

Sheffield Hallam University

The structural interaction of pipe couplings used for trenchless construction.

HILL, Matthew Jamieson.

Available from the Sheffield Hallam University Research Archive (SHURA) at:

<http://shura.shu.ac.uk/19792/>

A Sheffield Hallam University thesis

This thesis is protected by copyright which belongs to the author.

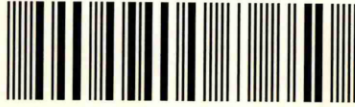
The content must not be changed in any way or sold commercially in any format or medium without the formal permission of the author.

When referring to this work, full bibliographic details including the author, title, awarding institution and date of the thesis must be given.

Please visit <http://shura.shu.ac.uk/19792/> and <http://shura.shu.ac.uk/information.html> for further details about copyright and re-use permissions.

LEARNING CENTRE
CITY CAMPUS, POND STREET,
SHEFFIELD, S1 1WB.

101 610 909 1



REFERENCE

ProQuest Number: 10697094

All rights reserved

INFORMATION TO ALL USERS

The quality of this reproduction is dependent upon the quality of the copy submitted.

In the unlikely event that the author did not send a complete manuscript and there are missing pages, these will be noted. Also, if material had to be removed, a note will indicate the deletion.



ProQuest 10697094

Published by ProQuest LLC (2017). Copyright of the Dissertation is held by the Author.

All rights reserved.

This work is protected against unauthorized copying under Title 17, United States Code
Microform Edition © ProQuest LLC.

ProQuest LLC.
789 East Eisenhower Parkway
P.O. Box 1346
Ann Arbor, MI 48106 – 1346

**SCHOOL OF CONSTRUCTION
SHEFFIELD HALLAM UNIVERSITY**

**THE STRUCTURAL INTERACTION OF PIPE
COUPLINGS USED FOR TRENCHLESS
CONSTRUCTION**

by

MATTHEW JAMIESON HILL

B.Eng. (hons) (Civil Engineering)

**A thesis submitted in partial fulfilment of the requirements of
Sheffield Hallam University
for the degree of Master of Philosophy**

Collaborating Organisation: Flex Seal Couplings Ltd., Sheffield, UK

June 1997



LEVEL 1

ABSTRACT

Trenchless construction of underground services by the pipe jacking method has radically increased over the past thirty years, particularly in sensitive urban areas. Spoil is removed at the cutting face and the entire pipeline is pushed through an oversized tunnel bore by large hydraulic jacks. The pipeline inevitably deviates from the intended alignment due to site conditions and the skill level of the workforce. Poor directional control of the pipeline can lead to pipe joints opening which induces high stresses in the pipe and produces a loading mechanism for the structural element of the coupling system.

This study has investigated the structural interaction of the pipe-packing-coupling system under installation conditions.

A theoretical model for the lateral force exerted on the joint/coupling under misaligned conditions was proposed and verified by full scale laboratory experiments. The differential eccentricity of the resultant jacking force at joints abutting a misaligned joint determines the lateral force exerted on the deflected joint and hence coupling system. It is shown that long pipes are beneficial in this respect.

This thesis considers the lateral force exerted on the joint under 'closed' and 'open' joint conditions. Such conditions occur due to minor deviations in the pipeline alignment with the open joint situation causing significant influence on the design of the coupling element.

The Australian Concrete Pipe Association Linear Stress Approach (ACPALSA) for open joint analysis was modified to predict the interaction between the packing material and the pipe joint for chipboard packing material and clay pipes. This is of benefit for the prediction of lateral force acting at an open misaligned joint.

A theoretical model for the prediction of principal tensile stresses induced in the structural element of the coupling was proposed and verified by full scale laboratory experiment. The design of the coupling should be based on points located at the centre of the coupling width due to edge effects associated with other locations. This point was shown to be critical in preliminary investigations and should be adopted for design purposes.

The findings of this thesis are of interest to the pipe jacking industry as a whole through improved knowledge of the structural interaction at misaligned joints and through a scientific approach to the design of the coupling system. The pipe-coupling unit cost maybe properly managed through implementation of this thesis.

DECLARATION

I hereby declare that no portion of the work referred to in this thesis has been submitted in support of an application for another degree or qualification of this or any university or other institution of learning. All sources of information have been duly acknowledged.

Matthew J. Hill

April 1997

ACKNOWLEDGEMENTS

The author wishes to express his sincere appreciation to DR F.A.N. Al-Shawi for his guidance and encouragement throughout the preparation of this thesis.

The author gratefully acknowledges the advise and facilities made available at Flex Seal Couplings Ltd. and in particular Mr. R. Prichatt, Mr. G. Woods and Mr. T Sykes.

CONTENTS

Page	
ABSTRACT	(ii)
DECLARATION	(iv)
ACKNOWLEDGEMENTS	(v)
CONTENTS	(vi)
NOTATION	(xiv)
GLOSSARY	(xii)
LIST OF FIGURES	(xvii)
LIST OF TABLES	(xx)
LIST OF PLATES	(xxii)

CHAPTER 1	<u>INTRODUCTION</u>	1
1.1.	INTRODUCTION	1
1.2.	THE PIPE JACKING TECHNIQUE	2
1.3.	JACKING PIPES	6
	1.3.1. Concrete jacking pipes	7
	1.3.2. Vitrified clay jacking pipes	7
	1.3.3. Glass reinforced plastic (GRP) jacking pipes	8
	1.3.4. Ductile iron jacking pipes	8
1.4.	JOINT DETAILS	9
1.5.	SCOPE OF PRESENT RESEARCH	11
1.6.	AIMS AND OBJECTIVES OF PRESENT RESEARCH	12

1.6.	AIMS AND OBJECTIVES OF PRESENT RESEARCH	12
1.6.1.	Aims of research	12
1.6.2.	Objectives of research	12
CHAPTER 2	<u>LITERATURE REVIEW OF RELATED WORKS</u>	14
2.1.	INTRODUCTION	14
2.2.	ALIGNMENT OF JACKED PIPELINES.....	15
2.3.	PIPE-JACKING FORCES	16
2.3.1.	Empirical methods of estimating total jacking forces	18
2.3.2.	Prediction of total jacking forces in rock stratum	19
2.3.3.	Prediction of total jacking forces in cohesive soils	21
2.3.4.	Prediction of total jacking forces in cohesionless soils	22
2.4.	THE STRUCTURAL INTERACTION OF JACKED PIPELINES.....	25
2.5.	THE STRUCTURAL INTERACTION OF OPEN JOINTS IN JACKED PIPELINES	27
2.6.	THE SPECIFICATION OF PACKING RING MATERIAL	32
2.7.	MAIN CONCLUSIONS	34
CHAPTER 3	<u>ANALYSIS OF LATERAL FORCE RESISTED BY</u> <u>COUPLING AT MISALIGNED JOINTS IN A JACKED</u> <u>PIPELINE</u>	36
3.1.	INTRODUCTION	36

CHAPTER 7 EXPERIMENTAL RESULTS AND DISCUSSION 139

7.1. INTRODUCTION 139

7.2. PIPE-PACKING INTERACTION140

7.3. LATERAL FORCE ACTING AT MISALIGNED JOINT 148

 7.3.1. Lateral force acting at open misaligned joint 148

 7.3.2. Lateral force acting at open/closed misaligned joint 153

 7.3.3. Lateral force sharing between structural element of coupling and
 frictional resistance of pipe-packing interface 157

7.4. EXPERIMENTAL STRESS ANALYSIS OF LOOSE SLEEVED PIPE-
 JACKING COUPLING 159

 7.4.1. Results of coupling test C1 for 400mm diameter clay pipes 160

 7.4.2. Results of coupling test C2 for 250mm diameter clay pipes 168

 7.4.3. Results of coupling test C3 for 250mm diameter clay pipes 170

7.5. MAIN CONCLUSIONS178

CHAPTER 8 CONCLUSIONS AND RECOMMENDATIONS 181

8.1. CONCLUSIONS FROM PRESENT STUDY181

8.2. RECOMMENDATIONS FOR FURTHER RESEARCH 184

REFERENCES185

APPENDICES

APPENDIX A1-A8 : Stress strain relationships for chipboard packing material . .A1-A8

GLOSSARY.

Few of the terms used to describe installation of underground services have been formally defined and definitions are not consistent between authors. The following definitions are presented for the purpose of this thesis and will be adopted hereafter.

Pipe jacking	Installation of underground service by forcing a series of pipes through an excavated tunnel by means of hydraulic jacks. Spoil is excavated at the face and transported through the constructed pipeline. Excavation is either manual or automatic and describes the technique used for man entry sized pipes.
Microtunnelling	Installation of underground service by forcing a series of pipes behind an automated excavation machine. Spoil is removed in the form of slurry and removed with an auger. The range of diameter of pipe is less than 900mm and therefore described as non-man entry.
Trenching	The technique of installing a pipeline by laying the pipes in the base of an excavated trench.
Misalignment	The angular displacement between successive pipe axes as a result of steering operations or differential ground conditions.
DN	The suffix DN refers to the Nominal Diameter of the pipe. The diameter refers specifically to the internal bore of the pipe.
Open joint	A situation resulting from excessive misalignment between two pipes whereby part of the pipe-end is not used for load transfer.

- Closed joint** A situation resulting from good tunnel alignment where the jacking load is transferred uniformly across the joint or near uniformly. All of the pipe end is used to transfer load to some degree.
- Coupling** The means of locating the pipe ends at the joint to prevent relative movement and ingress or egress of liquids. For the purpose of this thesis the coupling is considered as a structural ring element and a rubber sealing element.
- Packing material** A compressible material placed between pipe ends at the joint. Its function is to distribute the jacking load over a larger area as possible and to reduce stress concentrations at the joint as a result of misalignment.

NOTATION

a	Compressed thickness of packing material under load.
a_0	Nominal thickness of packing material before load application.
b	Width of rectangular coupling member.
d_{inside}	Diameter of Steinzeug clay pipe to internal bore.
d_{max}	Diameter of Steinzeug clay pipe to outside of barrel.
d_{spigot}	Diameter of Steinzeug clay pipe to milled spigot.
e	Eccentricity of resultant jacking force at misaligned joint measured from pipe axis.
E	Modulus of elasticity of coupling material.
E_c	Modulus of elasticity of pipe material.
E_j	Elasticity of pipe joint configuration.
E_p	Modulus of elasticity of packing material.
F	Applied jacking force.
F_r	Friction between packing material and pipe-end at misaligned joint.
G	Modulus of elasticity of coupling material in shear.
H	Lateral force component of applied jacking force at misaligned joint.
H_c	Lateral force resisted by structural element of coupling.
h_1	Offset distance between adjacent studs.
h_2	Offset distance between adjacent studs.
h_3	Offset distance between adjacent studs.
I	Second moment of area of coupling member.
J	Torsional constant for coupling member.
k	Dimensionless coefficient.
k_1	Dimensionless coefficient.
L_p	Length of pipe.
M	Applied moment at misaligned joint.
m	Dimensionless parameter defining packing-pipe contact zone at open joint.
M_0	Reactive moment about major member axis at boundary of half-coupling.
M_{m0}	Reactive moment about minor member axis at boundary of half-coupling.

M_{m0}	Distribution of bending moment induced in coupling ring about minor member axis.
M_0	Distribution of bending moment induced in coupling ring about major member axis.
P	Gauge pressure in hydraulic cylinder recorded on dial gauge.
p	Internal radial pressure distribution exerted on coupling ring.
P_θ	Distribution of tensile force induced in coupling ring.
R	Radius of coupling ring.
R_p	Radius of packing ring.
R_s	Radius to offset stud from pipe axis.
r	Ratio of minimum : maximum longitudinal jacking stress level in pipe at closed joint.
T_0	Reactive torque at boundary of half-coupling.
T_θ	Distribution of torsion induced in half-coupling.
t	Thickness of rectangular coupling member.
t_j	Width of packing material.
t_w	Thickness of pipe wall.
t_0	Applied torsion per unit circumferential length of coupling ring.
U	Strain energy.
y	Linear distance from $\sigma_{p_{min}}$ to σ_ϕ at misaligned joint.
z	Linear dispersion of longitudinal jacking stress distribution.
α_L	Inclination of applied jacking force through misaligned pipe.
β	Misalignment angle between successive pipe axes.
ϕ	Angular position defining longitudinal stress level in pipe at misaligned joint.
ϕ_A	Angular twist about longitudinal axis of member at boundary of half-coupling.
γ_L	Inclination of reactive jacking force through misaligned pipe.
η	Empirical coefficient.

ϕ	Parameter defining relative contribution of constant and varying internal radial pressure exerted on coupling ring.
κ	Angle, defining position of maximum compression of packing material measured from pipe invert.
λ	Constant pressure component of internal radial pressure exerted on coupling ring.
μ	Dimensionless parameter defining coupling mechanical and geometrical properties.
ν	Poisson's ratio for coupling material.
θ	Angular position measured from crown of coupling defining coupling stress distributions.
θ_c	Angular position measured from crown of pipe defining packing-pipe contact zone at open joint.
ρ	Coefficient, defining share of lateral force resisted by coupling.
σ_B	Direct bending stress about major member axis induced in coupling ring.
$\sigma_{p\phi}$	Longitudinal stress level in pipe joint at angular position ϕ .
σ_m	Direct bending stress about minor member axis induced in coupling ring.
σ_{max}	Maximum principal tensile stress induced in coupling ring.
σ_{min}	Minimum principal stress induced in coupling ring.
σ_{pmax}	Maximum longitudinal jacking stress level in pipe/packing.
σ_{pmin}	Minimum longitudinal jacking stress level in pipe/packing at closed joint.
σ_T	Hoop tensile stress induced in coupling ring.
τ_{max}	Maximum shear stress induced in coupling ring.
τ_{xz}	Surface shear stress component in x-z direction induced in coupling ring.
τ_{yz}	Surface shear stress component in y-z direction induced in coupling ring.
ω	Stress function for torsion of flat rectangular member.
ψ_A	Angular rotation about major member axis at boundary of half-coupling.
ψ_{mA}	Angular rotation about minor member axis at boundary of half-coupling.

LIST OF FIGURES

Figure Number	Page
1.1. The pipe jacking technique	5
1.2. Typical joint details used for jacking pipes	10
2.1. Prediction of total jacking force for different soil conditions	20
2.2. Model for predicting total jacking force in cohesionless material	24
2.3. Theoretical pipeline alignment	26
2.4. Australian Concrete Pipe Association Linear Stress Approach	28
2.5. Measured joint stress distributions with plywood packing material	31
3.1. Lateral force at a misaligned joint	37
3.2. Trapezoidal jacking stress distribution for closed misaligned joint	40
3.3. Relationship between r and the eccentricity of jacking force at a closed misaligned joint	44
3.4. Triangular jacking stress distribution for open misaligned joint	47
3.5. Relationship between θ_c and eccentricity of jacking force at an open misaligned joint	51
3.6. Relationship between m and θ_c for the prediction of pipe-packing-pipe interaction at an open misaligned joint	55
4.1. Flow diagram illustrating conceptual analysis of coupling stress model	59
4.2. Load sharing of pipe-packing-coupling system under installation conditions	61
4.3. Conceptual analysis of coupling under shear loading	63
4.4. Internal radial pressure exerted on coupling ring	64
4.5. Tensile force induced in coupling ring due to radial pressure distribution	66

4.6.	Bending moment about minor axis of coupling due to internal radial pressure distribution	68
4.7.	Vector free body diagram of quarter-coupling illustrating reactions at boundary (A), and applied loading	71
4.8.	Cartesian co-ordinate system adopted for shear stress distribution analysis . . .	79
4.9.	Distribution of shear stress for coupling cross-section	82
4.10.	Distribution of direct, bending and shear stresses acting on typical cross-section of coupling	84
4.11.	Mohr circle for stress at the critical point in the coupling cross-section	86
4.12.	Distribution of non-dimensional principal tensile stress induced at the surface of the middle of the coupling width	88
5.1.	Longitudinal section through experimental jacking frame	95
5.2.	Longitudinal section through Steinzeug clay pipe	101
5.3.	Relationship between applied axial stress and compression for chipboard packing sample CB1	104
5.4.	Relationship between applied axial stress and compression for chipboard packing sample CB2	105
5.5.	Relationship between applied axial stress and compression for chipboard packing sample CB3	106
5.6.	Illustration of typical coupling specimen	109
5.7.	Stress-strain relationship for tensile specimen S1	111
5.8.	Poisson's ratio for tensile specimen S1	112
5.9.	Stress-strain relationship for tensile specimen S2	113
5.10.	Poisson's ratio for tensile specimen S2	114
6.1.	Experimental measurement of joint deflection for central misaligned joint . .	119
6.2.	Relationship between hydraulic gauge pressure and applied force for cylinders HC1 and HC2	123
6.3.	Load cell arrangement for lateral force measurement	126

6.4.	Electrical strain gauge rosette location details for coupling stress analysis . . .	130
6.5.	Experimental arrangement for lateral force and coupling stress analysis tests	133
7.1.	Misaligned open joint characteristics during lateral force tests ST1A-ST1B for DN 250 mm pipes	141
7.2.	Misaligned open/closed joint characteristics during lateral force tests ST3A, ST3B and ST3C for DN 400mm pipes	142
7.3.	Misaligned open/closed joint characteristics for lateral force tests ST5A, ST5B, ST5C, ST5D and ST5E for DN 600 mm pipes	143
7.4.	Correlation between experimental results and theoretical relationship for θ_c and m, for pipe diameters in the range 250 mm to 600 mm	147
7.5.	Deviation of line of action of lateral force from vertical in open joint tests . . .	149
7.6.	Correlation between experimental measurement and theoretical prediction for lateral force based on joint alignment data for tests ST1A and ST1B for DN 250 mm pipes.	151
7.7.	Correlation between experimental measurement and theoretical prediction for lateral force based on joint alignment data for tests ST3B and ST3C for DN 400 mm pipes	152
7.8.	Misaligned joint characteristics and relationship between lateral force and applied jacking force for tests ST2A, ST2B, ST2C and ST2D for DN 250 mm pipes	154
7.9.	Misaligned joint characteristics and relationship between lateral force and applied jacking force for tests ST4A, ST4B, ST4C and ST4D for DN 400 mm pipes	155
7.10.	Misaligned joint characteristics and relationship between lateral force and applied jacking force for tests ST5A, ST5B, ST5C, ST5D and ST5E for DN 600 mm pipes	156
7.11.	Misaligned joint characteristics during test C1 for DN 400mm pipes	163
7.12.	Relationship between lateral force resisted by coupling and applied jacking force for test C1	164
7.13.	Correlation between theoretical model and experimental results for test C1 . .	165
7.14.	Correlation between theoretical model and experimental results for test C1 . .	166

7.15.	Correlation between theoretical model and experimental results for test C1. .	167
7.16.	Misalignment joint characteristics during test C2 for DN 250 mm pipes	171
7.17.	Relationship between lateral force resisted by coupling and applied jacking force for test C2	172
7.18.	Correlation between theoretical model and experimental results for rosettes 1,3 and 4 for test C2	173
7.19.	Misaligned joint characteristics for test C3 for DN 250 mm pipes	175
7.20.	Relationship between lateral force resisted by coupling and applied jacking force for test C3	176
7.21.	Correlation between theoretical model and experimental results for rosettes 1 and 2 for test C3	177

LIST OF TABLES

Table Number		Page
2.1.	Summary of frictional resistance's for different ground conditions	19
4.1.	Typical range of values for μ for coupling section sizes	76
5.1.	Dimensional specification of clayware pipes used for experimental investigation	100
5.2.	Properties of Steinzeug vitrified clay pipes	99
5.3.	Dimensional specification of chipboard packing rings	102
5.4.	Dimensional specification of chipboard blocks used for compression tests . .	103
5.5.	Summary of thickness of chipboard samples at start of load cycle	107
5.6.	Dimensional specification of coupling specimens	108

5.7.	Dimensional specification of stainless steel tensile specimens	110
5.8.	Summary of mechanical properties found by tensile tests	115
6.1.	Summary of offset stud alignment for experimental measurement of β	118
6.2.	Identification of correct range for κ [9]	120
6.3.	Summary of hydraulic cylinder details	121
6.4.	Summary of uncertainly analysis and accuracy of measurements recorded during experimental programme	132
6.5.	Summary of lateral force determination	136
6.6.	Summary of coupling stress analysis programme	137
7.1.	Typical joint elasticity's derived for experimental programme	145
7.2.	Summary of load sharing characteristics for closed joint tests	158
7.3.	Analysis of open joint phase of coupling test C1	161
7.4.	Analysis of open joint phase of coupling test C2	169

LIST OF PLATES

Plate Number	Page	
1.1.	Typical jacking pit set-up showing thrust wall, jacking frame and construction sequence	4
5.1.	Hydraulic jack arrangement for cylinder HC2 showing loading plate and reaction plate	96
5.2.	Illustration of experimental jacking frame	98
6.1.	Illustration of open joint showing packing ring and offset studs on DN 250 mm pipes	122
6.2.	Calibration of cylinder HC1 using servo-controlled testing machine	125
6.3.	Strain gauge rosettes fixed to coupling specimen C2 under test conditions . . .	128

CHAPTER 1

INTRODUCTION

1.1. INTRODUCTION.

Trenchless construction of underground services including pipelines, ducts and cables involves excavation without surface disturbance along the line of the service. Soil is removed by thrust displacement or enlargement of existing underground services which does not require conventional trenching.

Pipe jacking under roads and railways without interference to traffic was first introduced by the Northern Pacific railroad (USA) between 1896 and 1900 [1]. Since that time the method has evolved and become a standard accepted practice world wide. The pipe jacking method was first introduced to the United Kingdom in the late 1950's as a means of providing short pipelines beneath difficult obstacles such as canals, embankments etc.

The development of mechanised excavation plant and the increased awareness by clients to the social costs associated with traditional open cut construction has increased the viability of pipe jacking, particularly in urban environments. Today, trenchless construction is employed throughout the developed world.

1.2. THE PIPE JACKING TECHNIQUE.

The pipe jacking technique is a novel means of constructing flexible, structural, watertight pipelines with minimal disruption to the surrounding environment. A 'jacking pit' is excavated (typically at a manhole location) and shored either by sheet piles and falsework or segmental precast units for deeper excavations. A thrust wall is constructed in the base of the excavation to resist high jacking forces encountered during construction of the pipeline. A jacking frame with large capacity hydraulic jacks is aligned in the base of the pit to the correct grade and inclination of the intended pipeline. A typical jacking pit arrangement is illustrated in Plate 1.1.

The tunnel bore is excavated within a shield either manually or by mechanised plant and spoil is removed from the face to the jacking pit for removal. Jacking pipes are connected in turn to the excavation shield and pushed through the tunnel bore by means of large capacity hydraulic jacks. The excavation rate is matched by the rate of advancement of the pipes until the pipeline reaches a reception shaft, where the shield is removed. The technique is illustrated schematically in Figure 1.1.

Historically the main drawback from the pipejacking technique has been proper alignment control of the pipe train throughout the drive. Difficult ground conditions or voids can affect the alignment of the excavation machine, hence the subsequent pipeline. The pipeline alignment is controlled by laser beam fixed at the rear of the jacking pit and targeted at the rear of the shield. Steering corrections to the shield are made either automatically by microcomputer or manually by a technician, by means of

small hydraulic jacks located in the barrel of the shield. With recent advances in equipment the control of pipeline alignment has improved, however, rapid changes in alignment can give rise to opening of joints. Traditionally, misalignment between successive pipe axes has been the single cause of concern for the integrity of the pipeline in terms of:-

- 1) Controlling the total jacking force that can be safely transmitted through pipe joints.
- 2) Sealing performance of the coupling system.

Where longer lengths of pipeline are required between reception shafts, intermediate 'interjack' stations are invariably used to increase the jacking capability of the operation [2]. Here, a steel cylinder with hydraulic jacks placed around its periphery is introduced into the pipeline and pushed in the normal way until its operation becomes necessary. The pipes behind the interjack station are then held stressed back to the jacking pit, while the forward section of the pipeline is advanced via the interjack. At the end of the drive the interjack station is removed and the pipeline made good.

Lubrication in the form of bentonite/water slurry is also used frequently to reduce the skin friction along the drive between the external surface of the pipe and the soil. The reduction in jacking forces can be considerable providing the loss of slurry to the surrounding soil can be controlled [3].



Plate 1.1. Typical jacking pit set-up showing thrust wall, jacking frame and construction sequence.

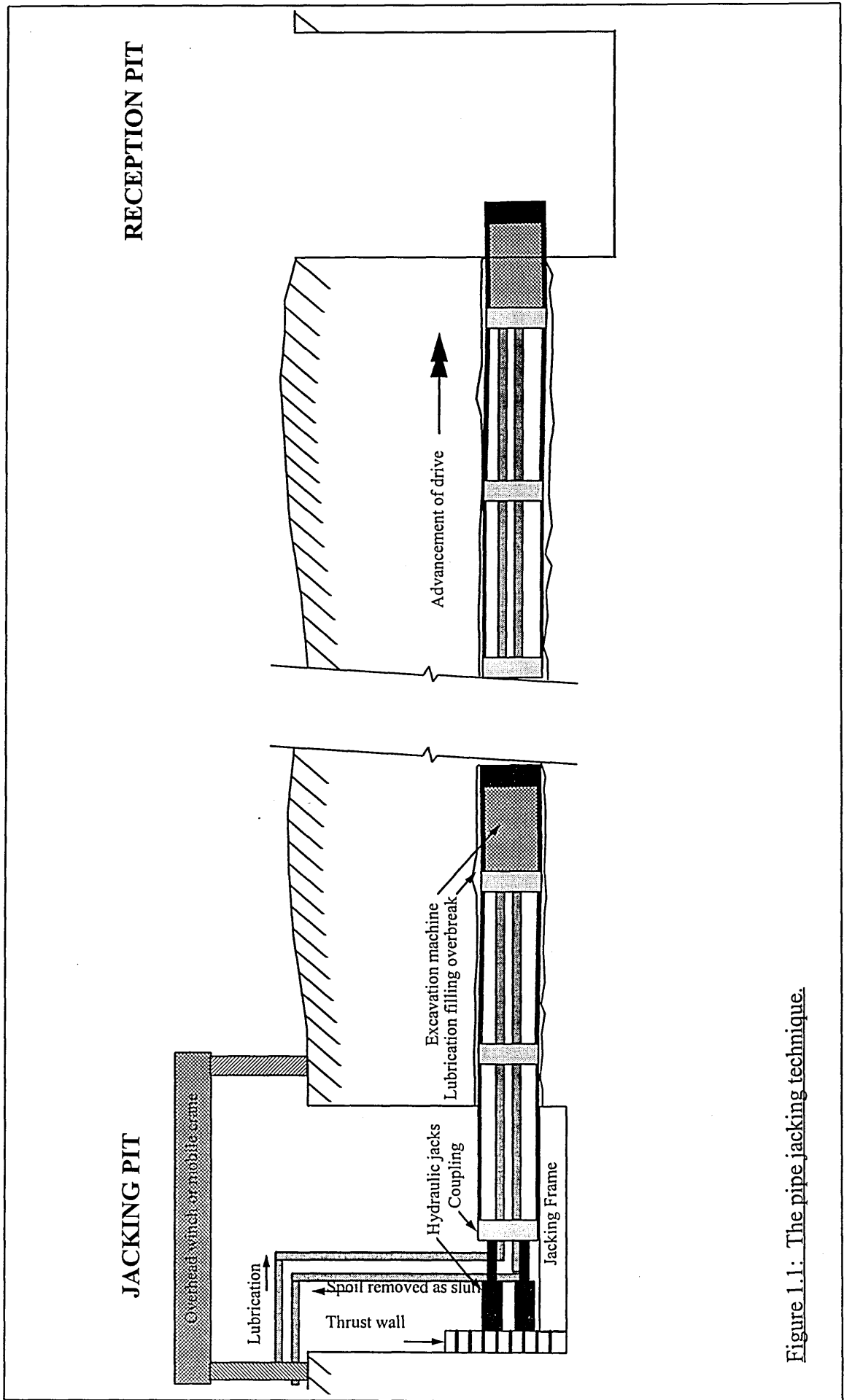


Figure 1.1: The pipe jacking technique.

1.3. JACKING PIPES.

Pipes and joints for installation by pipejacking are designed for both gravity and pressure applications. Due to the high axial loads required to push the whole pipeline through the ground, thick walled pipes are manufactured from a variety of materials as listed below:-

- 1) Reinforced concrete.
- 2) Vitrified clay.
- 3) Glass Reinforced Plastic (GRP).
- 4) Ductile iron.

The choice of material is dependant on the specific requirements of the service to be installed with concrete invariably used for pipe bores in excess of 1000mm and clayware/concrete used for microtunnelling applications. Ductile iron is mainly preferred for use with pressure pipeline applications.

Jacking pipes are typically manufactured in lengths of 2m. The length of the pipe is determined by economic factors, as longer pipes will require fewer joints, but the shaft dimensions have to be larger. It is recommended that the length of the pipe does not exceed the length of the excavation shield. As the pipeline is advanced, minor corrections in line and grade are continuously made. It is argued that longer pipes will not be able to follow the course of the shield and this will induce greater drag [3].

1.3.1. CONCRETE JACKING PIPES.

Reinforced concrete is the most common material used for production of jacking pipes as reinforcement can be used to resist longitudinal and hoop bending induced in the pipe. The range of pipe sizes is virtually limitless with typical ranges of internal bore between 250mm and 5000mm with wall thickness varying between 75mm and 200mm [4]. Pipes are factory produced by the pipe-spinning method or vertically cast with high frequency vibration.

1.3.2. VITRIFIED CLAY JACKING PIPES.

Clay drain and sewer pipes have been successfully used since the time that man first wanted to transport liquids by gravity. Clayware has traditionally been used for open cut installation for many years. However, vitrified clay pipes have become well established for trenchless construction in Europe in recent times due to the following reasons:-

- High chemical resistance with no need for any secondary lining.
- High compressive and bending strengths which can resist high jacking loads.

Vitrified clay pipes are available only for microtunnelling applications where the internal bore is limited to less than 1000mm. The pipes are vertically extruded and glazed to enhance their chemical resistance and reduce frictional forces during

construction. The degree of accuracy in manufacture of concrete pipes is higher than that attained for clay pipes [5]. The ends of the clay pipes are machined to give square ends and accurate spigots for use with a loose sleeved coupling. The poor dimensional accuracy frequently encountered with clay pipes leads to inefficient use of the wall thickness for load transfer in certain circumstances.

1.3.3. GLASS REINFORCED PLASTIC (GRP) JACKING PIPES.

GRP pipes manufactured by the centrifugal casting method have been used since the early 1980's in Europe, Japan and North America on sewer applications by trenchless construction. The main manufacturer of GRP pipes is Hobas Durotec GmbH [6], producing pipes from 200 mm to 2400 mm internal diameter, with wall thickness varying between 30mm to 60mm. The load capacity of the pipes compared with concrete and clayware is poor with the safe working load being approximately 40 percent lower than clay pipes and 60 percent lower than reinforced concrete pipes [3].

1.3.4. DUCTILE IRON JACKING PIPES.

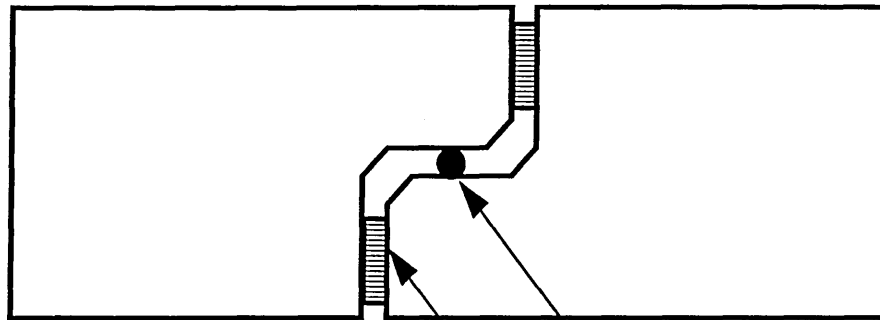
The greatest application for ductile iron for pipejacking and microtunnelling has been for pressurised pipelines in Japan. Ductile iron is available in a range of diameters from DN 300 to DN 2600 mm in 4m length sections.

1.4. JOINTS DETAILS.

Joints details for jacking pipes are divided into two categories, rebated and sleeved. Each type is illustrated in Figure 1.2. The rebated joint limits the axial force that can be safely transmitted as only part of the wall thickness can be considered as load bearing particularly when the joint is opened. For this reason, the rebated joint is uncommon.

The fixed and loose sleeved coupling joints utilise more of the wall thickness for load transfer during installation and is therefore commonly used world-wide. The joint in all cases is sealed by an elastomeric ring (Figure 1.2. (a,b)) or profiled seal (Figure 1.2. (c)) to prevent ingress or egress of fluids. The coupling needs to be adequately protected against corrosion and typical materials include GRP, stainless steel and mild steel.

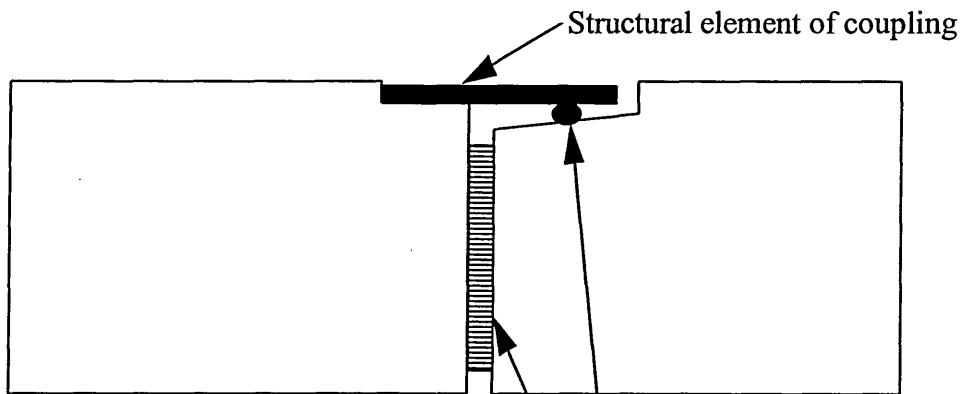
In addition a packing ring is inserted between the pipe faces to distribute longitudinal jacking stresses around the pipe annulus. Typical materials commonly used include chipboard and Medium Density Fibreboard (MDF).



Elastomeric ring

Packing ring

(a) : Rebated joint for concrete jacking pipe.

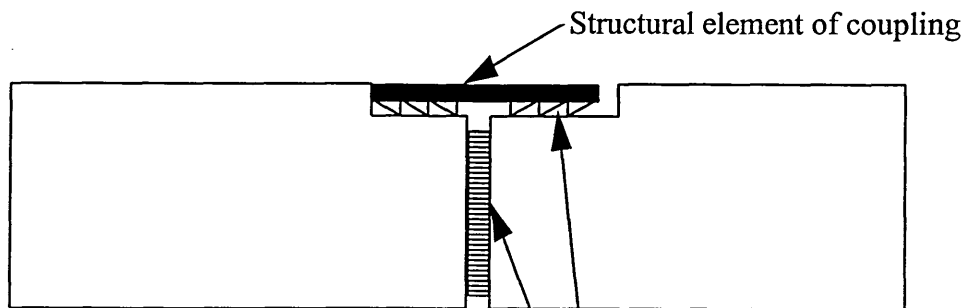


Structural element of coupling

Elastomeric ring

Packing ring

(b) : Fixed sleeve joint for concrete jacking pipe.



Structural element of coupling

Profiled seal

Packing ring

(c) : Loose sleeve joint incorporating profiled sealing element for clayware pipes.

Figure 1.2: Typical joint details used for jacking pipes.

1.5. SCOPE OF PRESENT RESEARCH.

Jacking pipes are subjected to high cyclic loading especially during long drives. Minor steering correction to line and level of the shield/machine introduce misalignment between successive pipes. Research has been focused on the pipe-soil and pipe-packing interaction with little thought given to the pipe-packing-coupling interaction.

The basic composition of a jacking pipe coupling consists of:-

- A structural ring element (typically stainless steel/mild steel) to resist any lateral forces and to locate the pipe ends, and,
- A sealing element to prevent ingress/egress of fluids both in the short and long term.

The use of corrosion resilient materials such as stainless steel can have a dramatic affect on the cost of the pipe-coupling unit. Therefore, better understanding of the behaviour of the joint may lead to more efficient use of materials.

This thesis will identify the lateral forces acting on a stainless steel structural ring and determine the optimum design requirements of the coupling in terms of its structural behaviour based on a scientific methodology.

1.6. AIMS AND OBJECTIVES OF PRESENT RESEARCH.

1.6.1. AIMS OF RESEARCH.

The main aim of the thesis is to investigate the structural interaction of the pipe-packing-coupling system under installation conditions in order to give recommendations to aid the structural design of jacking pipe couplings. The contribution to knowledge made by this thesis will be of benefit to the pipe jacking industry, not only in terms of the coupling design but through the joint interaction at misaligned joints.

1.6.2. OBJECTIVES OF RESEARCH.

In order to meet the aims stated above, the following objectives were fulfilled:-

- 1) To review the current knowledge base with respect to the structural interaction of jacking pipe joints.
- 2) To review published works concerning the scale of the problem in terms of achievable pipeline alignments, jacking forces, joint design etc.
- 3) To formulate and refine a mathematical model for the prediction of lateral force exerted on the coupling member under installation conditions.

- 4) To formulate and refine a mathematical model for the prediction of principal tensile stresses induced in the coupling member under installation conditions.
- 5) To design and construct a purpose built experimental jacking frame in order to verify the mathematical models proposed.
- 6) To investigate the magnitude of lateral forces resisted by the structural element of the coupling under full scale misaligned experimental conditions.
- 7) To investigate the principal tensile stress distribution induced in the structural element of the coupling under full scale misaligned experimental conditions
- 8) To perform materials tests on coupling system components.
- 9) To review the theoretical and experimental investigations in order to propose recommendations to aid the structural design of jacking pipe couplings.

CHAPTER 2

LITERATURE REVIEW OF RELATED WORKS

2.1. INTRODUCTION.

The pipe-jacking industry has evolved radically over the past thirty years and new techniques and plant have led to an increase in the use of the method particularly in sensitive environmental areas. As with all new technologies, research into the fundamental mechanics of the pipe-soil interaction has led to the development of state-of-the-art methods of construction. The main areas researched over recent years have been the pipe-soil and pipe-packing interaction with little regard to the pipe-packing-coupling interaction.

The current knowledge base is critically reviewed in this chapter giving a starting point for the present study. As the structural interaction of the coupling has not been studied before, the models presented in chapters 3 and 4 are based on related works for the global interaction of the pipeline and considerations of ground conditions. The review of literature is therefore divided into two main themes:-

- 1) Construction related issues.
- 2) The structural interaction of jacked pipelines.

2.2. ALIGNMENT OF JACKED PIPELINES.

The alignment of the pipeline is crucial to the structural and hydraulic performance in the short term (i.e. construction phase) and long term. Irregularities in ground conditions and steering adjustments will inevitably create misalignment between pipes. Minor joint deflections may be accommodated by the compression characteristics of the packing material, however, larger joint displacements will lead to opening of joints.

Field Monitoring carried out by Stein et al. [7] in Hamburg showed that good line and level tolerances can be achieved with deviations from theoretical axes of ± 15 mm. However, the change in alignment is more important than the overall alignment profile, for which no data was presented.

Boot et al [8] established the behaviour of misaligned pipes tending to re-align under applied jacking force through laboratory testing of clay pipes. This straightening of the pipe train was observed by Milligan et al [9] in field monitoring of full scale pipe-jacks although typical changes in misalignment under load were limited to approximately 0.08° . Haslam [10] developed the concept of joint closing under load and attributed the phenomenon to measurable bending of the pipes adjoining the deflected joint due to eccentric loading, thereby reducing the joint gap.

Field monitoring of misaligned joints for actual pipe-jacked schemes by Milligan et al [9] in the UK showed that four of the five schemes monitored were within specified line and level tolerance with well controlled drives creating joint angles between zero and

0.3° and maximum values up to approximately 0.75° where directional control was poor. Peak pipe joint stresses were recorded at large joint deflections confirming the danger of over-stressed pipes.

Moss [11] argued that the difference between tolerance for line and level of the pipeline and tolerance for angular deflection of pipe joints should be addressed. It is possible to maintain line and level tolerance at the expense of large joint deflections due to rapid over-steering of the shield which could lead to pipe failure. At present BS 5911: part 120 [12] and EN 295: part 7 [13] do not refer to construction tolerances which leaves the judgement of the corrective measures taken during drives with the engineers specification, which may not always be beneficial to the structural integrity of the pipe joints. Normal practice has been to specify the errors in line and level at any one point, typically 50 or 75 mm [9,14], however, this does not limit safe working joint deflections.

2.3. PIPE-JACKING FORCES.

The force required to push the entire pipeline through the excavated tunnel bore is dependant on a number of factors. An assessment of the jacking forces likely to be encountered during the drive must be made in order to ensure that the jacks to be used are adequate and secondly whether interjack stations are required. Thompson [3] attributed the total jacking force to main two sources:-

- 1) Forces arising from the prevailing site conditions.
- 2) Forces that are influenced by the construction process.

The main contribution to the total jacking force is the force required to overcome frictional resistance between the pipe and the soil, while resistance at the tunnel face is comparatively small - due only to friction forces acting on the external surface of the shield.

There are a multitude of factors affecting the total jacking force which will vary from site to site. Thompson suggests the following parameters to be dominant for assessing total jacking forces [3]:-

- 1) The size, shape and self-weight of the pipes.
- 2) The length of the pipeline.
- 3) The soil type and its variation along the length of the drive.
- 4) The stability of the soil, both immediately and over the construction process.
- 5) The cover depth and unit weight of the overlying soil.
- 6) The amount of overcut during excavation.
- 7) The use of lubricant.
- 8) Steps at joints and/or joint deformation.
- 9) Misalignment of the pipeline along its length.
- 10) The use of intermediate jacking stations.
- 11) The frequency and duration of stoppages.

Points (1-5) are determined by site conditions while points (6-9) are determined by the construction process. Numerous models have been proposed for the prediction of the jacking force required to push the pipeline through different soil types. It is clear that any one model can not take into account all of the factors outlined above, however, some correlation has been noted between analytical models and site observations. Analytical models that consider the soil properties have received most credit.

2.3.1. EMPIRICAL METHODS OF ESTIMATING TOTAL JACKING FORCES.

Many factors influence the frictional resistance between the external surface of the pipe and the tunnel bore. Stein [7] and Craig [14] expressed the jacking force as a 'rules of thumb' measure in terms of the drag per unit area of pipeline based on empirical data obtained from pipe jacking records. Variations in recorded jacking forces in the UK and Germany illustrate the need for analytical models which identify the influencing parameters.

Table 2.1. shows the frictional resistance for different ground conditions observed in the UK and Germany:-

Soil type	Frictional resistance (kN/m ²)	
	UK [14]	Germany [7]
Rock	2 to 3	
Boulder clay	5 to 18	2.8 to 18.4
Firm clay	5 to 20	5.3 to 9.3
Wet sand	10 to 15	2.2 to 16.1
Silt	5 to 20	4.9 to 8.5
Dry dense sand		1.1 to 6.7
Dry loose sand	25 to 45	
Fill	up to 45	
Dense gravel		6.4 to 23

Table 2.1. Summary of frictional resistance's for different ground conditions, after Stein [7] and Craig [14].

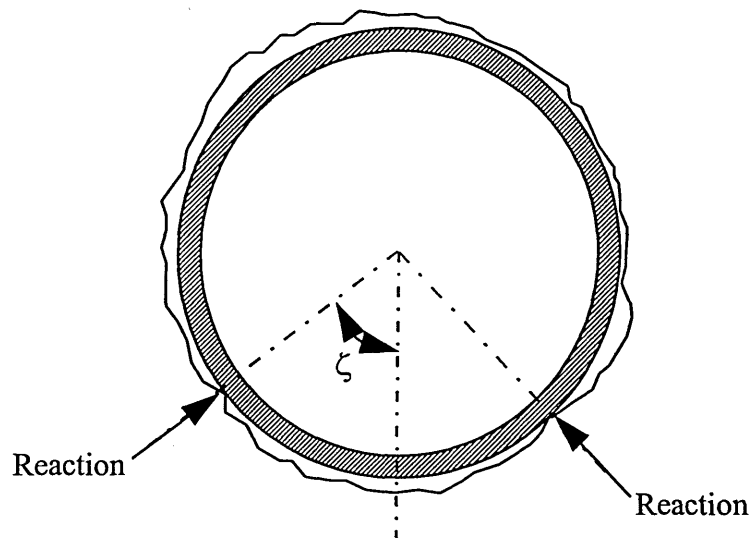
2.3.2. PREDICTION OF TOTAL JACKING FORCES IN ROCK STRATUM.

The over-excavation necessary when tunnelling through rock causes the pipe to rest on point contacts within the cavity. With reference to Figure 2.1(a), Rodges [15] proposed the following formula for the prediction of jacking force through rock stratum:-

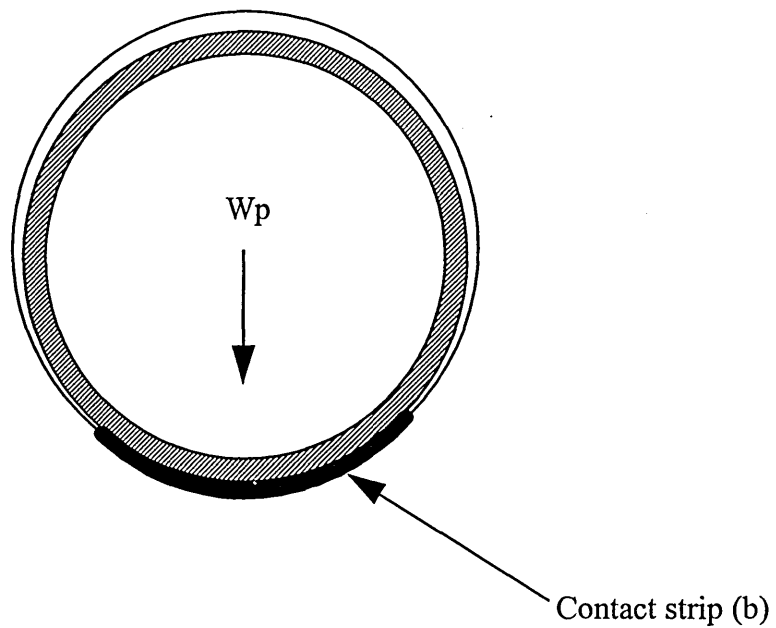
$$F_p = \frac{W_p \tan \delta_p}{\cos \zeta} \quad (2.1)$$

Where:-

F_p = Jacking force (in kN/m run).



(a) Model for predicting total jacking force in rock stratum [15]



(b) Model for predicting total jacking force in cohesive soil with stable bore, after Haslam [16].

Figure 2.1. Prediction of total jacking force for different soil conditions.

W_p = Weight of pipe.

δ_p = Angle of friction between pipe and rock (in degrees) - from laboratory experiment.

ζ = Angle made by the reaction with the vertical (in degrees).

Rodges found satisfactory correlation with the model for sandstone, however, the appropriate value for δ_p was critical in order to predict the jacking force through varying rock stratum. In addition, the value of ζ is unknown in practice, therefore a value must be assumed so that the jacking force (F_p) can be evaluated from equation 2.1. Thompson [3] recommended the use of ζ equal to 30° for design purposes.

2.3.3. PREDICTION OF TOTAL JACKING FORCES IN COHESIVE SOILS.

Haslam [16] considered the case of a pipeline resting in the bottom of a stable bore of cohesive soil. Elastic analysis of the soil response to load was assumed to determine the contact strip between the pipe and the soil, hence determine the resistance to sliding due to pipe-soil friction. The model is defined with reference to Figure 2.1(b) as:-

$$F_p = \alpha s_u b \quad \text{kN / m run} \quad (2.2)$$

Where:-

αs_u = 'adhesion' between pipe and clay

$$b = 1.6 \sqrt{P_u K_d C_e}$$

P_u = contact force per unit length.

$$K_d = D_1 D_2 / (D_1 - D_2).$$

$$C_c = (1 - n_1^2) / E_1 + (1 - n_2^2) / E_2$$

E_1 = elastic modulus of the soil.

E_2 = elastic modulus of pipe.

D_1 = diameter of tunnel bore.

D_2 = external diameter of pipe.

n = Poisson's ratio as for E .

The main drawback to the model was in the prediction of contact area between the pipe and the tunnel bore on account of plastic yielding of the soil.

Later work by Rodges et al [15] to verify the deviation from elastic behaviour of the soil was carried out. Experimental results showed that the elastic model underestimated the contact area by a factor of 2.5. In addition the water content of the clay was found to influence the contact area in a time dependant manner. Field monitoring by Milligan et al [9] also gives support to the contact strip model for cohesive soils although under estimating the actual jacking force by a factor of 1.2.

2.3.4. PREDICTION OF TOTAL JACKING FORCES IN COHESIONLESS SOILS.

The jacking force required to push the pipeline through cohesionless soil is generally greater than for cohesive/rock stratum due to soil collapsing onto the pipe. With

reference to Figure 2.2., Auld [17] using Terzaghi's earth pressure theory [18], derived an expression for the total jacking force per unit length of the pipe for un-lubricated drives as:-

$$F_p = \frac{\pi D}{2} (\sigma_v + \sigma_h) \tan \delta \quad (2.3)$$

Where:-

$$\sigma_v = \frac{\gamma B}{k \tan \phi} (1 - e^{-k \frac{H}{B} \tan \phi}) \quad (2.4)$$

$$\sigma_h = k(\sigma_v + 0.5\gamma D) \quad (2.5)$$

D = external diameter of pipe.

ϕ = angle of internal friction of the soil

δ = angle of friction between pipe and soil.

γ = unit weight of soil (kN/m²).

k = active pressure coefficient.

Field monitoring by Milligan et al [9] showed good correlation with the above analysis for loose to medium-dense cohesionless materials for un-lubricated conditions. The use of lubrication filling the overbreak reduces the angle of friction (δ) between the pipe and the soil and the jacking force required to push the pipeline. Clearly, effective lubrication should allow longer pipelines to be jacked, provided that the lubrication can be controlled.

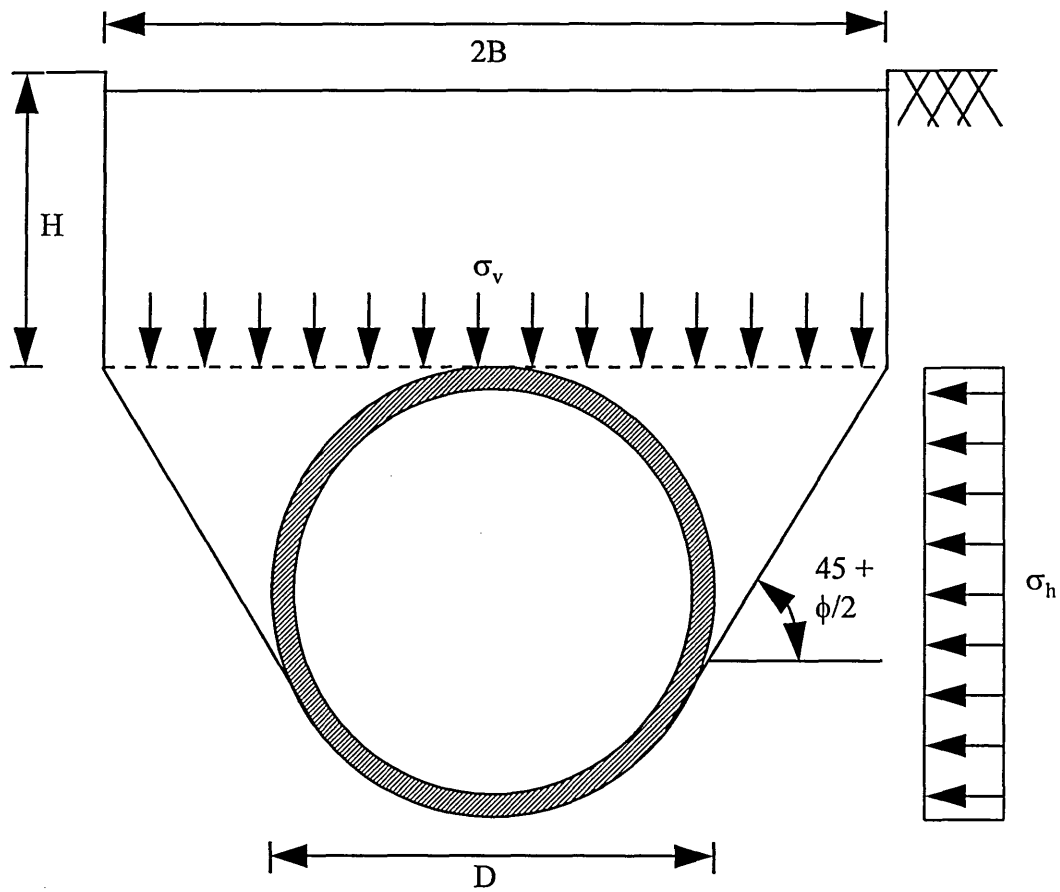


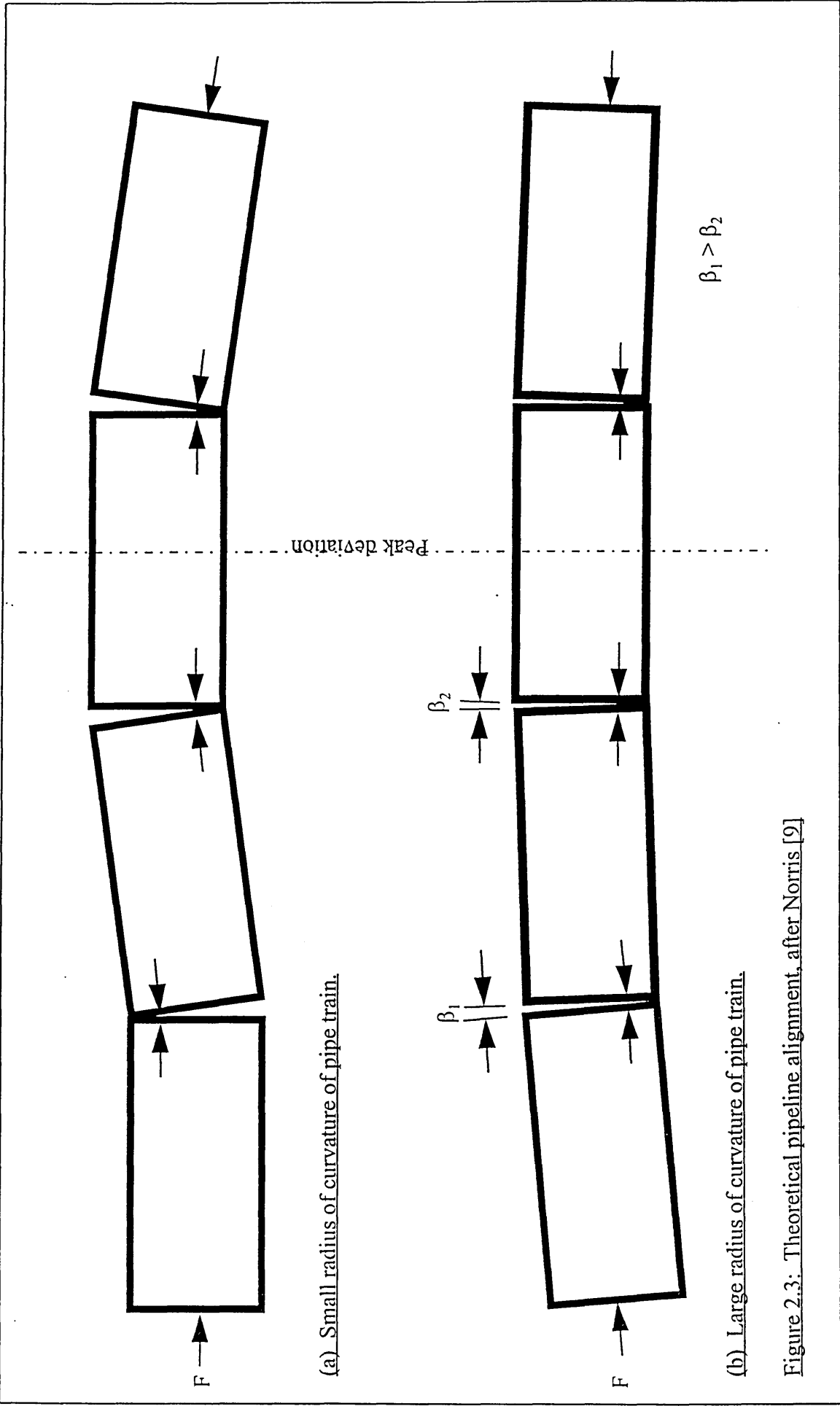
Figure 2.2. Model for predicting total jacking force in cohesionless material [17,18].

2.4. THE STRUCTURAL INTERACTION OF JACKED PIPELINES.

Haslam [16] was the first to propose a model for the global interaction of the pipe train as it proceeds through the tunnel bore. In this, he recognised that a misaligned tunnel produced a component of jacking force perpendicular to the pipeline axis. When combined with the self-weight of the pipe the resultant force would produce a contact strip with the surrounding soil. Haslam assumed an infinitely stiff response to longitudinal jacking force but complete flexibility for force normal to the pipe axis.

Milligan and Norris [9] identified a number of different ground reactions depending upon the alignment of the pipeline. These were dealt with by distinguishing between large and small radius of curvatures shown in Figure 2.3. The results of the study showed that the case of small radius of curvature only occurred close behind the shield where quite rapid changes in alignment occurred as a result of steering operations, or at very small joint misalignments as the pipeline passes through a point of contraflexure in the tunnel. From measured joint deflections in actual schemes [9], Milligan concluded that large radius of curvature was frequently encountered and this has the most adverse effect on the integrity of the pipeline.

Due to the effect of misalignment in three dimensions, Milligan showed that the load path through the pipe was dictated by the position of maximum compression in the packing material [9,19]. Therefore, the position of the resultant jacking force at each end of a pipe determines the load path through the pipe. By extending this concept, the inclination of the jacking force through the pipes abutting a deflected joint would



(a) Small radius of curvature of pipe train.

(b) Large radius of curvature of pipe train.

Figure 2.3: Theoretical pipeline alignment, after Norris [9]

produce a component of jacking force normal to the pipeline axis, and this is resisted by the packing-coupling system.

The ground reaction used in the present study assumes that the component of jacking force acting normal to the pipeline axis at a misaligned joint (the lateral force) is able to cause un-resisted shear in the joint. This assumption is based upon considerations of variable ground conditions. For example, a pipe joint extending through rock stratum into loose sand or voids in the tunnel bore. The condition of un-resisted shear produces an upper bound joint force and this is the case considered in the design of a coupling system.

2.5. THE STRUCTURAL INTERACTION OF OPEN JOINTS IN JACKED PIPELINES.

The only means to quantify the relationship between the maximum longitudinal jacking stress in the pipe wall and the misalignment of the pipeline is attributed to the Concrete Pipe Association of Australia [20] which gives the following equation for the calculation of the safe joint deflection for any open joint configuration.

With reference to Figure 2.4.:-

$$\beta = \frac{180a\sigma_{pmax}}{\pi E_j z} \quad (2.6)$$

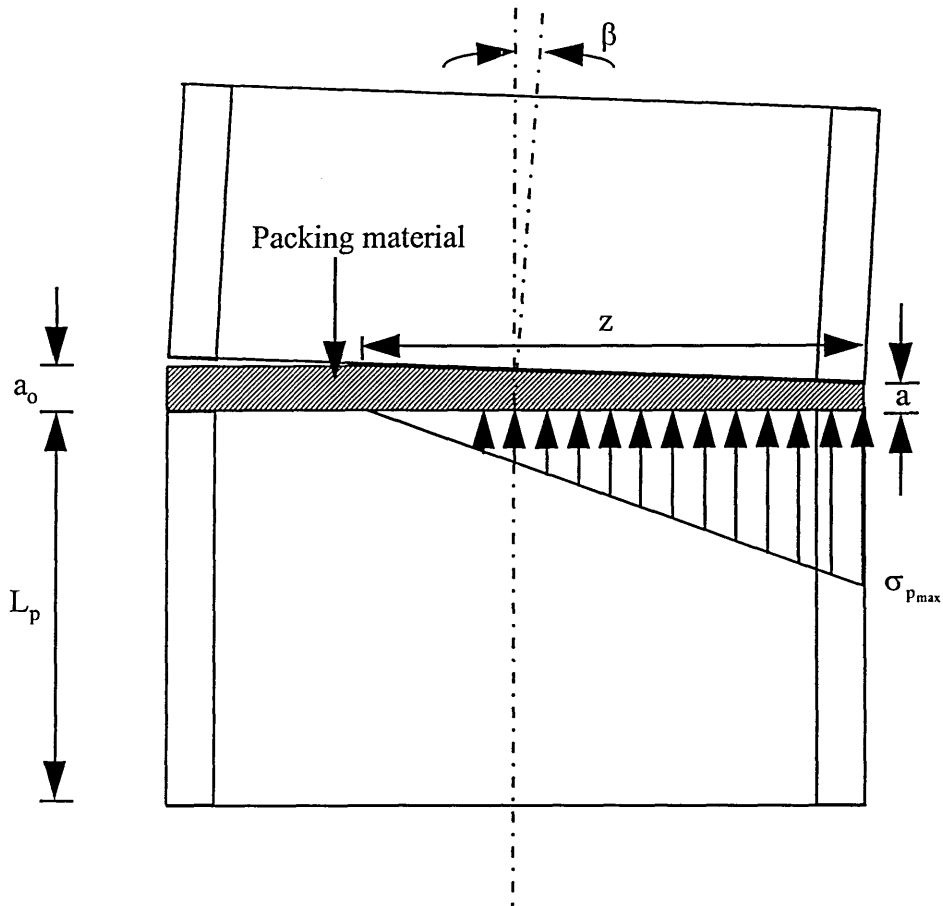


Figure 2.4. Australian Concrete Pipe Association Linear Stress Approach [20].

where:-

$$E_j = \frac{a t_w E_p E_c}{a t_w E_c + L_p t_j E_p} \quad (2.7)$$

a = Compressed thickness of packing material.

β = Misalignment angle of pipes abutting open joint.

$\sigma_{p_{max}}$ = Maximum longitudinal jacking stress level in pipe/packing.

E_c = Modulus of elasticity of pipe material.

E_j = Elasticity of joint arrangement.

E_p = Modulus of elasticity of packing material.

L_p = Length of pipe.

t_j = Width of packing material.

t_w = Thickness of pipe wall.

z = Linear dispersion of longitudinal jacking stress distribution pipe wall.

From equation 2.6. the maximum longitudinal stress level in the pipe is largely dependant on the misalignment angle (β) and the joint elasticity (E_j). The maximum joint stress must be controlled by good directional control of the pipeline so that damage does not occur at the joint. Milligan et al [9] noted highly localised joint stresses even at low misalignment angles, perhaps acting over less than a quarter of the pipe circumference.

Correlation with joint stresses measured during field monitoring by Milligan et al [9,19] reported satisfactory agreement and recommended equation 2.6. be used for design

purposes. The main drawback in the model is the estimation of the joint elasticity (E_j), as the elasticity of the packing material is not constant but stress dependant for common packing materials. Any correlation with joint stresses would require a complete history of the packing material stress-strain relationship. Since this is difficult to obtain in practice the analysis is considered to be conservative.

Kanari et al [21] investigated the effect of tensile strains induced in the pipe as a result of jacking in curved drives. By applying an eccentric force to a single pipe and observing the strains induced, tensile strains were measured when the eccentricity of the jacking force was approximately $R_p/2$ from the pipe axis. The following expression for the core radius of the cross-section of the pipe was given:-

$$K = \frac{R_o^2 + R_D^2}{4R_o} \quad (2.8)$$

Where:-

R_o = Radius to outside of pipe,

R_D = Radius to inside of pipe wall.

Kanari also measured the jacking stress distributions close to the pipe end under different eccentricities of load which are shown in Figure 2.5. It is clear from the Figure that the stress distributions are approximately linear. Curve A is for the case of a closed joint where the distribution is approximately trapezoidal and curves B and C are for the open joint case. The work carried out by Kanari et al confirms the distribution of longitudinal jacking stresses at open joints (given by equation 2.6.) and suggests that the distribution for closed joints can be

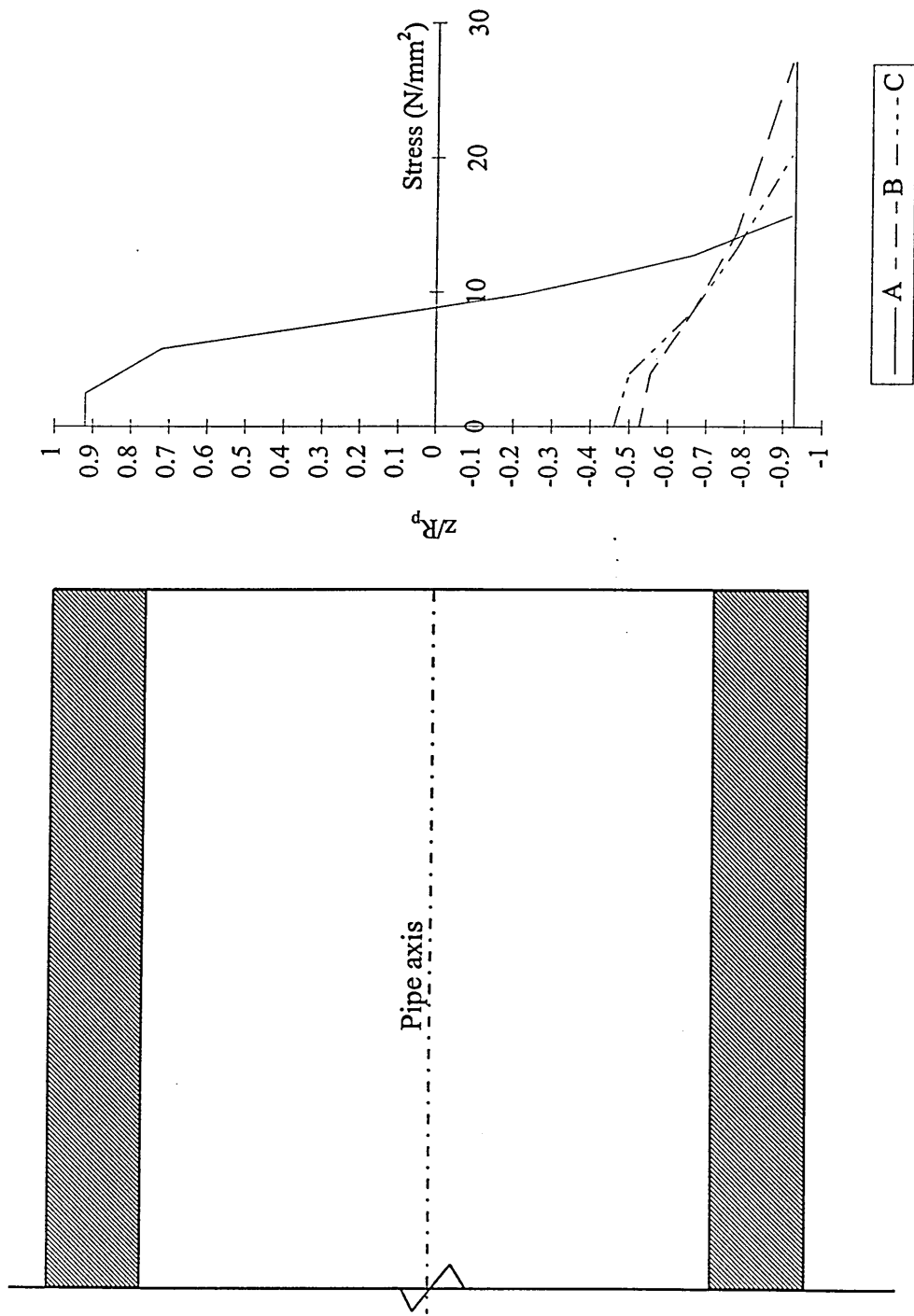


Figure 2.5. Measured joint stress distributions with plywood packing material, after Kanari et al [21].

modelled on a trapezoidal distribution.

The eccentricity of the jacking force at open and closed joints was investigated by Haslam [10] who proposed equations for the prediction of eccentricity for various joint displacement conditions. It would seem appropriate to derive the eccentricity of the resultant jacking force at the joint in terms of the contact area.

2.6. THE SPECIFICATION OF PACKING RING MATERIAL.

The presence of a compressible packing material inserted between adjacent pipe ends reduces the maximum stress level in the pipe wall by distributing the applied jacking force over a larger area and by compensating for irregularities in planarity in the pipe ends. Studies carried out by Husein et al [22] and Ripley et al [23] investigated the effect of different packing materials on the strength of the pipe in order to maximise its capability.

Husein investigated a wide range of wood based and rubber materials. He concluded that wood based materials with low Poisson's ratio were most suitable due to their compressibility and ability to distribute longitudinal jacking stresses over the pipe end.

Ripley conducted cyclic compression tests on a variety of wood based materials and compared them against the following criteria:-

- 1) The material should compress when loaded and recover to its original thickness when unloaded.
- 2) The material should have a Poisson's ratio in compression near to zero to eliminate lateral strains causing spalling of the pipe end.

From both studies, chipboard and Medium Density Fibreboard (MDF) were found to be most suitable. The results of stress-deformation tests on chipboard and fibreboard showed radically different characteristics for the first load cycle to that of subsequent load cycles [23]. The materials became permanently deformed after the first load cycle and consequently increased the modulus of elasticity. The modulus of elasticity was also shown to be stress dependant, giving higher values at high stress levels.

Ripley [23] found that packing material (chipboard and MDF) in a saturated state improved the load transfer capabilities as it was more compressible, therefore distributed the load over a larger pipe-end area.

Husein [22] and Ripley [23] both agreed that thick packing rings were beneficial to the joint system. Taking the pipe geometry and the compressibility of the packing material in to account, thick packing rings would distribute longitudinal jacking stresses over a greater pipe-end area at a deflected joint than thinner packing rings.

2.7. MAIN CONCLUSIONS.

The following conclusions may be drawn from the literature survey:-

- 1) Previous research projects have not concentrated on the pipe-packing-coupling interaction but provide valuable information regarding the possible global interaction of jacked pipelines.
- 2) The control of the pipeline alignment is critical in limiting stress levels in misaligned joints and to control the component of jacking force acting normal to the pipeline axis (lateral force).
- 3) With well controlled drives, the joint deflections measured in practice have been in the range of zero to 0.3 degrees with maximum values as high as 0.75 degrees.
- 4) Numerous models have been proposed for the prediction of jacking forces required to push the pipe train through the tunnel bore for different site conditions. Typical jacking forces can be in excess of 5000 kN for relatively short pipeline lengths.
- 5) Taking points (3) and (4) into account, the consequence of large jacking forces applied to misaligned pipe trains could have a damaging effect on the pipe and the coupling system.
- 6) The global interaction models reviewed in this chapter and the nature of variable

ground conditions has led to the structural interaction of the pipe-packing-coupling system being assumed to be loaded by un-resisted shear action due to the lateral force.

- 7) The Australian Concrete Pipe Association Linear Stress Approach (ACPALSA) for the prediction of longitudinal jacking stresses as a function of joint misalignment has been given credibility from field monitoring of actual pipe jacked schemes in the UK and experimental investigations in Japan.
- 8) Based on experimental evidence, the distribution of longitudinal jacking stress can be modelled on a trapezoidal distribution for the case of a closed joint.
- 9) The differential eccentricity of the resultant jacking force at each end of the pipe determines the load path through the pipe.
- 10) The properties of the packing material used to distribute longitudinal jacking stresses over the pipe-end have an effect on the strength capability of the pipes.
- 11) Chipboard and MDF have been found to be most suitable for use as packing material. The stress-strain characteristics of the material should be assessed for modelling the structural interaction of the pipe joint due to the stress-dependant modulus of elasticity and the cyclic nature of loading.

CHAPTER 3

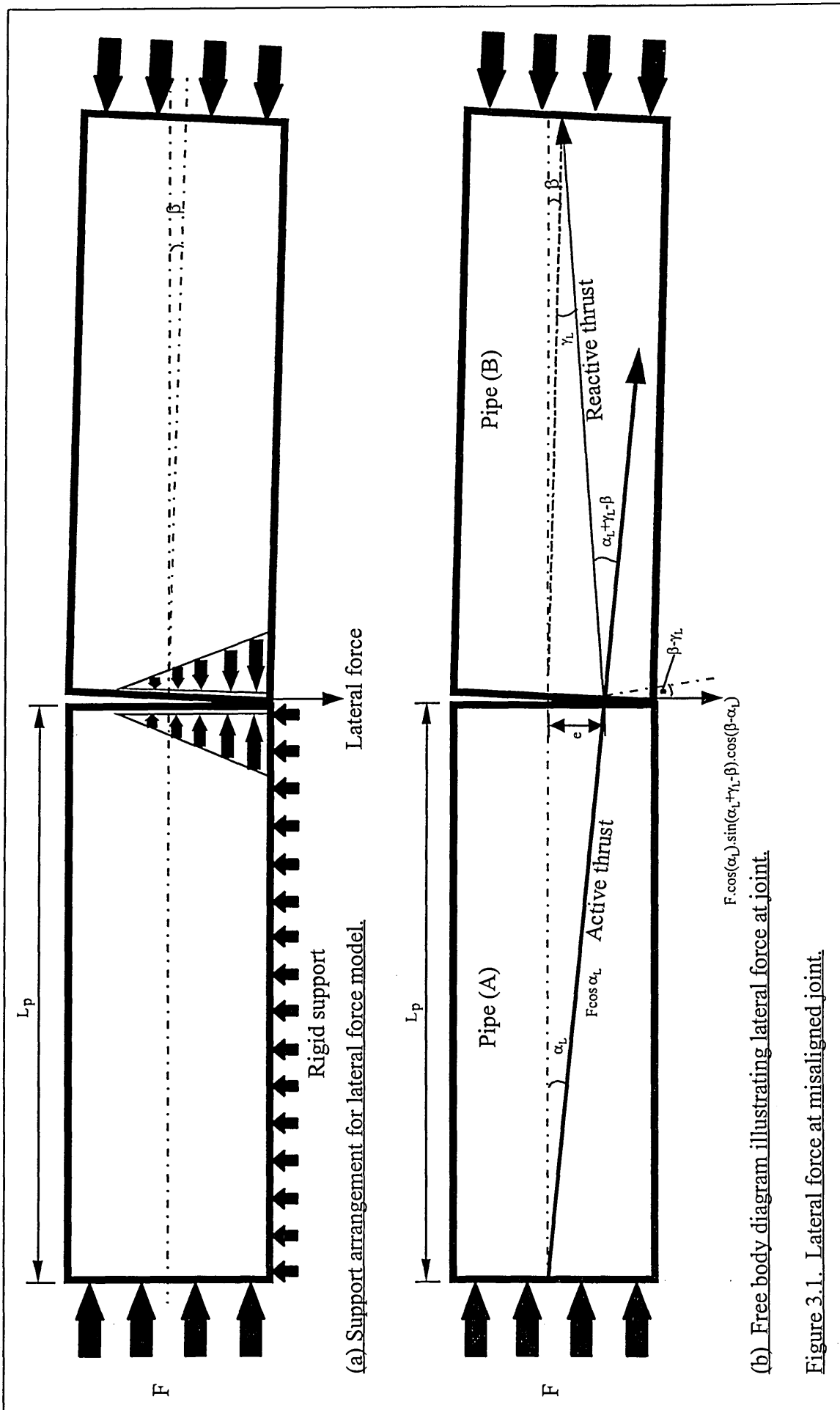
ANALYSIS OF LATERAL FORCE RESISTED BY COUPLING AT MISALIGNED JOINTS IN JACKED PIPELINES.

3.1. INTRODUCTION.

In order to derive a model for the prediction of principal stresses induced in the structural element of the coupling, a loading mechanism has to be established first.

The loading mechanism identified in this study takes the component of applied jacking force acting perpendicular to the pipe axis at a misaligned joint, when one of the pipes is rigidly supported by the surrounding soil and the subsequent pipe is free to act under the influence of the lateral force. Figure 3.1.(a) illustrates the general loading arrangement and Figure 3.1. (b) illustrates the free body forces acting at the misaligned joint. Figure 3.1.(b) has been simplified by assuming a straight line of action for the active thrust rather than the real case of a curved profile.

Ground conditions are typically variable and a pipe train passing through soils of differential stiffness would lead to the upper bound loading regime experienced by the coupling and this situation is used for the present study. A distinction is made between the joint when in a closed state, i.e. when all the packing ring is transferring load, and the joint in an open state (when a gap is formed between the packing ring and the adjacent pipe-end). Large angular misalignment at joints will



generally lead to the joint opening. Smaller misalignment can be accommodated by compression of the packing material and redistribution of jacking stresses. The angular misalignment at the joint will determine whether the joint is open or closed.

The lateral force at the joint is dependant on the relative eccentricities of jacking force in the local section of the pipe train. The determination of the eccentricity of jacking force is derived in the following sections for both closed and open joints.

With reference to Figure 3.1. (b), the lateral force acting at the joint on pipe B is derived by extending the line of acting of the force from pipe A and resolving relative to the reactive force. The line of action of the reactive force is defined by the relative eccentricities for pipe B. The resulting lateral force at the joint is defined by:-

$$H = F \cdot \sin(\alpha_L + \gamma_L - \beta) \cdot \cos(\beta - \alpha_L) \cdot \cos(\alpha_L) \quad (3.1)$$

The inclination of the jacking force α_L is simply given by equation 3.2. (below) and for the pipe alignment scenario illustrated by Figure 3.1(b) the inclination of the reactive force γ_L is also given by:-

$$\alpha_L = \gamma_L = \tan^{-1} \left(\frac{e}{L_p} \right) \quad (3.2)$$

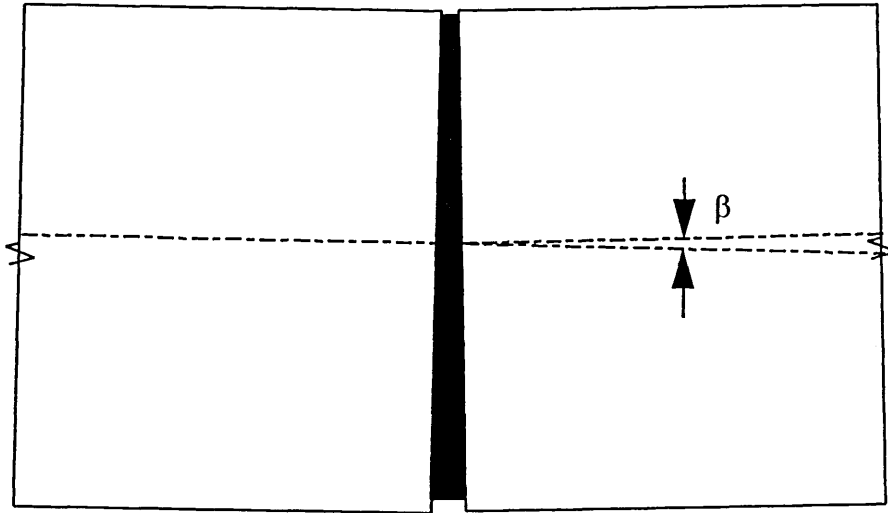
The aspect ratio of pipe length/diameter will influence the inclination of the jacking force through equation 3.2. Therefore longer pipes are desirable to reduce the inclination of jacking forces and resultant lateral forces acting on the coupling.

3.2. ANALYSIS OF CLOSED JOINTS.

As mentioned in 3.1., small angular deviations in line and level may be accommodated to some extent by compression of the packing material. The eccentricity of the jacking force due to the misalignment between the two opposite ends of the pipe will determine the inclination of the force relative to the pipe axis and the lateral force applied to the coupling. In order to calculate the inclination of the jacking force, the eccentricity at the pipe-ends has to be determined.

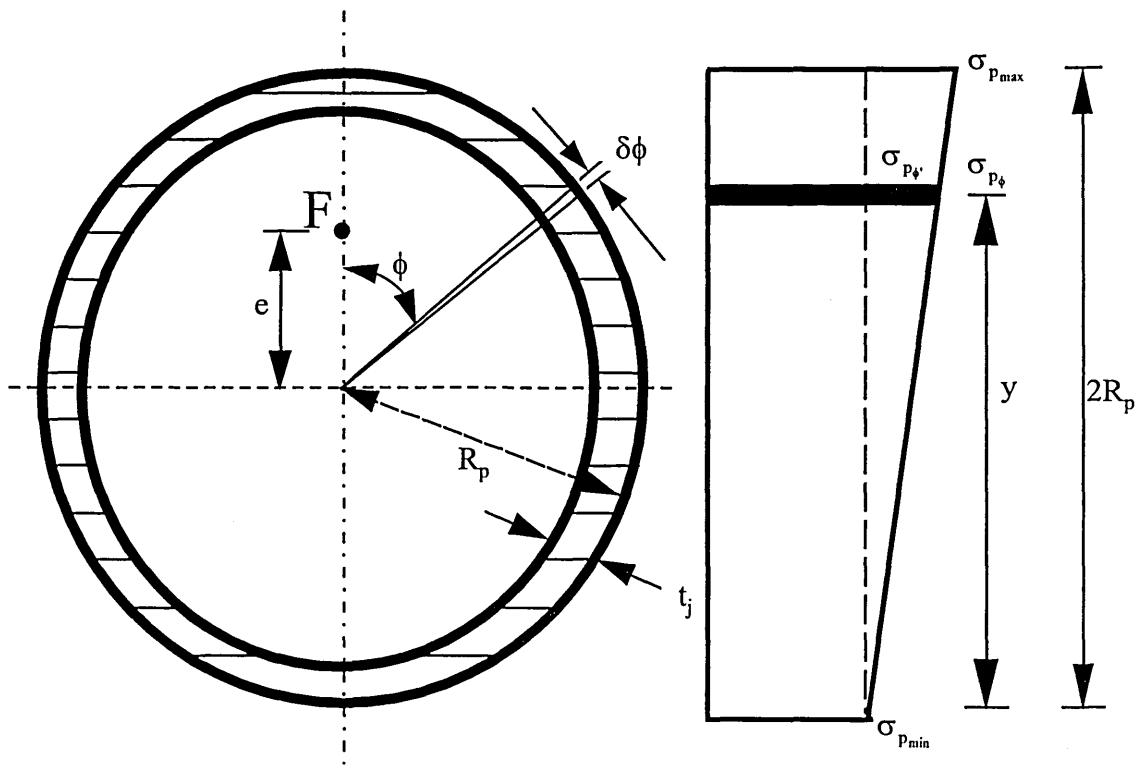
3.2.1. ECCENTRICITY OF JACKING FORCE AT A CLOSED JOINT.

The distribution of longitudinal jacking stresses at a closed joint is assumed to take a trapezoidal shape as illustrated in Figure 3.2. The justification for this assumption is made on the grounds that all the pipe wall is used to transfer jacking stresses due to its classification as closed. At the 'pivot' side of the joint, the jacking stress will be greatest with the opposite side of the joint under a lesser stress intensity. Therefore, trapezoidal distribution fits the physical considerations of the closed joint. The trapezoidal distribution has been shown to be applicable by Kanari et al [21].



Note:
Entire packing ring used to transfer longitudinal thrust.

(a) Closed joint.



(b) Eccentricity of jacking force at pipe/joint interface for closed joint.

Figure 3.2. Trapezoidal jacking stress distribution for closed misaligned joint.

With reference to Figure 3.2 (b) the derivation of the eccentricity for closed joints is based on the following relationships:-

$$y = R_p + R_p \cos\phi = R_p (1 + \cos\phi) \quad (3.3)$$

$$\frac{\sigma_{p_{max}} - \sigma_{p_{min}}}{2R_p} = \frac{\sigma_{p_\phi}}{y} \quad \text{from similar triangles.} \quad (3.4)$$

Therefore:-

$$\sigma_{p_\phi} = \frac{R_p (\sigma_{p_{max}} - \sigma_{p_{min}})(1 + \cos\phi)}{2R_p} \quad (3.5)$$

$$\text{From figure 3.2.(b)} \quad \sigma_{p_\phi} = \sigma_{p_{min}} + \sigma_{p_\phi} \quad (3.6)$$

Therefore σ_{p_ϕ} is explicitly defined by:-

$$\sigma_{p_\phi} = \frac{1}{2}(1 + \cos\phi)(\sigma_{p_{max}} - \sigma_{p_{min}}) + \sigma_{p_{min}} \quad (3.7)$$

By defining expressions for the total force and total moment acting on the pipe end, the eccentricity of the force can be deduced simply from the basic definition:-

$$e = \frac{M}{F} \quad (3.8)$$

3.2.1.1. TOTAL JACKING FORCE TRANSFERRED THROUGH CLOSED

JOINT.

The total jacking force at the closed misaligned joint is derived by summing the elemental components of force due to the assumed distribution of longitudinal jacking stresses over the range of available pipe cross-sectional area. The elemental force acting on pipe-end at angular position ϕ is given by:-

$$\delta F = \sigma_{p\phi} R_p t_j \cdot \delta\phi \quad (3.9)$$

The total force acting on pipe-end is give by solution to equation (3.10).

$$F = 2R_p t_j \int_0^\pi \left[\frac{1}{2}(1 + \cos\phi)(\sigma_{p_{\max}} - \sigma_{p_{\min}}) + \sigma_{p_{\min}} \right] \cdot d\phi \quad (3.10)$$

$$F = R_p t_j \pi (\sigma_{p_{\max}} + \sigma_{p_{\min}}) \quad (3.11)$$

3.2.1.2. TOTAL MOMENT ACTING AT A CLOSED JOINT.

The total moment acting on the pipe joint is derived by summing the product of the elemental force and its corresponding lever arm relative to the centroidal axis of the pipe over the range of available cross-sectional area. The elemental joint moment at position ϕ is given by equation 3.12:-

$$\delta M = \sigma_{p_j} R_p^2 t_j \cos \phi \cdot \delta \phi \quad (3.12)$$

The total moment at the closed joint is therefore the solution to equation 3.13.

$$M = 2R_p^2 t_j \int_0^\pi \cos \phi \left\{ \frac{1}{2}(1 + \cos \phi)(\sigma_{p_{\max}} - \sigma_{p_{\min}}) + \sigma_{p_{\min}} \right\} \cdot d\phi \quad (3.13)$$

$$M = \frac{R_p^2 t_j \pi}{2} (\sigma_{p_{\max}} - \sigma_{p_{\min}}) \quad (3.14)$$

From equation 3.8. $e = \frac{M}{F}$

Therefore substitution of equations 3.11. and 3.14. yields the eccentricity of the jacking force at the closed joint. Hence:-

$$e = \frac{R_p}{2} \left[\frac{\sigma_{p_{\max}} - \sigma_{p_{\min}}}{\sigma_{p_{\max}} + \sigma_{p_{\min}}} \right] \quad (3.15)$$

$$\frac{e}{R_p} = \frac{1}{2} \left[\frac{1-r}{1+r} \right] \quad (3.16)$$

Where $r = \frac{\sigma_{p_{\min}}}{\sigma_{p_{\max}}}$

The relationship between $\frac{e}{R_p}$ and r is illustrated in Figure 3.3.

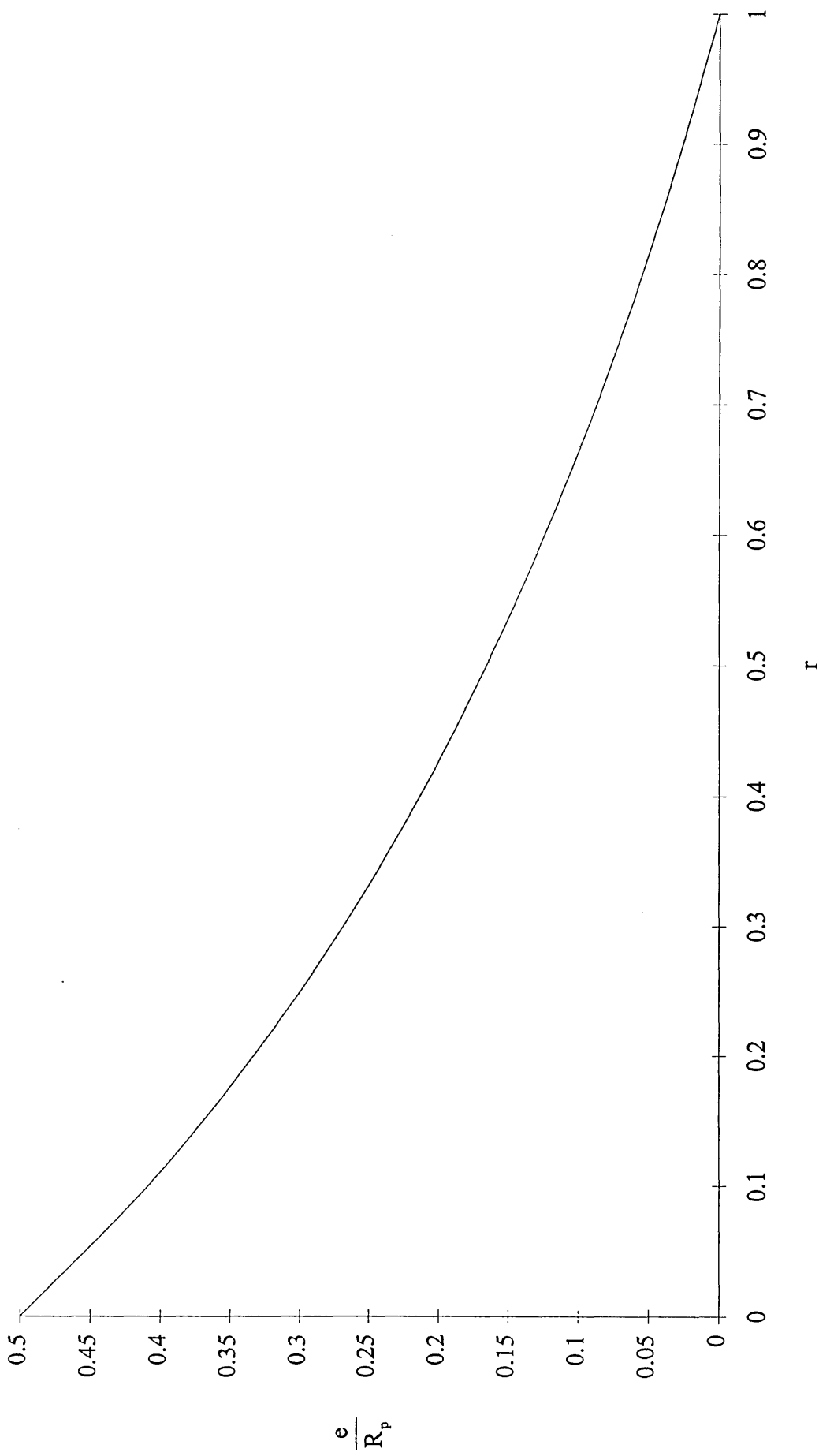


Figure 3.3. Relationship between r and the eccentricity of jacking force at a closed misaligned joint.

3.2.1.3. CONCLUSIONS.

The eccentricity of jacking force at a closed joint can be theoretically derived using equation 3.16. In practice the ratio of $\frac{\sigma_{p_{min}}}{\sigma_{p_{max}}}$ is required which is not quantifiable from the local jacking parameters (misalignment angle, jacking force, packing characteristics etc.).

The extreme values of $\frac{e}{R_p}$ for the closed joint as defined by equation 3.16. are as follows:-

1) When $\sigma_{p_{min}} = \sigma_{p_{max}}$ $\frac{e}{R_p} = 0$

2) When $\sigma_{p_{min}} = 0$ $\frac{e}{R_p} = 0.5$

Point (1) illustrates the case of axial loading where the pipes are perfectly aligned and the jacking stress distribution is uniform. Point (2) illustrates the case where the joint is about to open.

3.3. ANALYSIS OF OPEN JOINTS.

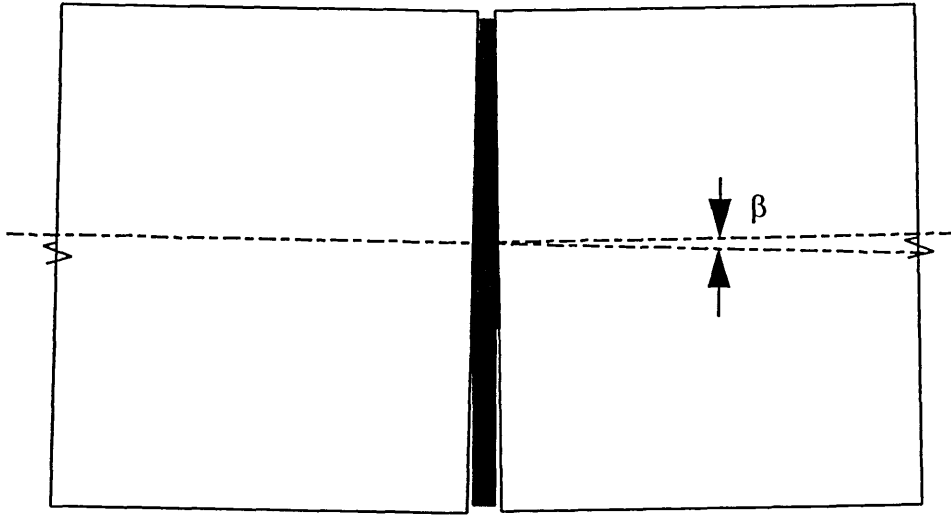
Open joints represent a much more severe loading regime on the pipe and on the coupling. The jacking force is transferred at the joint through a reduced cross sectional area and creates high stress concentrations in the pipe wall and the packing ring. The eccentricity of the jacking force at an open joint is located further from the centroidal axis of the pipe than for the closed joint case. This will have the effect of increasing the inclination of the jacking force from the pipe axis and therefore the lateral force.

As mentioned in 2.5, the distribution of jacking stresses at an open joint has been shown to be linear or approximately linear. For the theoretical analysis of the open joint a triangular stress distribution is assumed at the joint acting over the available pipe/packing area. The typical stress distribution considered for the open joint is illustrated in Figure 3.4. The same process was used to determine the eccentricity of the open joint as was for the closed case.

3.3.1. ECCENTRICITY OF JACKING FORCE AT AN OPEN JOINT.

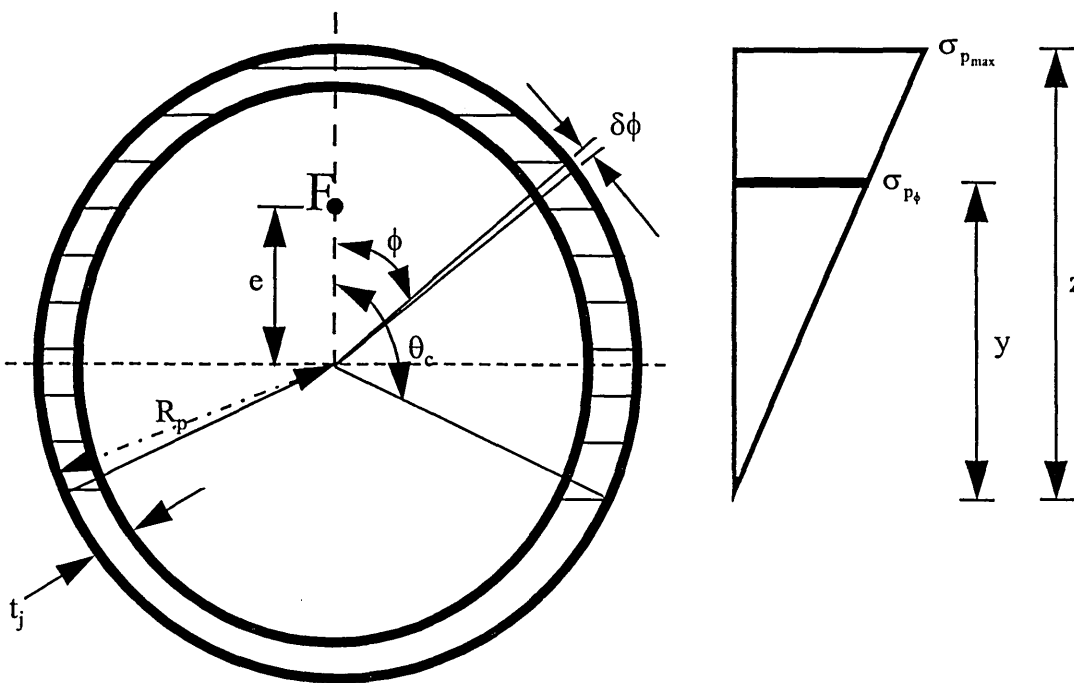
With reference to Figure 3.4. the derivation for the eccentricity for open joints is based on the following relationships:-

$$\sigma_{p\phi} = \sigma_{p_{max}} \cdot \frac{y}{z} \quad (3.17)$$



Note:
 Partial packing ring contact used to transfer longitudinal thrust.

(a) Open joint.



(b) Eccentricity of jacking force at pipe/joint interface for open joint.

Figure 3.4.: Triangular jacking stress distribution for open misaligned joint.

Where:-

$$y = R_p \cos\phi + R_p \sin\left(\theta_c - \frac{\pi}{2}\right) = R_p \left(\cos\phi + \sin\left(\theta_c - \frac{\pi}{2}\right) \right) \quad (3.18)$$

$$z = R_p + R_p \sin\left(\theta_c - \frac{\pi}{2}\right) = R_p \left(1 + \sin\left(\theta_c - \frac{\pi}{2}\right) \right) \quad (3.19)$$

Therefore:-

$$\sigma_{p\phi} = \frac{\sigma_{pmax} \left(\cos\phi + \sin\left(\theta_c - \frac{\pi}{2}\right) \right)}{1 + \sin\left(\theta_c - \frac{\pi}{2}\right)} \quad (3.20)$$

3.3.1.1. TOTAL JACKING FORCE TRANSFERRED THROUGH AN OPEN JOINT.

The total force at the joint is derived by summing the elemental components of force due to the assumed distribution of longitudinal jacking stresses over the range of available pipe cross-sectional. The elemental force acting on pipe end at angular position ϕ is given by:-

$$\delta F = \sigma_{p\phi} t_j R_p \delta\phi \quad (3.21)$$

The total force acting on the pipe end is given by solution to equation 3.22.

$$F = 2 \int_0^{\theta_c} \sigma_{p_s} t_j R_p \cdot d\phi \quad (3.22)$$

Substituting σ_{p_s} from equation 3.20. in equation 3.22. and solving gives:-

$$F = \frac{2R_p t_j \sigma_{p_{max}}}{1 + \sin\left(\theta_c - \frac{\pi}{2}\right)} \left[\sin\theta_c + \theta_c \sin\left(\theta_c - \frac{\pi}{2}\right) \right] \quad (3.23)$$

3.3.1.2. TOTAL JACKING MOMENT ACTING AT AN OPEN JOINT.

The total jacking moment acting on the pipe joint is derived by summing the product of the elemental force and its corresponding lever arm relative to the centroidal axis of the pipe over the range of available cross-sectional area. The elemental joint moment at position ϕ is given by:-

$$\delta M = \sigma_{p_s} R_p t_j d\phi \cdot R \cos\phi \quad (3.24)$$

The total moment at the pipe end is given by:-

$$M = 2R_p^2 t_j \int_0^{\theta_c} \sigma_{p_s} \cos\phi \cdot d\phi \quad (3.25)$$

Substituting σ_{p_s} from equation 3.20. into equation 3.25. and solving gives:-

$$M = \frac{2R_p^2 t_j \sigma_{pmax}}{1 + \sin\left(\theta_c - \frac{\pi}{2}\right)} \left[\frac{\theta_c}{2} + \frac{\sin 2\theta_c}{4} + \sin\theta_c \sin\left(\theta_c - \frac{\pi}{2}\right) \right] \quad (3.26)$$

and since, $e = \frac{M}{F}$

The substitution of equations 3.23. and 3.26. gives the eccentricity of the jacking force at the open joint as:-

$$e = R \left[\frac{\frac{\theta_c}{2} + \frac{\sin 2\theta_c}{4} + \sin\theta_c \sin\left(\theta_c - \frac{\pi}{2}\right)}{\sin\theta_c + \theta_c \sin\left(\theta_c - \frac{\pi}{2}\right)} \right] \quad (3.27)$$

The relationship between $\frac{e}{R_p}$ and θ_c is illustrated in figure 3.5.

3.3.1.3. CONCLUSIONS.

The eccentricity of jacking force at an open joint can be predicted by equation 3.27. with knowledge of the contact area at the joint (in terms of θ_c). The following extremes are noteworthy:-

1) When $\theta_c=0$ $\frac{e}{R_p}=1$

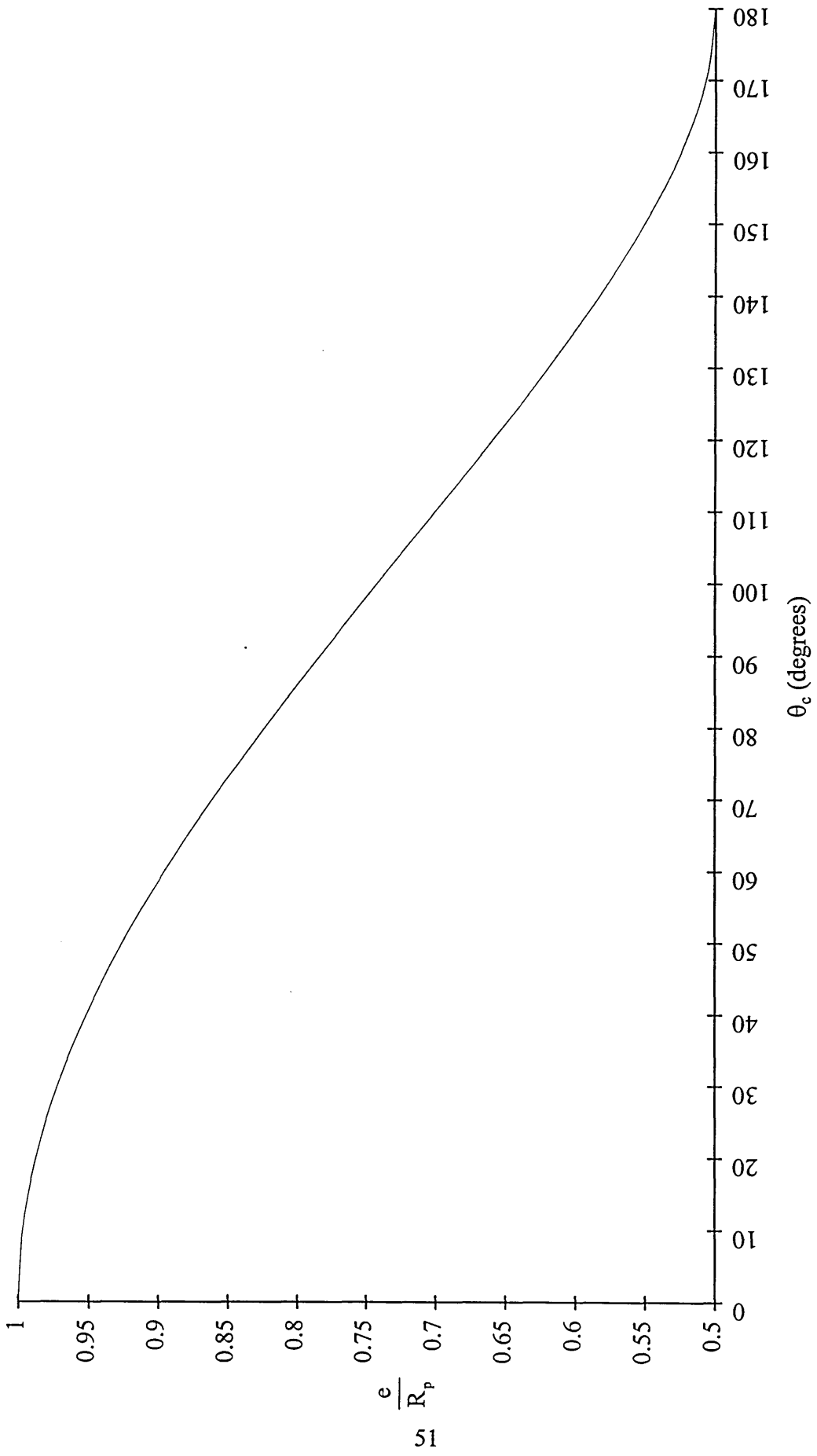


Figure 3.5. Relationship between θ_c and eccentricity of jacking force at an open misaligned joint.

2) when $\theta_c = \pi$ $\frac{e}{R_p} = 0.5$

Comparison between point (2) above and 3.2.1.3 point (2) show identical results for the case where the joint is about to open/close.

3.4. PREDICTION OF ECCENTRICITY FOR OPEN JOINTS BASED ON AUSTRALIAN LINEAR STRESS APPROACH.

The prediction of eccentricity for an open joint requires knowledge of the contact area at the interaction between the pipe-end and the packing material. The Australian Concrete Pipe Association Linear Stress Approach (ACPALSA) defines the contact zone in terms of the maximum stress in the pipe wall, the misalignment angle and packing characteristics (see 2.5.). This model has been modified to relate the local jacking parameters at the displaced joint with the defining contact area angle (θ_c).

From the open joint model, the total jacking force is defined by equation 3.23., repeated here as:-

$$F = \frac{2R_p t_j \sigma_{pmax}}{1 + \sin\left(\theta_c - \frac{\pi}{2}\right)} \left[\sin\theta_c + \theta_c \sin\left(\theta_c - \frac{\pi}{2}\right) \right]$$

From 2.5., the ACPALSA defines the misalignment angle β as:-

$$\beta = \frac{180a\sigma_{p_{max}}}{\pi E_j z} \quad (2.6. \text{ repeated})$$

$$\text{Where } E_j = \frac{at_w E_p E_c}{at_w E_c + L_p t_j E_p} \quad (2.7. \text{ repeated})$$

$$\text{and } z = R_p \left[1 + \sin\left(\theta_c - \frac{\pi}{2}\right) \right] \quad (3.19. \text{ repeated})$$

Rearranging equation 2.6. and substituting equation 3.19. yields the maximum stress at the open joint at a distance R_p from the centreline of the pipe as:-

$$\sigma_{p_{max}} = \frac{\pi \beta E_j R_p \left[1 + \sin\left(\theta_c - \frac{\pi}{2}\right) \right]}{180a} \quad (3.28)$$

Substituting 3.28. into 3.23. yields the total jacking force at the open joint in terms of all the relevant parameters given as:-

$$F = \frac{2R_p^2 t_j \beta E_j \pi}{180a} \left[\sin \theta_c + \theta_c \sin\left(\theta_c - \frac{\pi}{2}\right) \right] \quad (3.29)$$

Rearranging equation 3.29. yields the definition of the contact zone for an open joint in terms of the local jacking parameters as follows:-

$$\frac{90Fa}{R_p^2 t_j \pi \beta E_j} = \sin \theta_c + \theta_c \sin \left(\theta_c - \frac{\pi}{2} \right) \quad (3.30)$$

The parameters on the left hand side of 3.30. are known or assumed, leaving a theoretical function of θ_c which defines the contact zone of the joint.

$$\text{Let } m = \frac{90\eta Fa}{R_p^2 t_j E_j \beta \pi}$$

Where η is a empirical coefficient characterising the packing ring material (see 7.2).

$$\text{Therefore, } m = \sin \theta_c + \theta_c \sin \left(\theta_c - \frac{\pi}{2} \right)$$

A plot of the above equation is illustrated in Figure 3.6.

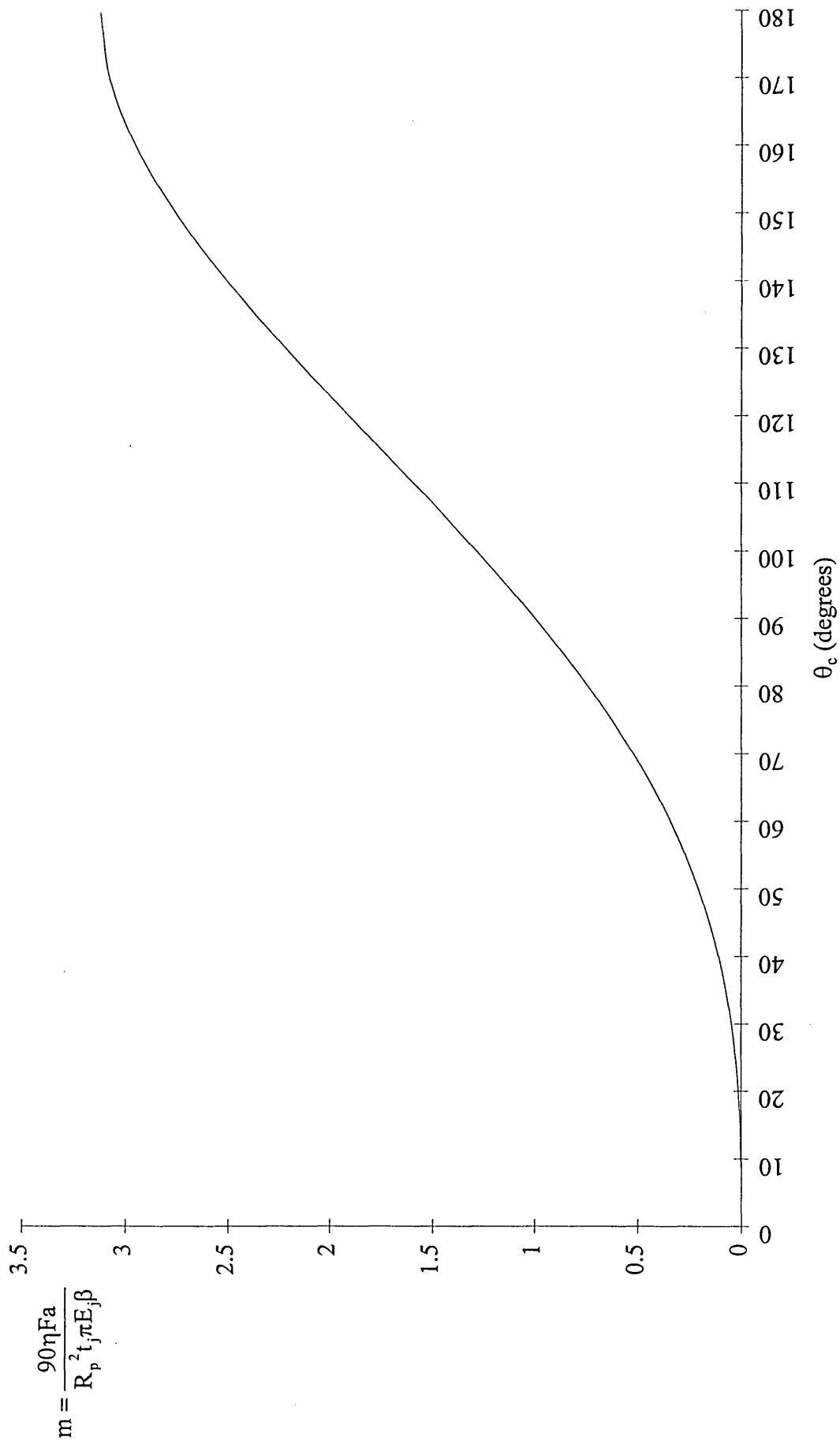


Figure 3.6.: Relationship between m and θ_c for the prediction of pipe-packing-pipe interaction at an open misaligned joint.

3.5. MAIN CONCLUSIONS.

The following conclusions may be drawn from the theoretical analysis of the structural interaction of misaligned joints:-

- 1) The eccentricity of the jacking force at pipe joints due to angular deviations in the pipeline alignment will cause localised stress peaks in the pipe wall and induce lateral forces on the coupling. The eccentricity of the jacking force is derived for closed joints and open joints and is given by equations 3.16. and 3.27. respectively.

- 2) Figures 3.3. and 3.5. can be used to determine the eccentricity of jacking force relative to the centroidal axis of the pipe joint for closed and open joints respectively. The maximum eccentricity possible for the closed joint being $R_p/2$ where the joint is about to open. The minimum eccentricity being zero where the jacking load is evenly distributed around the annulus of the pipe joint.

- 3) The maximum eccentricity for an open joint being the radius of the pipe for the case of point load contact between pipe-packing-pipe with an infinitely rigid packing material. This is unlikely to occur in practice due to the use of compressible packing rings. The minimum eccentricity for an open joint being $R_p/2$ where the joint is about to close. This scenario is also verified using the closed joint analysis where the joint is about to open.

- 4) The prediction of pipe-packing-pipe contact area used for jacking force transfer for the open joint model can be deduced from Figure 3.6. (modified for the properties of the packing material - see chapter 7).

- 5) The case of the open joint leads to a more critical situation because the eccentricity of jacking force is located outside the core of the cross section thereby increasing the lateral force on the coupling as described by equation 3.1. and 3.2.

- 6) The aspect ratio of the pipe will influence the magnitude of the misaligned lateral force through equation 3.2. Long pipes will reduce the inclination of misaligned jacking force and further reduce the magnitude of any lateral force acting on the coupling.

CHAPTER 4

MATHEMATICAL MODEL FOR THE PREDICTION OF PRINCIPAL TENSILE STRESSES INDUCED IN THE STRUCTURAL ELEMENT OF LOOSE SLEEVED JACKING PIPE COUPLINGS.

4.1. INTRODUCTION.

The formulation of a mathematical model for the prediction of principal tensile stresses induced in the structural element a loose sleeved coupling system is based on the lateral force model for closed and open joints, presented in chapter 3. The methodology used to formulate a mathematical model is outlined in Figure 4.1.

In the absence of published material concerning the pipe-packing-coupling interaction, the concept of a pipe loading mechanism on the coupling was assumed and verified by experiment. This chapter identifies the structural interaction of the pipe-coupling system and derives equations for the prediction of principal tensile stresses induced in the coupling during installation.

Symmetry of the coupling profile and loading enables the analysis to be simplified by considering half of the coupling only in the mathematical analysis and the experimental investigation.

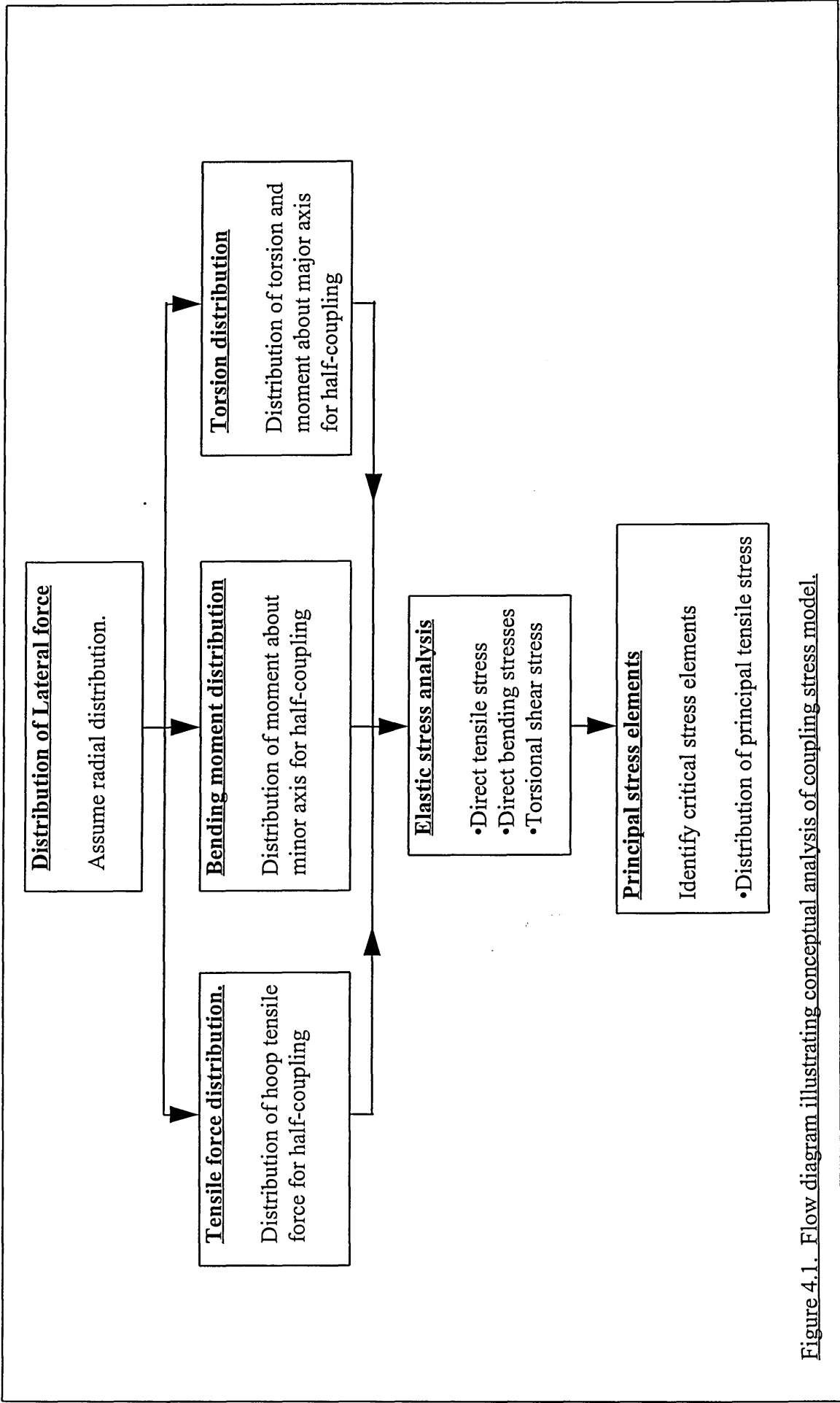


Figure 4.1. Flow diagram illustrating conceptual analysis of coupling stress model.

4.2. STRUCTURAL INTERACTION OF PIPE-COUPLING SYSTEM.

4.2.1. LOAD SHARING BETWEEN STRUCTURAL ELEMENT OF COUPLING AND FRICTIONAL RESISTANCE OF PIPE-PACKING INTERFACE.

When constrained by the structural element of the coupling, the lateral force induced as a result of misalignment will tend to cause the pipe spigots to react against the coupling in equal but opposite directions due to the shear effect of the loading.

The presence of a compressible rubber sealing element facilitates load sharing between the pipe-packing interface friction and the coupling. Hence:-

$$H_c = \rho H \quad (4.1)$$

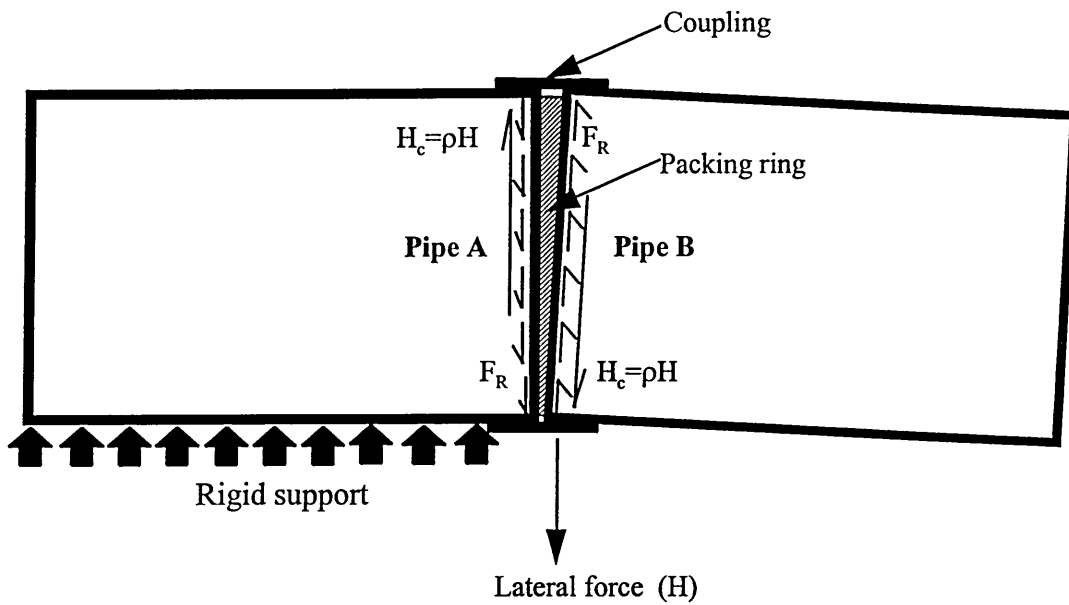
Where:-

H = Lateral force due to misalignment at joint,

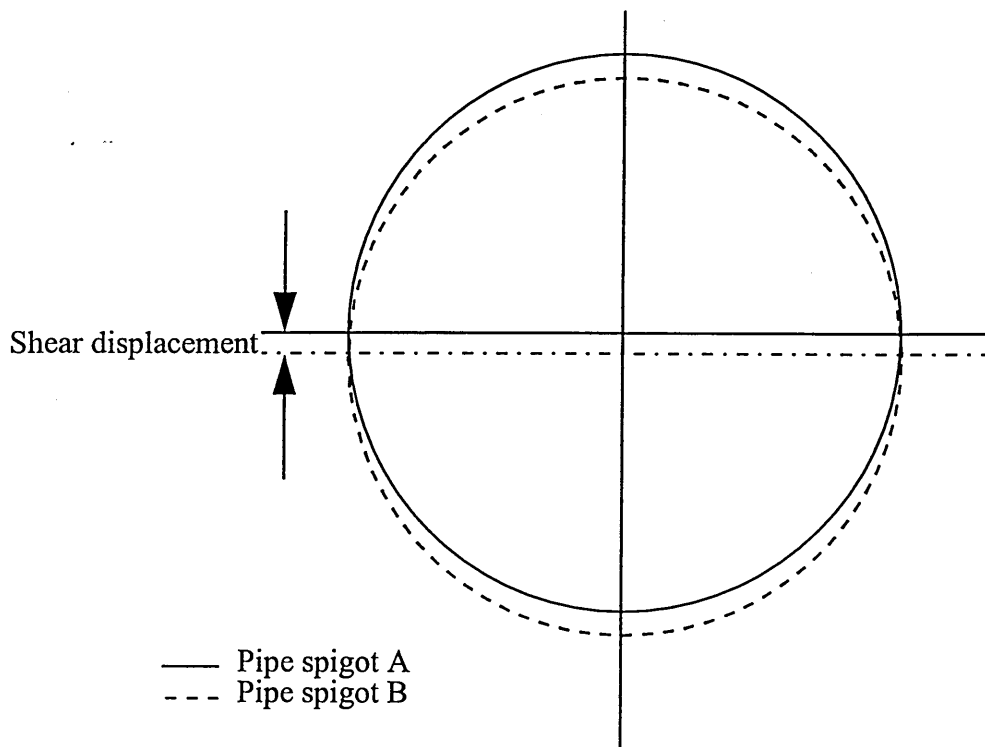
and H_c = Lateral force resisted by structural element of coupling.

and ρ = Coefficient, defining share of lateral force resisted by coupling.

The presence of compressible rubber between the pipe spigot and the metal ring allows the packing material to shear, thereby mobilising frictional resistance between the packing material and the pipe-end (Figure 4.2). Under high lateral loads the shear



(a): Resultant lateral force resisted by coupling/packing system.



(b) Relative shear displacement of pipe spigots facilitated by rubber seal element.

Figure 4.2: Load sharing of pipe-packing-coupling system under installation conditions.

deformation of the packing material will be greatest, therefore the value of ρ maybe dependent on the lateral force induced across the joint.

4.2.2. INTERNAL RADIAL PRESSURE DISTRIBUTION EXERTED ON COUPLING DUE TO LATERAL FORCE AT A MISALIGNED JOINT.

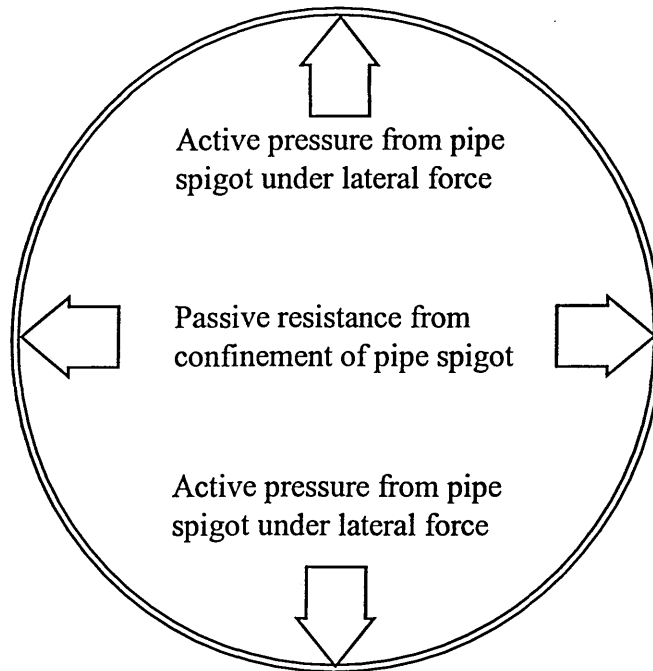
Under the action of a lateral force at a misaligned joint, relative displacement of the two pipe spigots is facilitated by the presence of the compressible rubber seal element. With reference to Figure 4.3(a), the active pressure at the crown will induce passive resistance at the springing due to the confined nature of the system. Therefore, the assumed deformation of the coupling profile under the shear loading described in chapter 3 is illustrated in Figure 4.3 (b). The compressible rubber seal allows inward deformation at the springing and outward deformation at the crown. With reference to Figure 4.4. the internal radial pressure distribution exerted on the coupling used in this study is given by:-

$$p = \lambda(1 + \varphi \cos\theta) \quad (4.2)$$

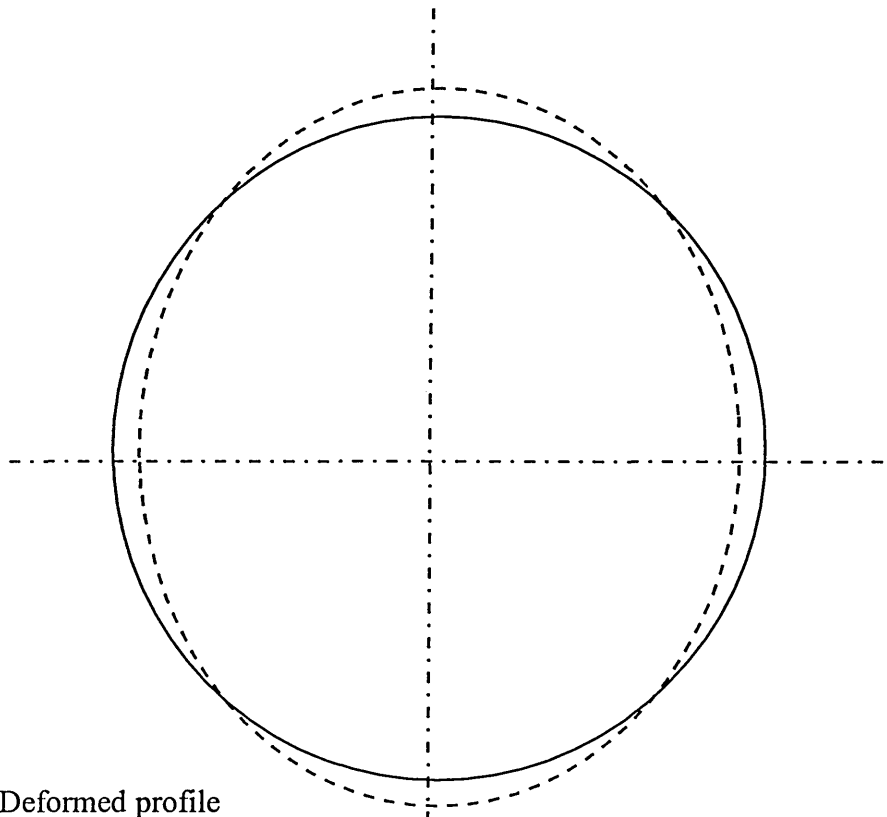
The lateral force resisted by the coupling is distributed radially around each half-coupling. The magnitude of λ is determined from consideration of static equilibrium.

With reference to Figure 4.4, the radial pressure is defined as:-

$$\frac{H_c}{2} = \int_0^{\frac{\pi}{2}} [\lambda(1 + \varphi \cos\theta)] \cos\theta . R . d\theta \quad (4.3)$$



(a) Conceptual analysis of internal radial pressure exerted on coupling under lateral force.



(b) Deformed profile of coupling under lateral force due to presence of compressible rubber seal.

Figure 4.3. Conceptual analysis of coupling under shear loading.

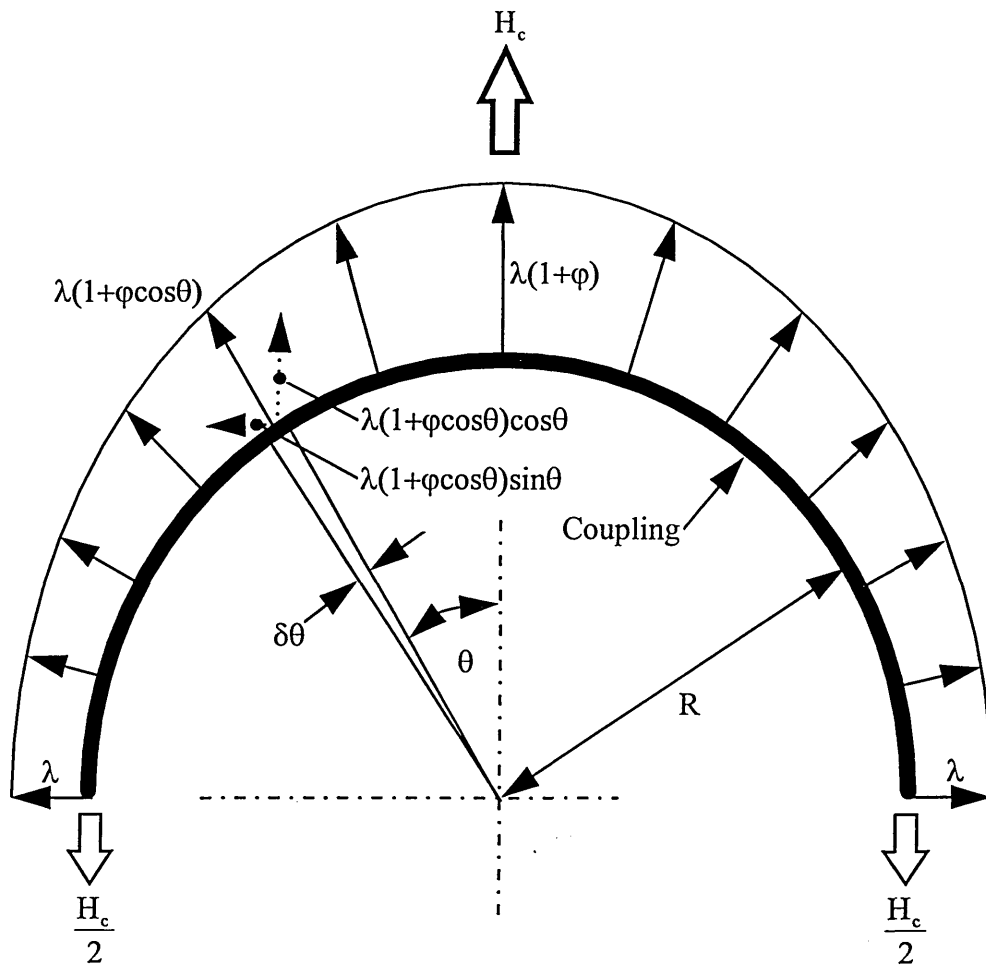


Figure 4.4. Internal radial pressure exerted on coupling ring.

Therefore:-

$$\lambda = \frac{2H_c}{R(\pi\phi + 4)} \quad (4.4)$$

4.3. ANALYSIS OF COUPLING LOADING MECHANISMS.

The conceptual analysis of the coupling system identified several loading mechanisms which were investigated for the internal radial pressure distribution exerted on the coupling. The following were investigated in detail:-

- 1) Tension distribution induced in coupling ring.
- 2) Bending distribution about minor axis of member induced in coupling ring.
- 3) Bending distribution about major axis of member induced in coupling ring.
- 4) Torsion distribution induced in coupling ring.

4.4. TENSION DISTRIBUTION INDUCED IN COUPLING DUE TO INTERNAL RADIAL PRESSURE.

With reference to Figure 4.5. the following derivation is made for the distribution of hoop tension induced in the ring as a result of internal radial pressure.

For static equilibrium:-

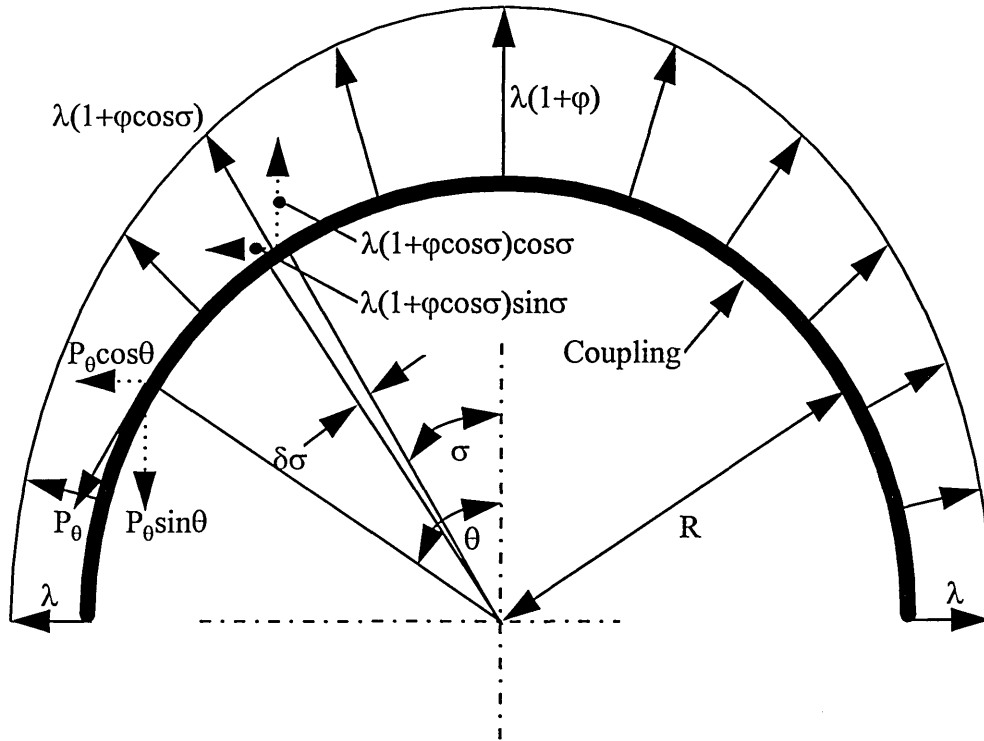


Figure 4.5. Tensile force induced in coupling ring due to internal radial pressure distribution.

$$2P_0 \sin \theta = 2 \int_0^{\theta} [\lambda(1 + \varphi \cos \sigma)] \cos \sigma \cdot R \cdot d\sigma \quad (4.5)$$

Substitution of λ from equation 4.4. gives the tension distribution as:-

$$P_\theta = \frac{H_c}{\pi\varphi + 4} \left[\varphi \cos \theta + \frac{\varphi\theta}{\sin \theta} + 2 \right] \quad (4.6)$$

4.5. BENDING DISTRIBUTION ABOUT MINOR MEMBER AXIS DUE TO INTERNAL RADIAL PRESSURE.

The internal radial pressure exerted on the coupling ring will cause the ring to deform as illustrated in Figure 4.3 (b). The non-uniform loading will induce bending about the minor axis. The distribution of bending moment is derived from consideration of static equilibrium.

With reference to Figure 4.6. the following expression for the bending moment at position θ is defined. Positive bending is assumed to cause tension on the inside fibres of the ring.

$$M_{m\theta} = M_{m0} - \frac{H_c R}{2} (1 - \sin \theta) + \int_0^{\frac{\pi}{2}-\theta} [\lambda(1 + \varphi \sin \sigma)] [\cos \theta - \sin \sigma] \cos \sigma \cdot R^2 \cdot d\sigma \quad (4.7)$$

$$+ \int_0^{\frac{\pi}{2}-\theta} [\lambda(1 + \varphi \sin \sigma)] [\cos \sigma - \sin \theta] \sin \sigma \cdot R^2 \cdot d\sigma$$

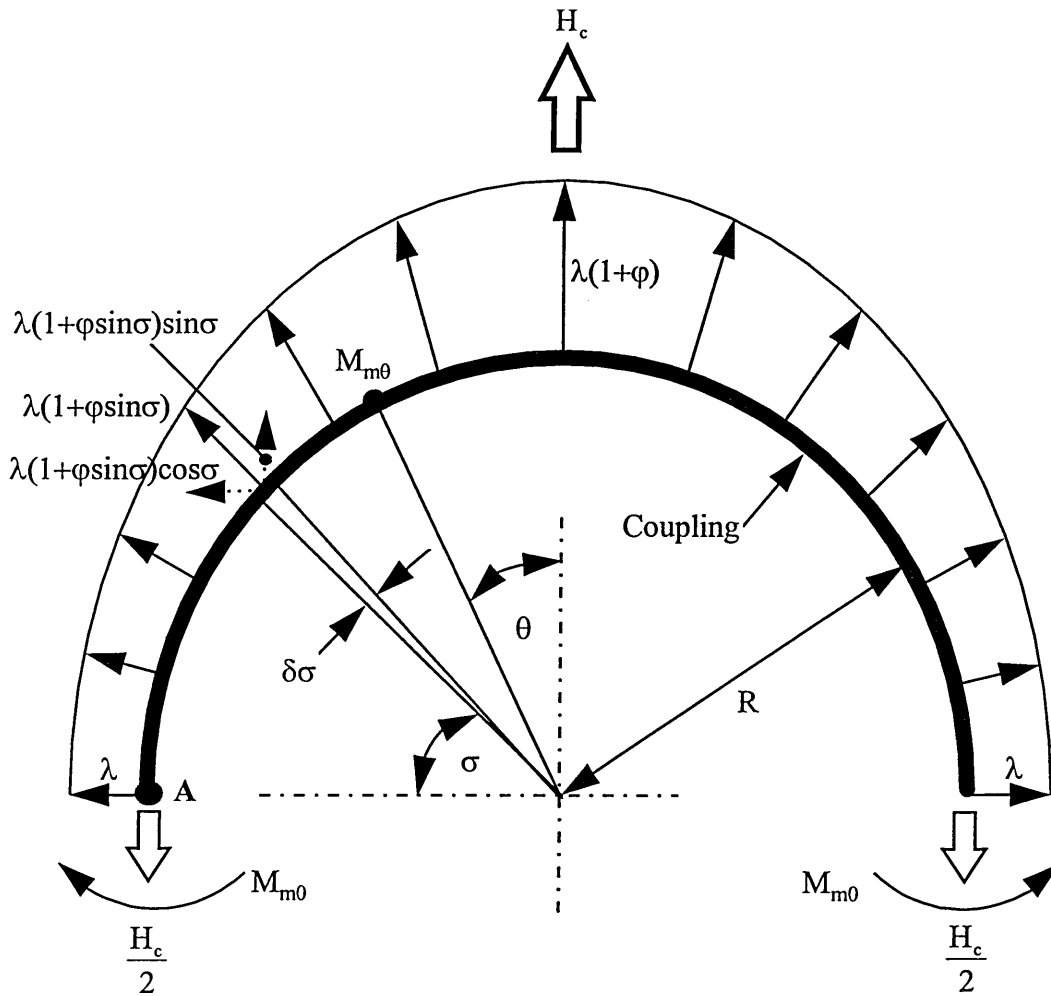


Figure 4.6. Bending moment about minor axis of coupling due to internal radial pressure distribution.

The reactive moment M_{m0} is found by applying Castigliano's second theorem [24] and noting that the angular rotation at Point A (Figure 4.6.) is zero on account of symmetrical loading.

Therefore:-

$$\Psi_{mA} = \frac{\partial U}{\partial M_{m0}} = 2 \int_0^{\frac{\pi}{2}} \frac{M_{m\theta}}{EI} \cdot \frac{\partial M_{m\theta}}{\partial M_{m0}} \cdot R \cdot d\theta = 0 \quad (4.8)$$

From equation 4.7.

$$\frac{\partial M_{m\theta}}{\partial M_{m0}} = 1 \quad (4.9)$$

Therefore the solution to equation 4.8. gives:-

$$M_{m0} = \frac{H_c R \phi}{2\pi} \left[\frac{\pi^2 - 8}{\pi\phi + 4} \right] \quad (4.10)$$

Substituting equations 4.4. and 4.10. into equation 4.7. gives:-

$$M_{m\theta} = H_c R \left[\frac{\phi(\pi \cos\theta + \pi\theta \sin\theta - 4)}{\pi(\pi\phi + 4)} \right] \quad (4.11)$$

4.6. TORSION / BENDING DISTRIBUTION INDUCED IN COUPLING DUE TO INTERNAL RADIAL PRESSURE.

The radially distributed force resisted by the half-coupling acts eccentrically about the longitudinal axis of the member due to the relative movement of the pipe spigots under shear loading. The resulting torsion is illustrated vectorially in Figure 4.7. The internal pressure is assumed to act over half the width of the coupling member therefore the lever arm for the force is $b/4$, where b is the width of the member.

The torque per unit length of coupling is given by:-

$$t_o = [\lambda(1 + \phi \sin \sigma)] \frac{b}{4} \text{ per unit length} \quad (4.12)$$

The applied torsion acting about the longitudinal axis of the coupling section is represented in Figure 4.7. by the vector acting tangentially to the coupling profile. The applied torque also induces bending to the section due to its component in the radial direction.

For equilibrium of the half-coupling, reactive torque's and moments are assumed at the boundary. These are represented by the vectors T_o and M_o respectively in the Figure.

In order to obtain the distribution of torsion and bending around the circumference of the half-coupling, equations of equilibrium are set up for the system.

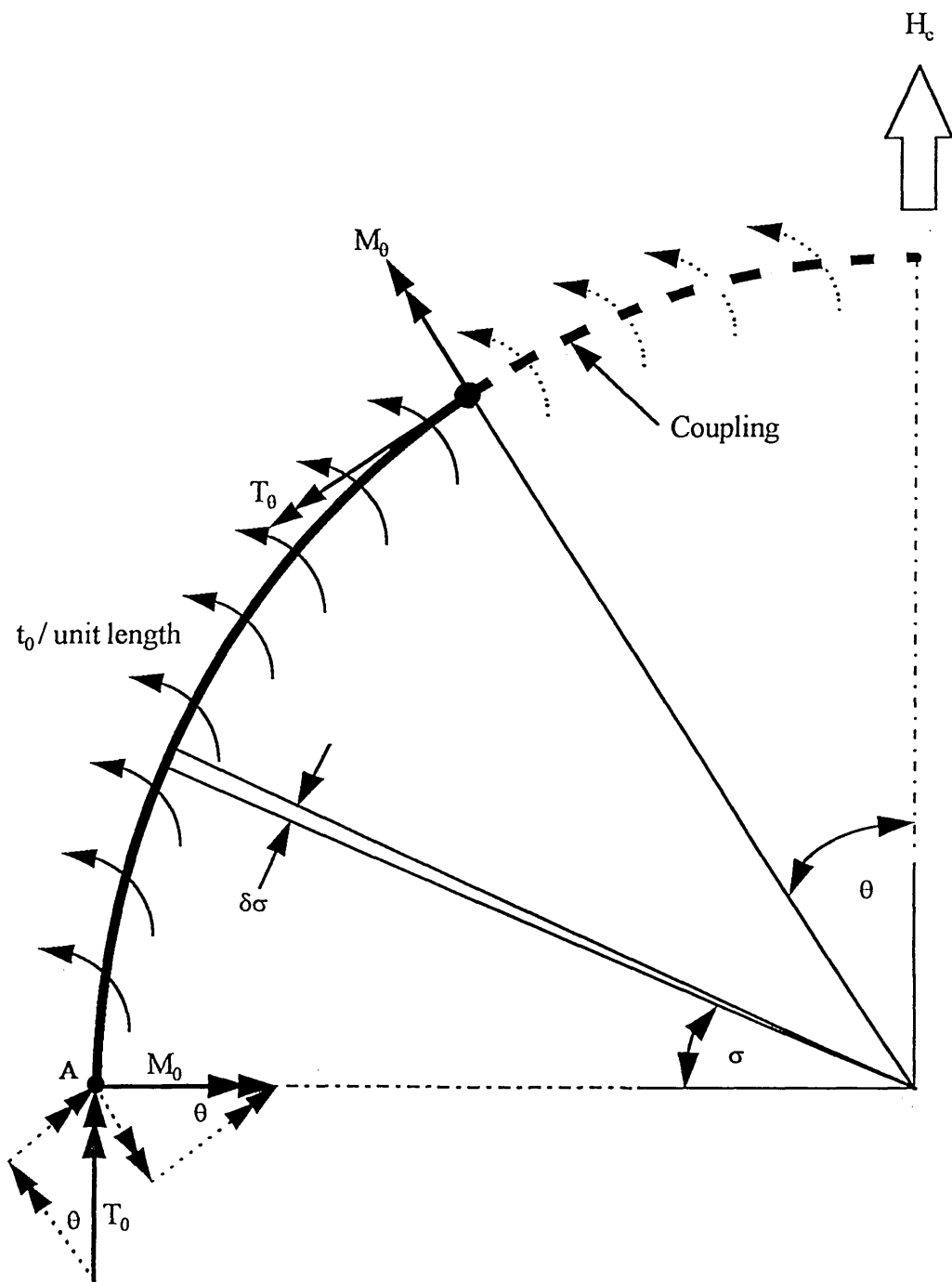


Figure 4.7. Vector free body diagram of quarter-coupling illustrating reactions at boundary (A), and applied loading.

With reference to Figure 4.7. the following equations of equilibrium are defined.

Resolving all vectors in the radial direction leads to:-

$$T_{\theta} = T_0 \sin \theta + M_0 \cos \theta + \int_0^{\frac{\pi}{2}-\theta} t_0 \cos\left(\frac{\pi}{2} - \theta - \sigma\right).R.d\sigma \quad (4.13)$$

Therefore:-

$$T_{\theta} = T_0 \sin \theta + M_0 \cos \theta + \frac{bR}{16} [\pi\phi - 2(\phi\theta - 2)] \cos \theta \quad (4.14)$$

Resolving all vectors in the tangential direction leads to:-

$$M_{\theta} = -T_0 \cos \theta + M_0 \sin \theta - \int_0^{\frac{\pi}{2}-\theta} t_0 \sin\left(\frac{\pi}{2} - \theta - \sigma\right).R.d\sigma \quad (4.15)$$

Therefore:-

$$M_{\theta} = -T_0 \cos \theta + M_0 \sin \theta - \frac{b\lambda R}{16} [2\phi \cos \theta + \{2(\phi\theta - 2) - \pi\phi\} \sin \theta + 4\lambda] \quad (4.16)$$

The derivations for the reactive torque's and moments, T_0 and M_0 are made using Castigliano's second theorem [24] noting that the angular twist (ϕ_A) and rotation (ψ_A) at the boundary (Point A, Figure 4.7.) are zero due to the symmetry of the radial pressure distribution.

Therefore:-

$$\phi_A = \frac{\partial U}{\partial T_0} = 2 \int_0^{\frac{\pi}{2}} \frac{T_{\theta}}{GJ} \cdot \frac{\partial T_{\theta}}{\partial T_0} \cdot R.d\theta + 2 \int_0^{\frac{\pi}{2}} \frac{M_{\theta}}{EI} \cdot \frac{\partial M_{\theta}}{\partial T_0} \cdot R.d\theta = 0 \quad (4.17)$$

$$\psi_A = \frac{\partial U}{\partial M_0} = 2 \int_0^{\frac{\pi}{2}} \frac{T_\theta}{GJ} \cdot \frac{\partial T_\theta}{\partial M_0} \cdot R \cdot d\theta + 2 \int_0^{\frac{\pi}{2}} \frac{M_\theta}{EI} \cdot \frac{\partial M_\theta}{\partial M_0} \cdot R \cdot d\theta = 0 \quad (4.18)$$

The geometric and mechanical properties of the coupling section are grouped as:-

$$\mu = \frac{EI}{GJ} \quad (4.19)$$

From equation 4.14. the partial derivatives with respect to torsion are:-

$$\frac{\partial T_\theta}{\partial T_0} = \sin \theta \quad (4.20)$$

$$\frac{\partial T_\theta}{\partial M_0} = \cos \theta \quad (4.21)$$

From equation 4.16. the partial derivatives with respect to bending are:-

$$\frac{\partial M_\theta}{\partial T_0} = -\cos \theta \quad (4.22)$$

$$\frac{\partial M_\theta}{\partial M_0} = \sin \theta \quad (4.23)$$

Therefore, solving equations 4.17. and 4.18. simultaneously gives the reactive torque and moment as:-

$$T_0 = \frac{bR\lambda[\pi^2\varphi(\mu+1) + 8\pi(\mu+1) + 2(\mu-1)\{\varphi(\mu-3) - 8\}]}{8[4(\mu-1)^2 - \pi^2(\mu+1)^2]} \quad (4.24)$$

$$M_0 = \frac{bR\lambda(\mu+1)[\pi^3\varphi(\mu+1) + 8\pi^2(\mu+1) - 8\pi(\varphi+4) + 32(\mu-1)]}{32[4(\mu-1)^2 - \pi^2(\mu+1)^2]} \quad (4.25)$$

Substituting equations 4.4., 4.24. and 4.25. in equation 4.14. and simplifying gives the distribution of torsion due to internal radial pressure as:-

$$T_\theta = \left\{ \frac{H_c b}{16(\pi\varphi+4)[\pi^2(\mu+1)^2 - 4(\mu-1)^2]} \right\} \left\{ \begin{array}{l} \cos\theta \left[\begin{array}{l} \pi^3\varphi(\mu+1)^2 - 4\pi^2\varphi\theta(\mu+1)^2 + 8\pi(4(\mu+1)) \\ -\varphi\mu(\mu-3) + 16(\mu-1)(\varphi\theta(\mu-1)+4) \end{array} \right] \\ -4\sin\theta [\pi^2\varphi(\mu+1) + 8\pi(\mu+1) + 2(1-\mu)(\varphi(\mu-3) - 8)] \end{array} \right\} \quad \dots(4.26)$$

Similarly for the bending about the major axis of the member, substitution of equations 4.4., 4.24 and 4.25. in equation 4.16. gives:-

$$M_\theta = \left\{ \frac{H_c b}{16(\pi\varphi+4)[4(\mu-1)^2 - \pi^2(\mu+1)^2]} \right\} \left\{ \begin{array}{l} 4\cos\theta [\pi^2\varphi\mu(\mu+1) - 8\pi(\mu+1) + 2(1-\mu)(\varphi(\mu+1) + 8)] \\ -\sin\theta \left[\begin{array}{l} \pi^3\varphi(\mu+1)^2 - 4\pi\varphi\theta(\mu+1)^2 + 8\pi(4(\mu+1)) \\ -\varphi\mu(\mu-3) + 16(\mu-1)(\varphi\theta(\mu-1)+4) \end{array} \right] \\ +8[\pi^2(\mu+1)^2 - 4(\mu-1)^2] \end{array} \right\} \quad \dots(4.27)$$

4.7. GEOMETRIC AND MECHANICAL PROPERTIES OF COUPLING MEMBER.

The parameter μ is introduced in equation 4.19. to group the mechanical and geometrical properties of the coupling section for convenience. The parameters which define μ are the second moment of area for the section, the elastic modulus of the material, the shear modulus of the material and the torsional constant for the section.

These parameters are summarised below:-

$$I = \frac{b^3 t}{12} \quad (4.28)$$

$$G = \frac{E}{2(1 + \nu)} \quad (4.29)$$

$$J = \frac{bt^3}{3} \quad (4.30)$$

Substitution of the above equations in equation 4.19. gives:-

$$\mu = \frac{b^2(1 + \nu)}{2t^2} \quad (4.31)$$

Table 4.1. gives of values of μ for typical coupling section sizes in stainless steel.

Section	b (mm)	t (mm)	μ
2 x 127	127	2	2620
3 x 150	150	3	1625
5 x 150	150	5	585

Table 4.1. Typical range of values for μ for coupling section sizes.

From equation 4.26. the torsion is dependant on the value of μ . Large values of μ are derived from relatively slender coupling sections which in turn induce a greater torsional shear stress.

4.8. ELASTIC STRESS ANALYSIS OF COUPLING UNDER INSTALLATION CONDITIONS.

In order to assess the coupling width to thickness ratio, the model is transformed from loads to stresses. Elastic theories of structural mechanics were used to derive two dimensional plane stress elements, which in turn were transformed to principal stress elements for critically stressed locations.

4.8.1. HOOP TENSILE STRESS DISTRIBUTION FOR COUPLING.

The hoop tensile stress for a two dimensional stress element is derived from the hoop tensile force and is given by:-

$$\sigma_T = \frac{P_\theta}{bt} \quad (4.32)$$

4.8.2. BENDING STRESS DISTRIBUTION ABOUT MINOR MEMBER AXIS OF COUPLING.

The bending stress acting on a two dimensional stress element is derived from the external moment ($M_{m\theta}$) using simple theory of flexural bending about the y-y axis of the member. Therefore the bending stress about the minor coupling axis is given by:-

$$\sigma_m = \frac{M_{m\theta}t}{2I} = \frac{6M_{m\theta}}{bt^2} \quad (4.33)$$

4.8.3. BENDING STRESS DISTRIBUTION ABOUT MAJOR MEMBER AXIS OF COUPLING.

The bending stress acting on a two dimensional stress element is derived from the external moment (M_θ) using simple theory of flexural bending about the x-x axis of the member.

The bending stress is given by:-

$$\sigma_B = \frac{M_\theta b}{2I} = \frac{6M_\theta}{b^2 t} \quad (4.34)$$

4.8.4. TORSIONAL SHEAR STRESS DISTRIBUTION FOR COUPLING MEMBER.

The solid rectangular coupling member is torsionally loaded as described by equation 4.26. The resulting shear stress acting on a two-dimensional plane stress element is derived using Timoshenko's theory of elasticity for flat bars under torsion [25]. The stress function for this case is given by equation 4.35. (below).

With reference to figure 4.8., the following stress function is defined:-

$$\omega = \frac{8T_\theta}{\pi^3 k_1 b t} \sum_{n=1,3,5,\dots}^{\infty} \frac{1}{n^3} (-1)^{(n-1)/2} \left[1 - \frac{\cosh(n\pi y / t)}{\cosh(n\pi b / 2t)} \right] \cos \frac{n\pi x}{t} \quad (4.35)$$

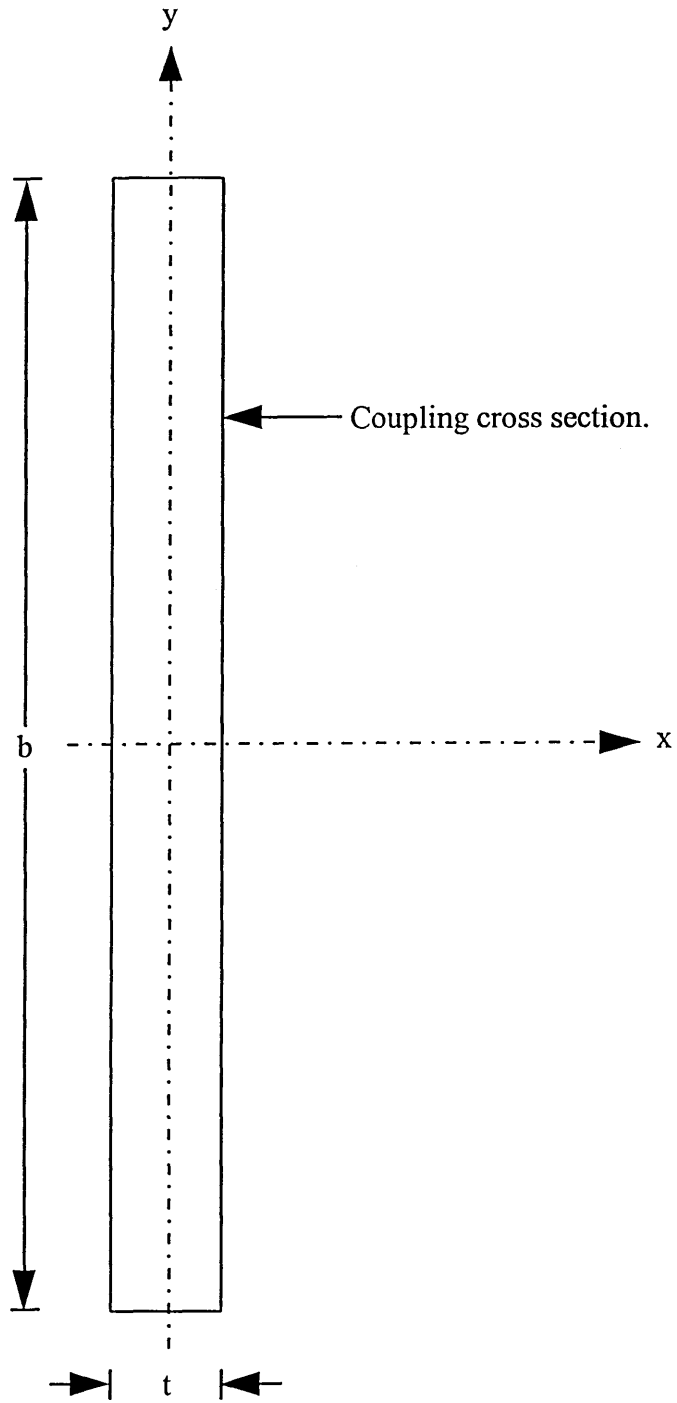


Figure 4.8. Cartesian co-ordinate system adopted for shear stress distribution analysis.

The shear stress components are obtained from equation 4.35. by differentiating with respect to x or y.

4.8.4.1. SHEAR STRESS DISTRIBUTION FOR LONG SIDE OF COUPLING CROSS SECTION.

The distribution of shear stress for the long side of the coupling section was obtained for the Cartesian position $x=t/2$ along $0 < y < b/2$ by differentiating with respect to x, hence:-

$$\tau_{yz} = -\frac{\partial \omega}{\partial x} \quad (4.36)$$

$$\tau_{yz} = \frac{8T_0}{k_1 t^2 b \pi^2} \sum_{n=1,3,5,\dots}^{\infty} \frac{1}{n^2} (-1)^{(n-1)/2} \left[1 - \frac{\cosh(n\pi y / t)}{\cosh(n\pi b / 2t)} \right] \sin \frac{n\pi x}{t} \quad (4.37)$$

Simplification leads to:-

$$\tau_{yz} = \frac{8T_0}{k_1 t^2 b \pi^2} \sum_{n=1,3,5,\dots}^{\infty} \frac{1}{n^2} \left[1 - \frac{\cosh(n\pi y / t)}{\cosh(n\pi b / 2t)} \right] \quad \text{for } x=t/2 \quad (4.38)$$

By taking $\frac{b}{2t} = \text{constant}$ and taking values of $0 < y < b/2$ for equation 4.38., the distribution of shear stress along the long side of the coupling section can be plotted.

This distribution is illustrated in Figure 4.9(a). Two extremes for the constant $\frac{b}{2t}$ were taken as 12 and 30 to match the typical range of coupling dimension ratios.

4.8.4.2. SHEAR STRESS DISTRIBUTION FOR SHORT SIDE OF COUPLING CROSS SECTION.

The component of shear stress acting along the short side of the coupling was found by differentiating equation 4.35. with respect to the variable y, hence:-

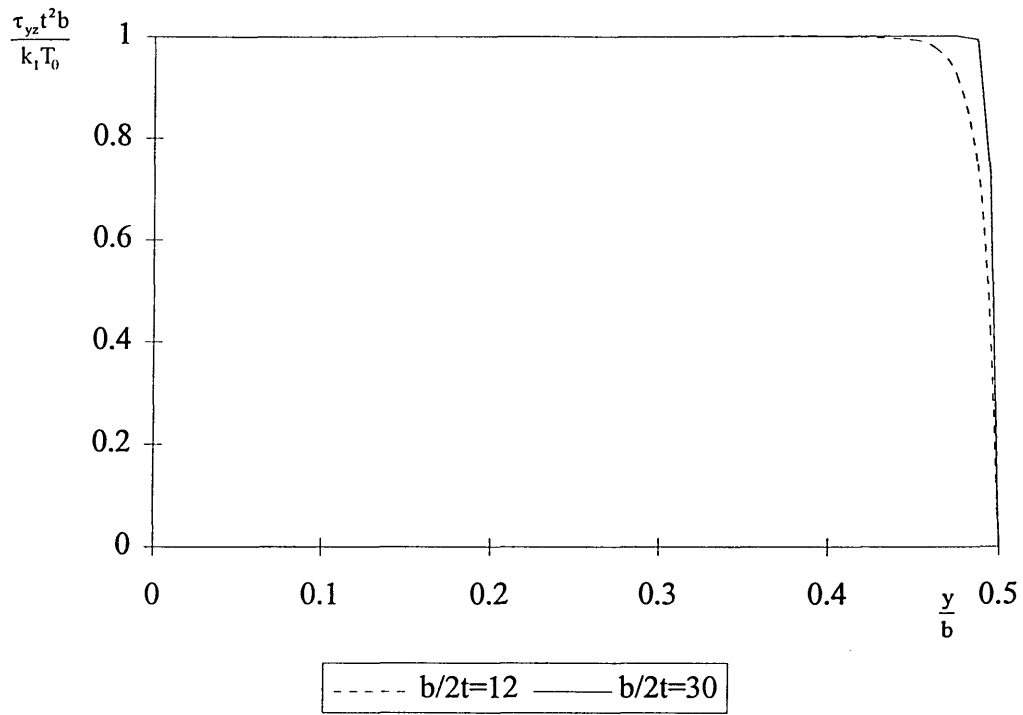
$$\tau_{xz} = -\frac{\partial\omega}{\partial y} \quad (4.39)$$

$$\tau_{xz} = -\frac{8T_0}{k_1bt\pi^3} \sum_{n=1,3,5,\dots}^{\infty} \frac{1}{n^3} (-1)^{(n-1)/2} \left[-\frac{\pi n}{t} \cdot \frac{\sinh(n\pi y / t)}{\cosh(n\pi b / 2t)} \right] \cdot \cos \frac{n\pi x}{t} \quad (4.40)$$

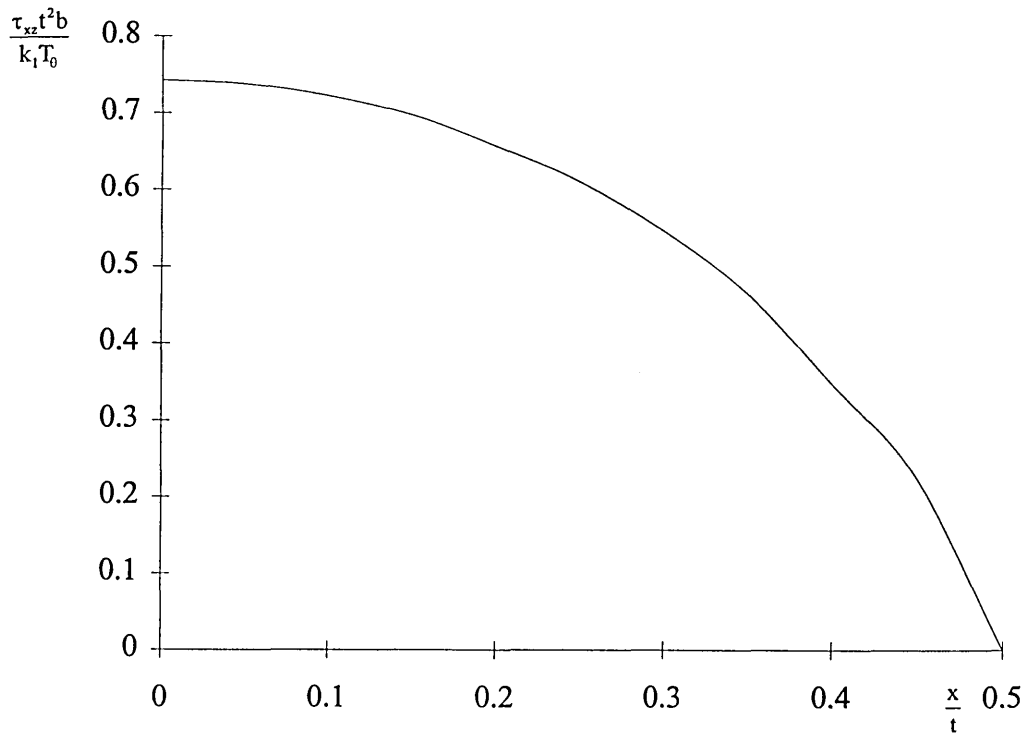
For the short side of the member when $y=b/2$, the shearing stress in the x-z direction is given by:-

$$\tau_{xz} = \frac{8T_0}{k_1t^2b\pi^2} \sum_{n=1,3,5,\dots}^{\infty} \frac{1}{n^2} (-1)^{(n-1)/2} \cdot \cos \frac{n\pi x}{t} \quad (4.41)$$

Taking the series to $n=49$, the plot of equation 4.41. is illustrated in Figure 4.9(b) for the shear stress distribution along the short side of the member at $0 < x < t/2$, $y=b/2$.



(a) Shear stress distribution along the long side of the coupling.



(b) Shear stress distribution along the short side of the coupling.

Figure 4.9. Distribution of shear stress for coupling cross section.

From comparison of Figure's 4.9(a) and (b) it is clear that the maximum surface shear stress acts along the long side of the section and is constant for $\frac{b}{2t}=30$ and $0 < y < 0.49b$.

The maximum shear stress has the value of:-

$$\tau_{\max} = \frac{T_0 k}{k_1 t^2 b} \quad (4.42)$$

where:-

$$k=1.00 \text{ for } b/t > 10 \text{ [25]}$$

$$k_1 = 0.33 \text{ for } b/t > 10 \text{ [25]}$$

For the case of the coupling section the maximum shear stress is given by:-

$$\tau = \frac{3.T_0}{t^2.b} \quad (4.43)$$

The distribution of applied stress for a typical coupling cross-section is illustrated in Figure 4.10. for tension, bending and torsion.

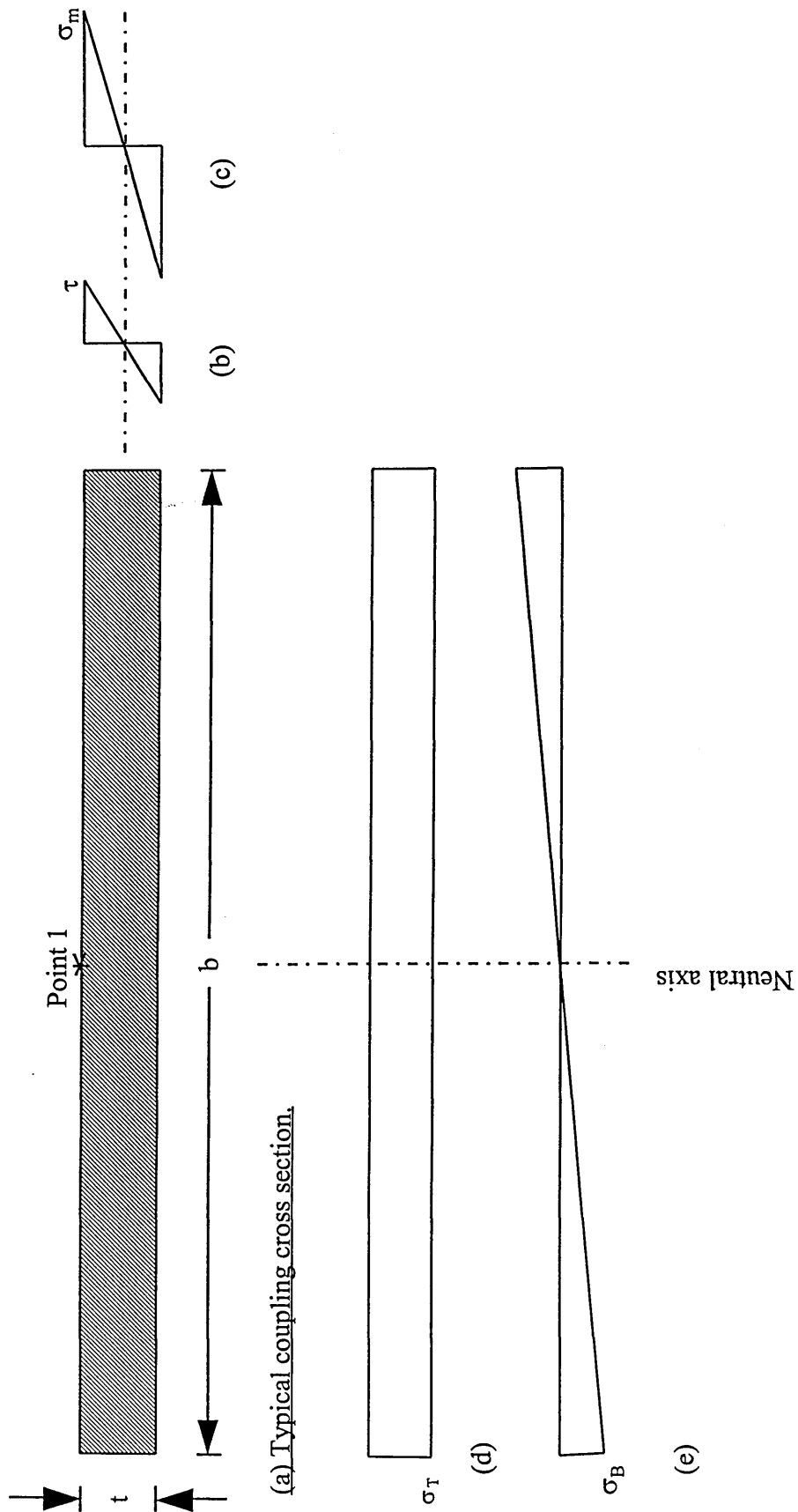


Figure 4.10. Distributions of direct, bending and shear stresses acting on typical cross section of coupling. (b) Torsional shear stress, (c) Bending stress about minor axis, (d) Tensile stress, (e) Bending stress about major axis.

4.9. PRINCIPAL STRESS DISTRIBUTION INDUCED IN COUPLING.

The principal stresses induced in the coupling are derived from the plane stress components derived in 4.8. The derivation of principal tensile stresses is made by considering a stress element located at the centre of the long side of the coupling at the surface. This point will be free from edge effects, and from the initial experimental investigation was found to be the critical design location for the coupling.

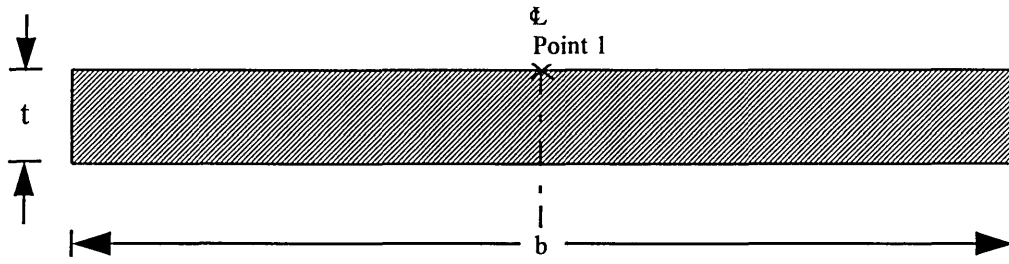
With reference to Figure 4.11. the magnitude of the principal stresses are derived as:-

For element at location 1:-

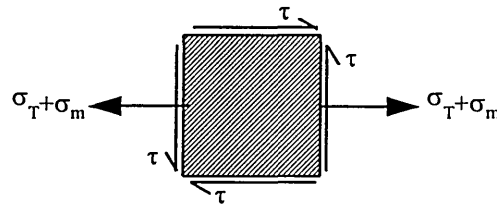
$$\begin{matrix} \sigma \\ \sigma \end{matrix} \begin{matrix} \text{max} \\ \text{min} \end{matrix} = \frac{\sigma_T + \sigma_m}{2} \pm \sqrt{\left(\frac{\sigma_T + \sigma_m}{2}\right)^2 + \tau^2} \quad (4.44)$$

and the maximum shear stress has the value:-

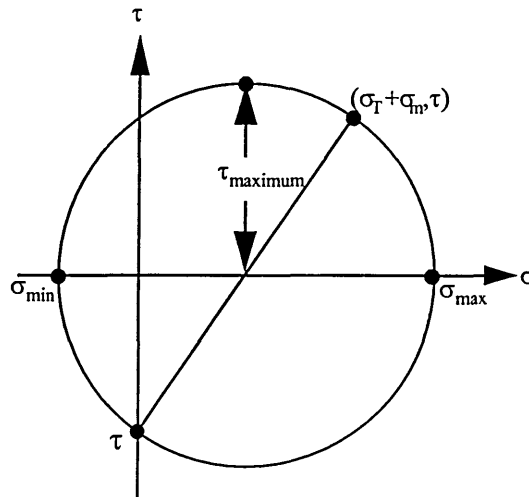
$$\tau_{\text{maximum}} = \sqrt{\left(\frac{\sigma_T + \sigma_m}{2}\right)^2 + \tau^2} \quad (4.45)$$



(a) Typical cross section of coupling showing the location of the critical point 1.



(b) Element at location (1).



(c) Mohr circle of stress for point at location (1).

Figure 4.11. Mohr circle for stress at the critical point in the coupling cross section.

The predicted distribution of principal tensile stress is illustrated in Figure 4.12. for the following coupling section sizes for a 800mm diameter coupling:-

- 1) 2mm x 127mm
- 2) 5mm x 150mm

The peak stress occurs at the crown of the coupling for the range of section sizes of interest. From Figure 4.12. it is clear that the peak stresses reduce with increasing coupling dimensions due to the increased section properties.

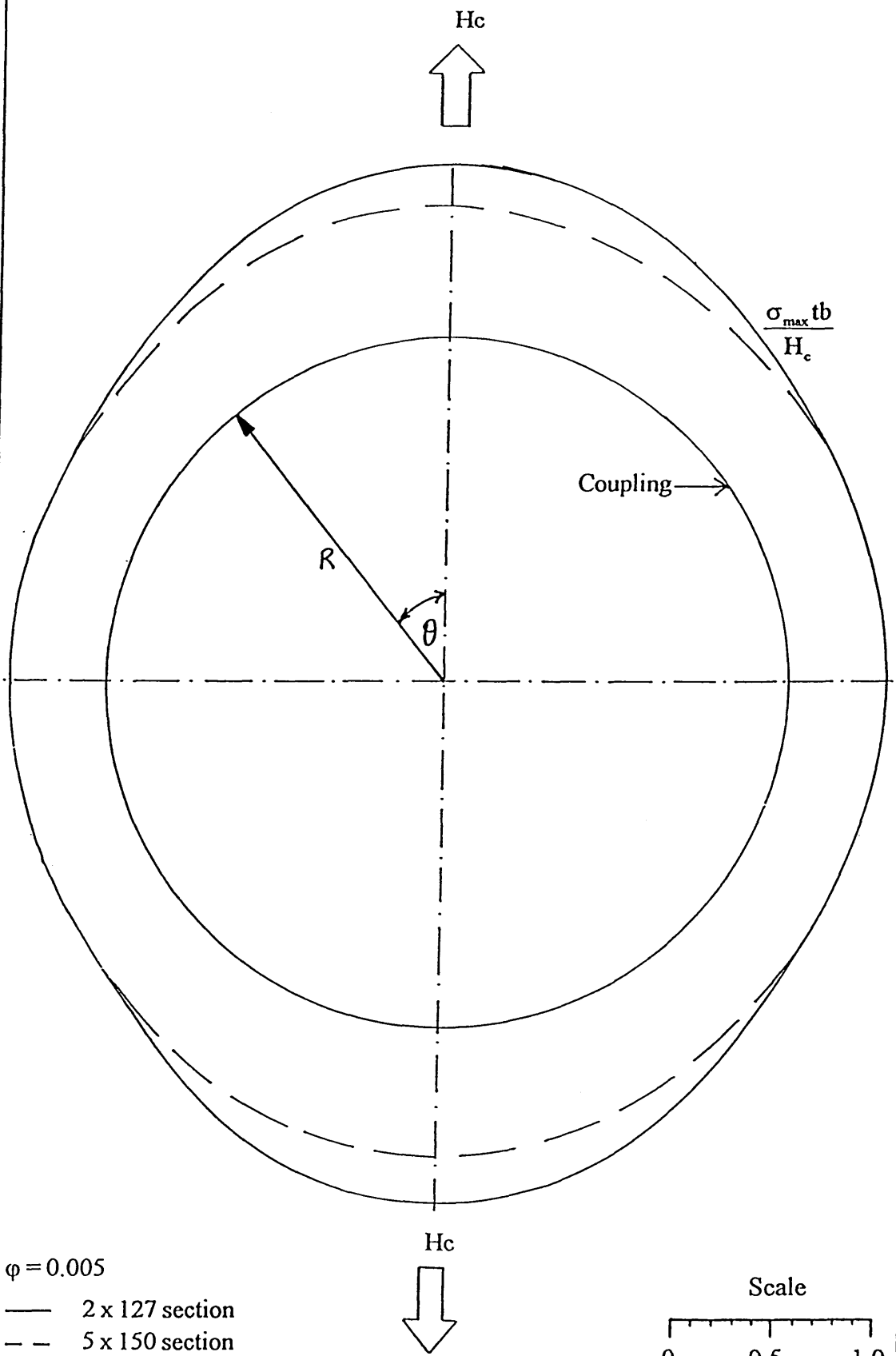


Figure 4.12. Theoretical distribution of non-dimensional principal tensile stress induced at the surface of the middle of the coupling width.

4.10. MAIN CONCLUSIONS.

The following conclusions maybe drawn from the theoretical analysis of the coupling:-

- 1) The lateral force acting across the packing ring due to a misaligned joint is resisted by both the structural element of the coupling, and the shear resistance between pipe-packing-pipe interface, due to the presence of the compressible rubber seal element.

- 2) The shear deformation of the packing material and the relative movement of the pipe spigots will cause a loose sleeved coupling ring to deform as shown in Figure 4.3(b). The active pressure due to the lateral force causes outward deformation of the coupling profile at its crown while inward deformation at the springing. Due to the confinement of the pipe-coupling system and the presence of the rubber seal, the inward deformation is resisted by passive pressure from the pipe.

- 3) The distribution of radial pressure used in this study simulates the pipe-coupling interaction and is given by equation 4.2. The value of ϕ was found by correlating theoretical and experimental principal stresses. The value of 0.005 was found to be most appropriate (see chapter 7).

- 4) From (3) above it is clear that the distribution of radial pressure for the coupling system is virtually constant, with slight increment towards the crown. This observation is expected due to the confinement of the coupling and its limited freedom to deform.

- 5) The hoop tension distribution was significant due to the nature of the radial pressure distribution. The resulting tensile stress distribution is given by equation 4.32.

- 6) The bending stress distribution about the minor axis due to the varying radial pressure component was significant due to the low value of section modulus for the plane of bending.

- 7) The coupling is loaded eccentrically about its longitudinal axis thereby inducing torsion and bending about the major axis (given by equations 4.26. and 4.27. respectively). These quantities are dependant on both the radial pressure distribution (in terms of φ), and the properties of the coupling member (in terms of μ).

- 8) The shear stress distribution for a solid thin rectangular section was investigated for the coupling in light of the torsional behaviour outlined in 4.6. The maximum shear stress was found to occur along the long side of the cross-section. The maximum shear stress was found to be constant over the range illustrated by Figure 4.9(a). The contribution of shear stresses to the overall principal tensile stresses was limited due to low torsional effect of the system.

- 9) The critical stress element identified in this study was located at the centre of the long side of the cross-section at the surface (see Figure 4.11.). The resulting principal tensile stress for this location is given by equation 4.44.

10)The effect of increasing the coupling thickness is readily seen in Figure 4.12. Large peak stresses coinciding with peak radial pressure for thin coupling sections are due to the relatively small bending stiffness and tensile resistance. As the coupling thickness increases, the peak stresses decrease showing a smooth distribution of principal tensile stress.

11)The model for the prediction of principal tensile stresses induced in loose sleeved coupling rings was verified by full scale experiment. The details of which are shown in chapter 7.

CHAPTER 5

DESCRIPTION OF EXPERIMENTAL APPARATUS AND SPECIMENS.

5.1. INTRODUCTION.

The experimental verification of the structural interaction models presented in chapters 3 and 4 was carried out using a purpose built jacking frame located at Flex Seal Couplings Ltd. of Sheffield. This chapter reviews the experimental apparatus used in relation to real pipe-jacking conditions and describes the experimental specimens, along with their engineering characteristics.

5.2. AIMS AND OBJECTIVES OF EXPERIMENTAL PROGRAMME.

The main aim of the experimental programme was to verify the structural interaction models of the pipe-packing-coupling system (chapters 3 and 4) under simulated full scale laboratory conditions.

The objectives set to fulfil this aim are listed below:-

1) Verify structural interaction of pipe-packing-coupling system (including packing-pipe contact zone prediction, lateral force acting at misaligned joint and load sharing characteristics of joint arrangement) for the following cases:-

- Open joint.
- Closed joint.

2) Verify coupling stress model by monitoring strain gauged couplings for the following cases:-

- Open/closed joint.
- Open joint.

5.3. DESCRIPTION OF EXPERIMENTAL JACKING FRAME.

In order to meet the objectives described above a purpose built jacking frame was constructed for a two pipe 'in air' system at full scale. The requirements of the experimental apparatus for the two pipe 'in air' system are listed below:-

- 1) Full scale pipes / packing rings / couplings.
- 2) Jacking forces to simulate installation loads.
- 3) Facility to displace relative angular inclination of pipes.
- 4) Accommodation of a range of microtunnelling pipe sizes.

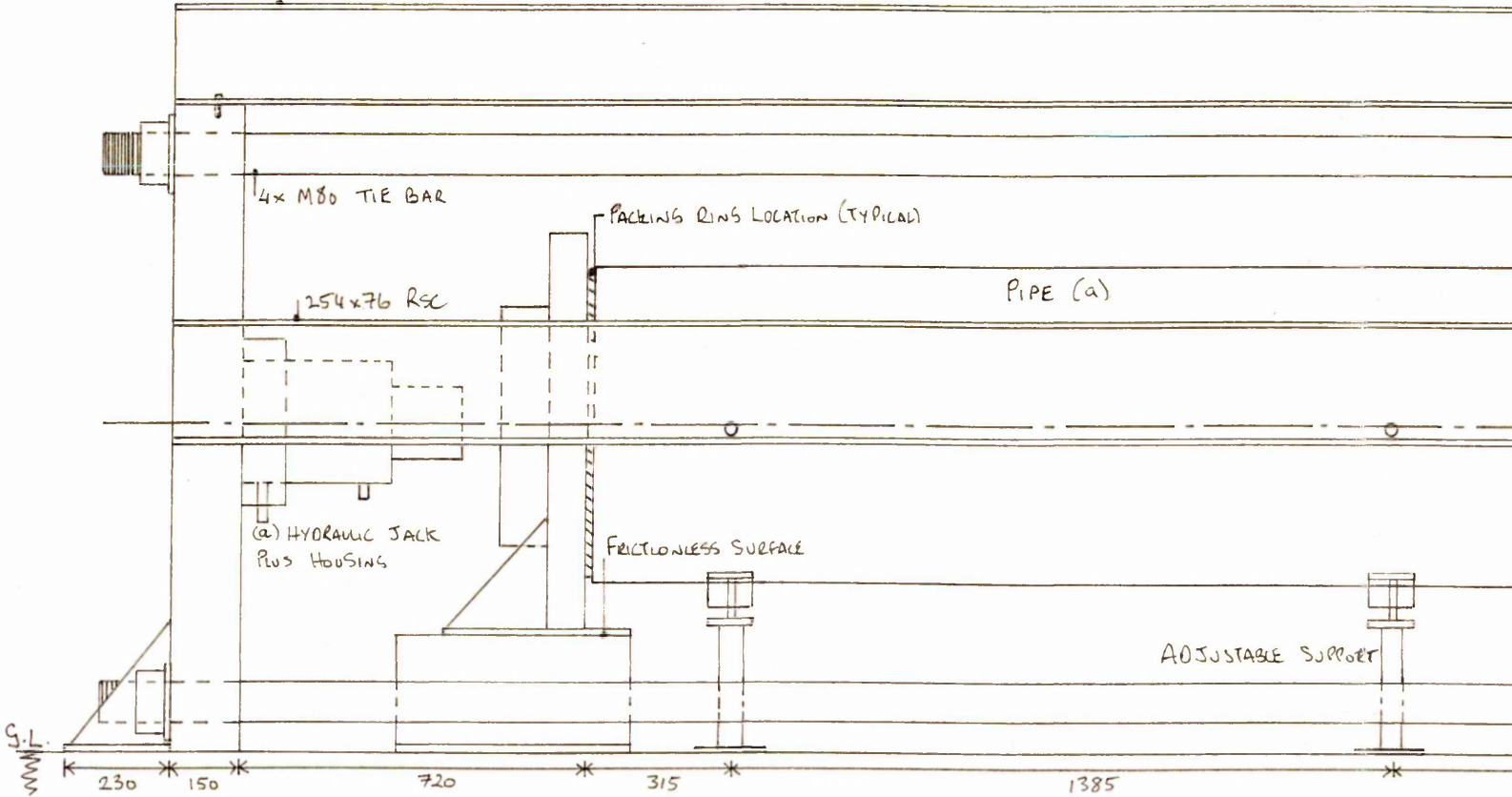
The experimental jacking frame shown in Figure 5.1. was designed for a maximum longitudinal jacking force of 2000 kN. The structural design and fabrication of the frame was carried out by Mayflower Engineering Ltd. of Sheffield. The frame was designed to accommodate 2m long Steinzeug vitrified clay pipes in the range of 250mm to 600mm nominal bore.

A removable hydraulic jack was used to provide the longitudinal force for the experiments and was housed in location (a). Two hydraulic cylinders were used during the course of the experimental programme. The capacities of cylinders HC 1 and HC 2 were 1500 kN and 2000 kN respectively. The details of the calibration of each cylinder can be found in 6.4. A constant pressure pump was used to control the flow to the cylinder during the experiments. Plate 5.1. illustrates the hydraulic jack arrangement.

The two pipes were deflected such that the resultant lateral force acted vertically towards ground. The eccentricity of the jacking thrust at the displaced central joint was therefore located in the lower half of the pipe-packing interface. Angular profiled reaction plates (location b) were used to provide full bearing to the displaced pipe (b) to control the eccentricity of jacking force at the pipe end. The frame was designed such that a range of initial misalignment angles of zero to 1 degree could be accommodated using different profiled reaction plates.

Pipe (a) was seated on metal 'v' profiled supports to simulate a solid reaction from the base of the excavation. Pipe (b) was displaced 'in air' to simulate the other extreme ground reaction of a void or very weak stratum. The justification of the pipe seating

203 x 133 x 25 UB LIFTING BEAM.



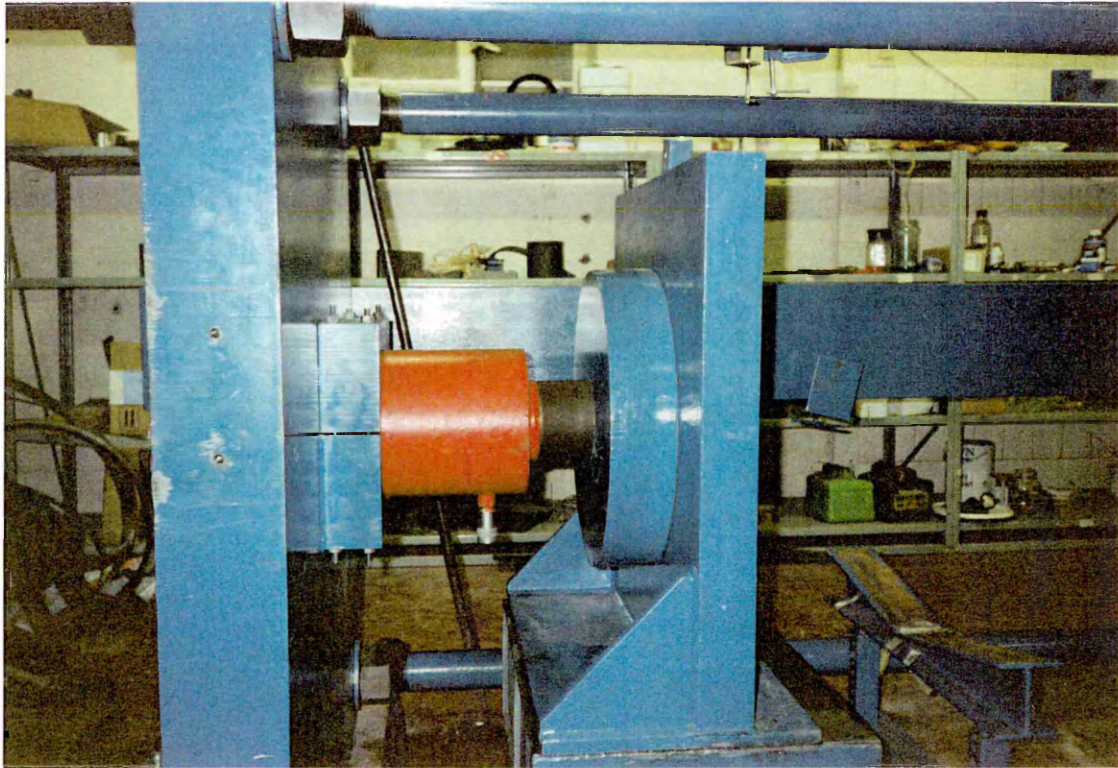


Plate 5.1. Hydraulic jack arrangement for cylinder HC2 showing loading plate and reaction plate.

arrangements is made on the basis of a worst case scenario of the lateral force at the misaligned joint, as mentioned in 2.4. and 3.1. Plate 5.2. illustrates the experimental jacking frame.

5.3.1. LIMITATIONS OF EXPERIMENTAL JACKING FRAME.

The two pipe 'in air' jacking frame had two main limitations:-

- 1) The ground reactions provided by the rigid supports could not simulate varying soil stiffness' but provided the upper bound condition of infinitely rigid/infinitely free support over the misaligned joint. On this basis the experimental arrangement was deemed satisfactory.

- 2) The large jacking forces applied to the two pipe 'in air' system (up to approximately 1500 kN) caused the misaligned joint to close. In addition, the combined effect of minor dimensional inaccuracies in the frame and the high jacking forces used during testing made the misaligned joint rotate out of the intended vertical plane. The joint rotation was monitored throughout each test, and the data adjusted accordingly.



(a) Experimental jacking frame prior to positioning of pipes.



(b) DN 400 pipe with strain gauged coupling C1 lifted into position.

Plate 5.2. Illustration of experimental jacking frame.

5.4. PROPERTIES OF STEINZEUG VITRIFIED CLAY JACKING PIPES.

Vitrified clayware microtunnelling pipes manufactured by Steinzeug GmbH (Germany) [5] were used to verify the theoretical analysis presented in chapters 3 and 4. Generality of the investigation was achieved using a representative range of pipe sizes. The dimensional specifications for the pipes used are presented in Table 5.1., with reference to Figure 5.2.

The engineering properties of the clay pipes are shown in Table 5.2. below:-

Specific weight	(kN/m ³)	22
Bending tensile strength	(N/mm ²)	15-40
Compression strength	(N/mm ²)	100-200
Tensile strength	(N/mm ²)	10-20
Modulus of elasticity	(N/mm ²)	50000

Table 5.2.: Properties of Steinzeug vitrified clay pipes. [5]

It is clear from Table 5.2. that vitrified clay possesses exceptional strength properties. The compressive strength is variable but in comparison with concrete, vitrified clay is an economical material for use with jacking pipes. The high compressive strength means that comparatively thinner pipe walls can be made in vitrified clay, compared with thick walled reinforced concrete jacking pipes.

	End (a)					End (b)					Length (mm) ± 0.5	
	d_{Spigot} (mm) ± 0.1	d_{Inside} (mm)	d_{max} (mm) ± 0.1	Average wall thickness (mm)	Milled length (mm) ± 0.5	d_{Spigot} (mm) ± 0.1	d_{Inside} (mm)	d_{max} (mm) ± 0.1	Average wall thickness (mm)	Milled length (mm) ± 0.5		
DN250												
Pipe 1	334.5	$250 \pm_1^2$	353.3	41.8	75	333.2	$250 \pm_0^4$	353.3	40.6	62		1991
Pipe 2	333.4	$250 \pm_1^0$	352.4	41.7	75	333.5	$250 \pm_0^2$	352.4	41.3	62		1991
DN 400												
Pipe 1	526.5	$401 \pm_0^4$	549.1	61.3	65	523.6	$400 \pm_0^2$	549.1	61.3	75		1998
Pipe 2	526.3	$402 \pm_0^4$	550.7	61.2	65	523.6	$400 \pm_0^4$	550.6	60.8	75		2001
DN 600												
Pipe 1	722.9	$600 \pm_0^5$	754	60.2	86	717.5	$600 \pm_2^7$	754	57.3	75		1985
Pipe 2	722.6	$600 \pm_0^{11}$	757	58.6	87	717.3	$600 \pm_1^4$	757	57.7	75		1985

Table 5.1: Dimensional specification of clayware pipes used for the experimental investigation.

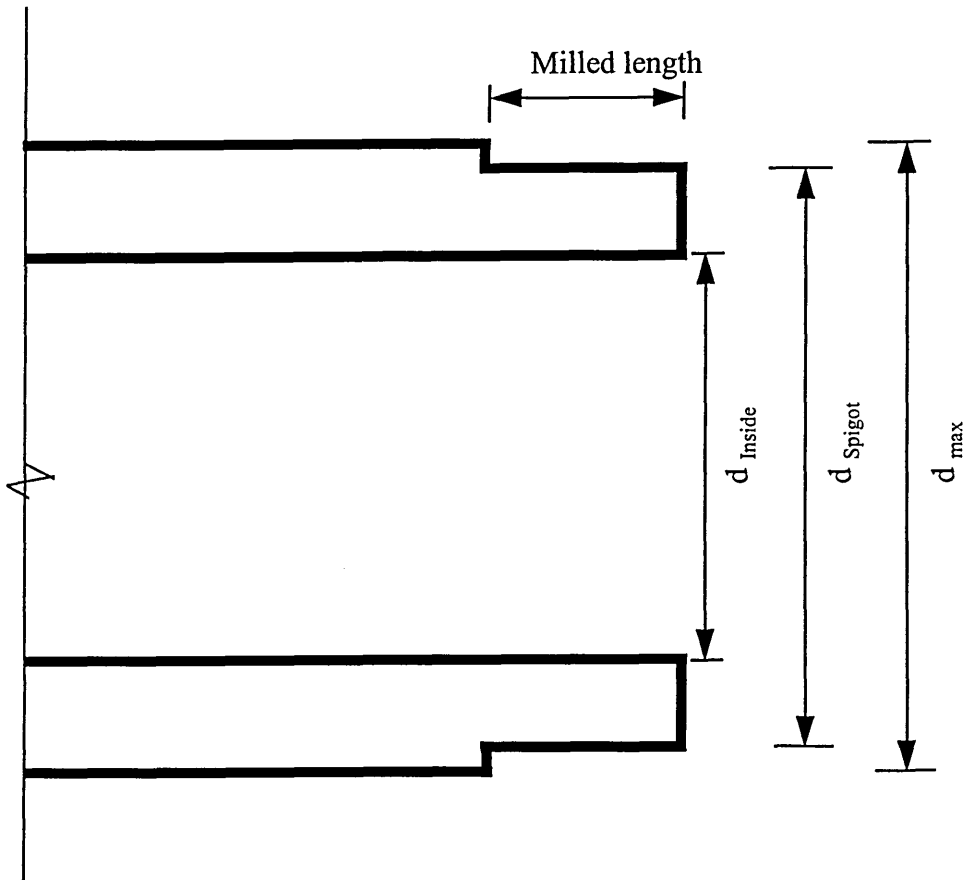


Figure 5.2. Longitudinal section through Steinzeug clay pipe [5].

5.5. PROPERTIES OF STEINZEUG CHIPBOARD PACKING MATERIAL.

Chipboard packing rings were supplied by Steinzeug GmbH conforming to prEN 312 [5]. The samples used for the experimental investigation were proprietary products and their design was pre-determined by Steinzeug GmbH. The dimensional specifications for the packing rings for the three pipe sizes are shown in Table 5.3. below:-

	Initial thickness (mm)	Diameter (outside) (mm)	Diameter (inside) (mm)
DN 250	8.12 ± 0.08	330 ± 1.0	253 ± 1.0
DN 400	10.22 ± 0.11	522 ± 1.0	414 ± 1.0
DN 600	16.36 ± 0.08	717 ± 1.0	619 ± 1.0

Table 5.3.: Dimensional specification of chipboard packing rings [5].

5.5.1. STRESS-STRAIN CHARACTERISTICS FOR CHIPBOARD PACKING MATERIAL.

Rectangular blocks sawn from the circular packing rings were edge prepared and subjected to compression load cycles in an ESH 600 kN testing machine. The dimensional specifications of the samples are shown in Table 5.4., below:-

	Sample Reference	Thickness (mm)	Width (mm)	Length (mm)	Average cross sectional area (mm)
DN 250	CB1	8.05 ± 0.03	34.45 ± 0.09	25.04 ± 0.28	862.63
DN 400	CB2	10.24 ± 0.02	36.78 ± 0.4	50.10 ± 0.26	1842.68
DN 600	CB3	16.38 ± 0.00	25.71 ± 0.45	39.15 ± 0.25	1006.55

Table 5.4.: Dimensional specification of chipboard blocks used for compression tests.

The specimens were loaded at a constant rate of 10 N/mm²/ 3mins [22] until the compressed thickness was reduced to 60 per cent of the original thickness for the loading cycle [20]. The specimen was allowed to recover for 15 minutes before re-loading. The specimens were loaded a total of five times to obtain the permanently deformed stress-strain characteristics of the materials used in subsequent lateral force and coupling stress analysis experiments (chapter 6).

The applied stress-deformation curves for the three samples tested are illustrated in Figures 5.3. to 5.5. The original thickness' of each sample at the start of each load cycle are shown in Table 5.5. below:-

APPLIED STRESS (N/MM²)

90

80

70

60

50

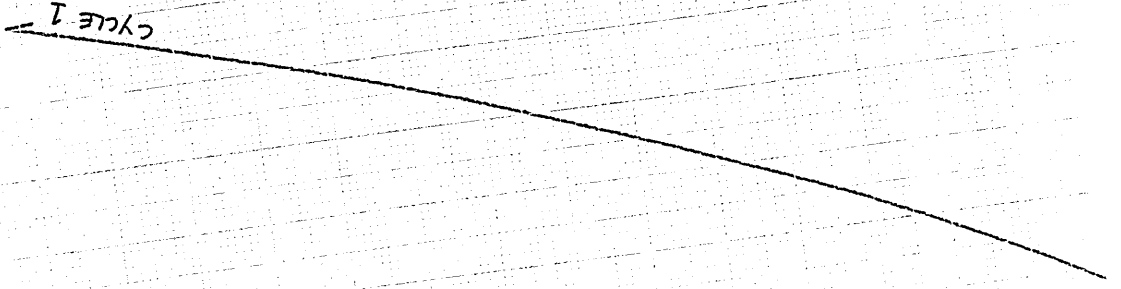
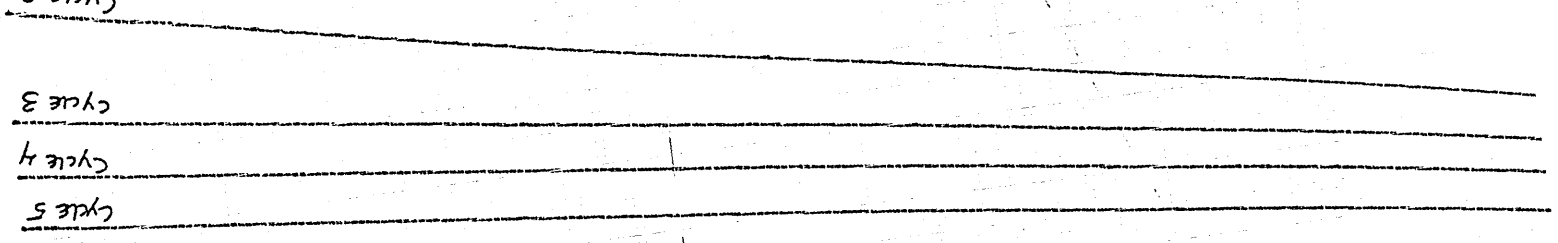
Cycle 2

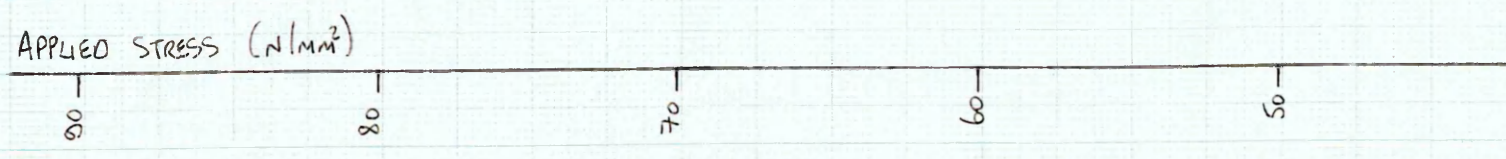
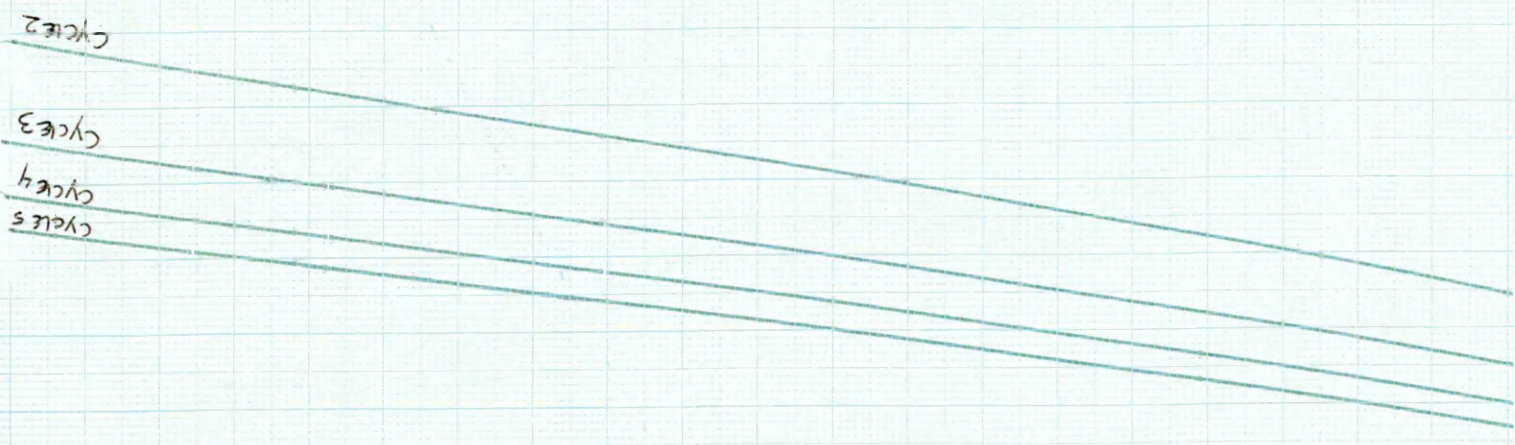
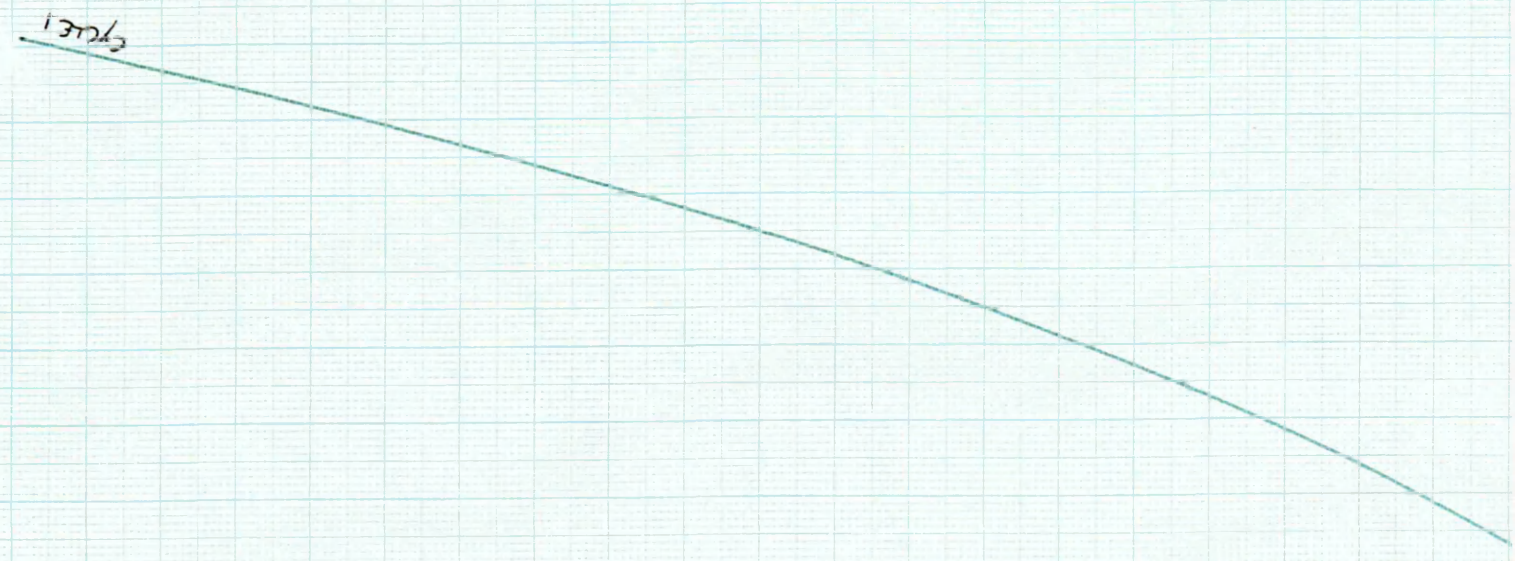
Cycle 3

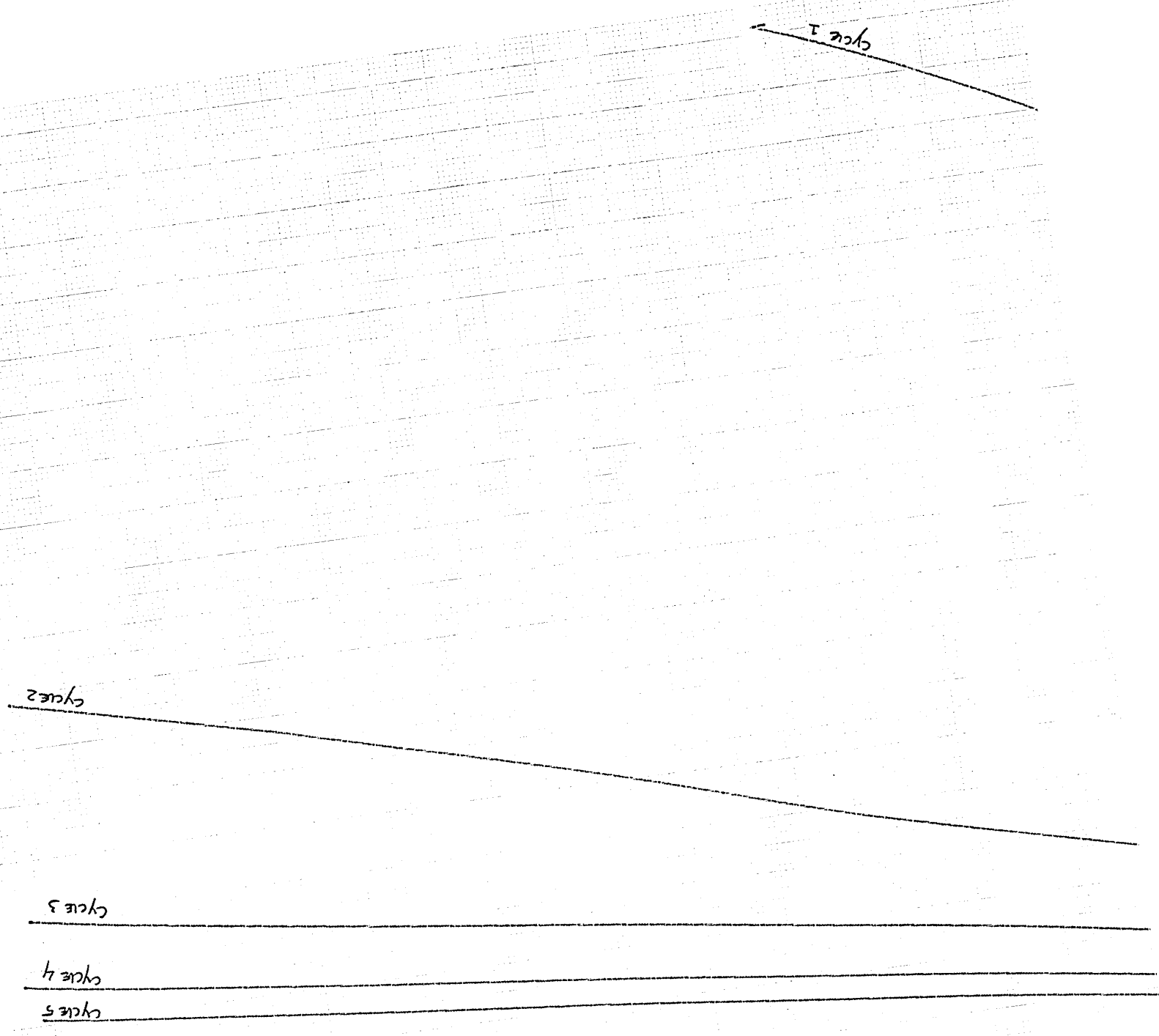
Cycle 4

Cycle 5

Cycle 1







APPLIED STRESS (N/mm^2)

80

70

60

50

cycles

1

2

3

4

5

cycles

Original thickness	CB 1	CB 2	CB 3
Start of cycle 1 (mm)	8.050	10.240	16.380
Start of cycle 2 (mm)	5.941	8.171	12.308
Start of cycle 3 (mm)	5.701	7.887	11.078
Start of cycle 4 (mm)	5.570	7.752	10.671
Start of cycle 5 (mm)	5.443	7.647	10.458
End of test (mm)	5.406	7.580	10.270

Table 5.5.: Summary of thickness' of chipboard samples at start of load cycle.

It is apparent that the chipboard material possesses a stiffening response to applied load. After the first load cycle, the material recovers by approximately 32.5 per cent (31 to 34). Upon reloading the material becomes stiffer - as illustrated by the non-linear stress / deformation curves, and its recovery reduces to approximately 26 per cent (25 to 28) after the fifth load cycle.

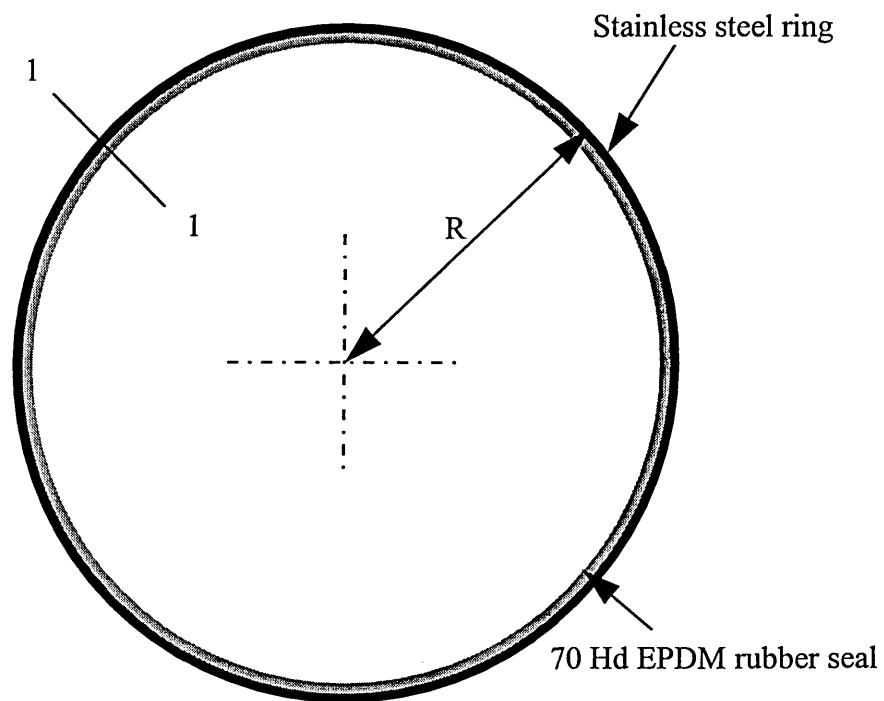
The modulus of elasticity of the chipboard packing material is stress dependant [22,23]. This is clearly shown by the non-linear response to applied stress in Figures 5.3. through 5.5. The modulus of elasticity of the material should be taken as the tangent modulus at the stress state of the loaded cycle under consideration. The modulus of elasticity at stress states above 40 N/mm² approaches a constant value with an increased number applications of load.

5.6. STAINLESS STEEL COUPLING SPECIMENS.

Coupling specimens were manufactured from grade 304S15 stainless steel to BS 1449:1983 [27]. Strips of stainless steel were passed through powered rolls to form a circular profile and butt welded by fusing the parent metal to form the weld. No filler material was added to the weld. In addition to the stainless steel structural element, a nominal 3mm thick Ethylene-Propylene-Di-Methyl (EPDM) rubber seal with Shore hardness value of 70 [28], was adhered to the inner of the ring in order to simulate the real coupling system. The rubber seal has the added benefit of distributing the applied radial force during pipe-packing-coupling experiments. A typical coupling specimen is illustrated in Figure 5.6. A schedule of coupling specimens used for the pipe-packing-coupling experiments is shown in Table 5.6. below:-

Pipe size (mm)	Specimen Reference	Section width (mm)	Section thickness (mm)	Outer radius (mm)
DN 400	C1	127.0	2.12	267.9
DN 250	C2	127.0	2.12	171.6
DN 250	C3	150.0	3.33	173.7

Table 5.6.: Dimensional specification of coupling specimens.



(a) Typical coupling profile.

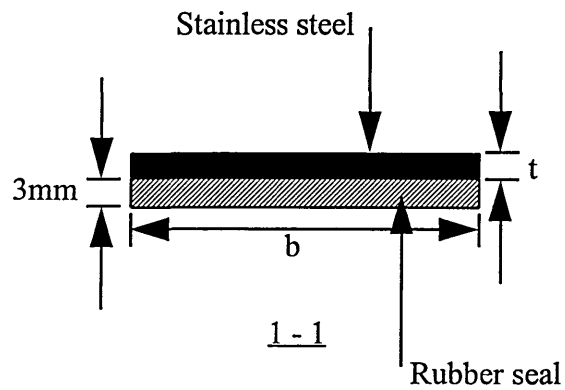


Figure 5.6.: Illustration of typical coupling specimen.

5.6.1. MECHANICAL PROPERTIES OF STAINLESS STEEL COUPLING SPECIMENS.

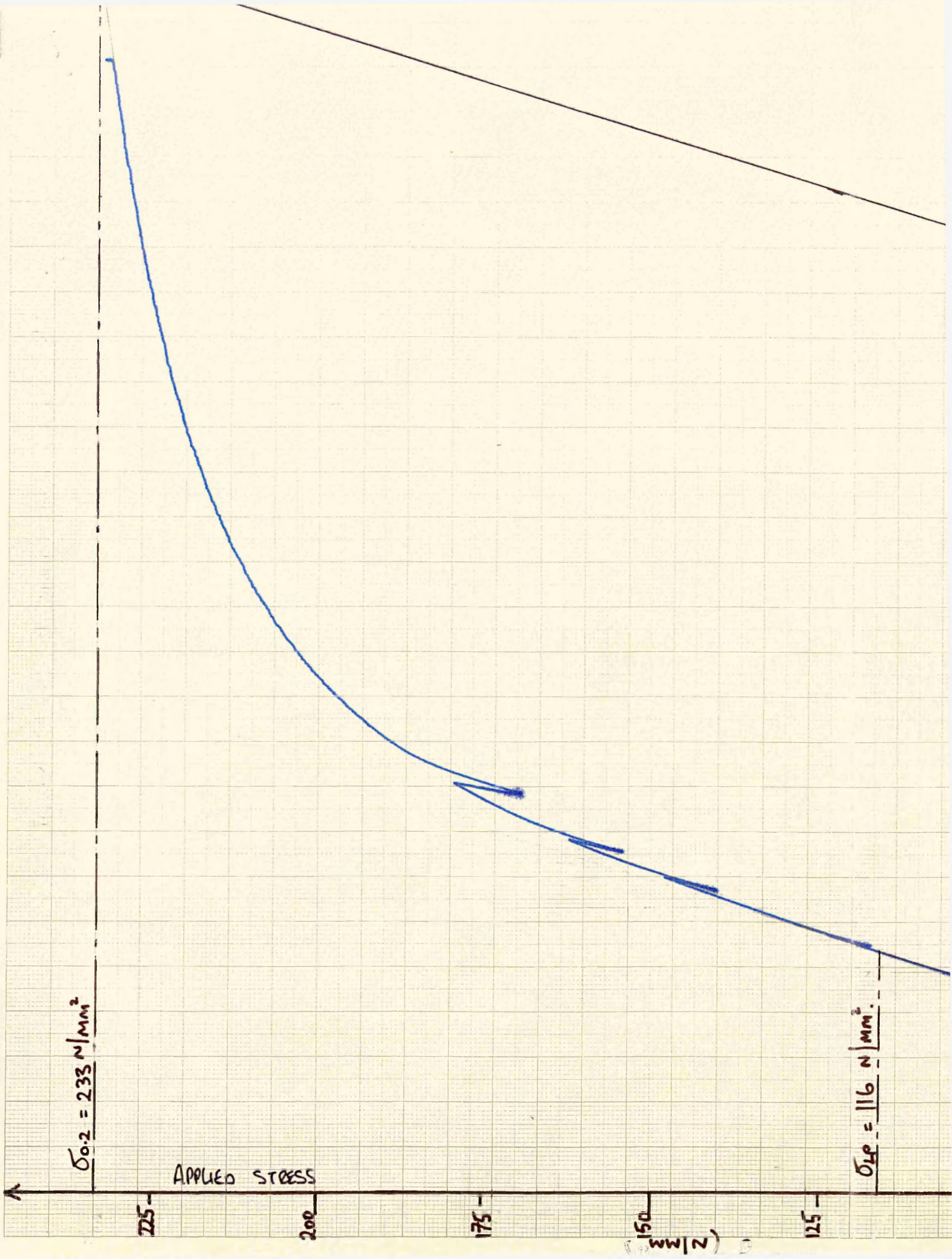
The mechanical properties of the stainless steel material used to manufacture the coupling specimens were determined from standard tensile tests conforming to BS 1449: Part 2: 1983 / BS EN 10 002-1: 1990 [27,29]. Tensile specimens were cut from similar material used to manufacture the coupling specimens. The specimens were tested using an ESH 600 kN testing machine. The specimens were loaded at a constant rate of 10 N/mm²/second [27] until failure. The elastic characteristics of the material were investigated.

The dimensional specifications of the tensile specimens are shown in Table 5.7. below:-

Reference	Proportional gauge length (mm)	Width (mm)	Thickness (mm)	Average C.S.A. (mm ²)
S1	120.0	24.30 ± 0.03	3.36 ± 0.03	81.65
S2	120.0	25.15 ± 0.04	5.26 ± 0.04	132.29

Table 5.7.: Dimensional specification of stainless steel tensile specimens.

Plots of stress-strain for tensile specimens S1 and S2 are illustrated in Figures 5.7. and 5.9 respectively. Plots of axial strain - lateral strain are given in Figures 5.8. and 5.10. for specimens S1 and S2 respectively.



$$\sigma_{0.2} = 233 \text{ N/mm}^2$$

APPLIED STRESS

$$\sigma_{LP} = 116 \text{ N/mm}^2$$

225

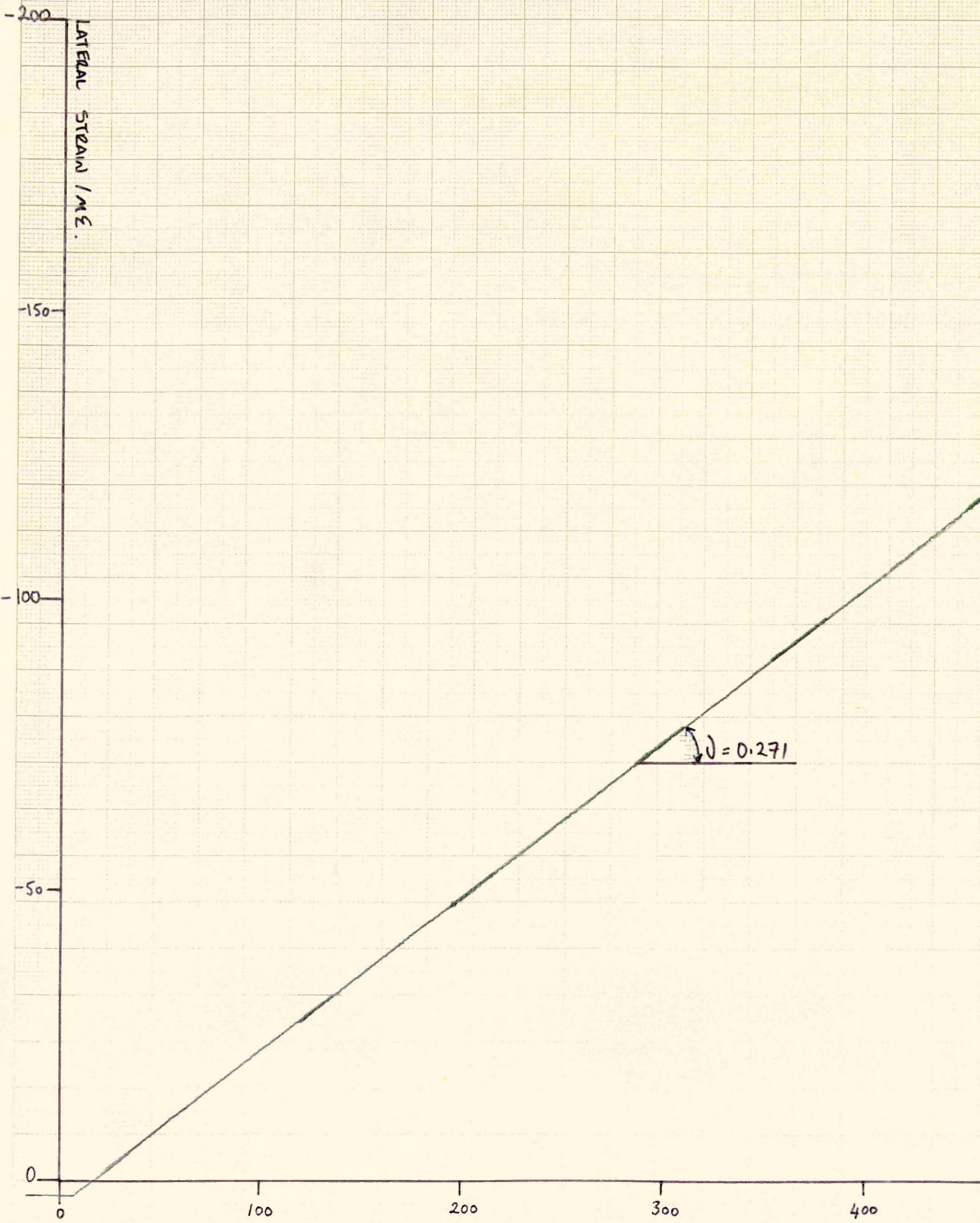
200

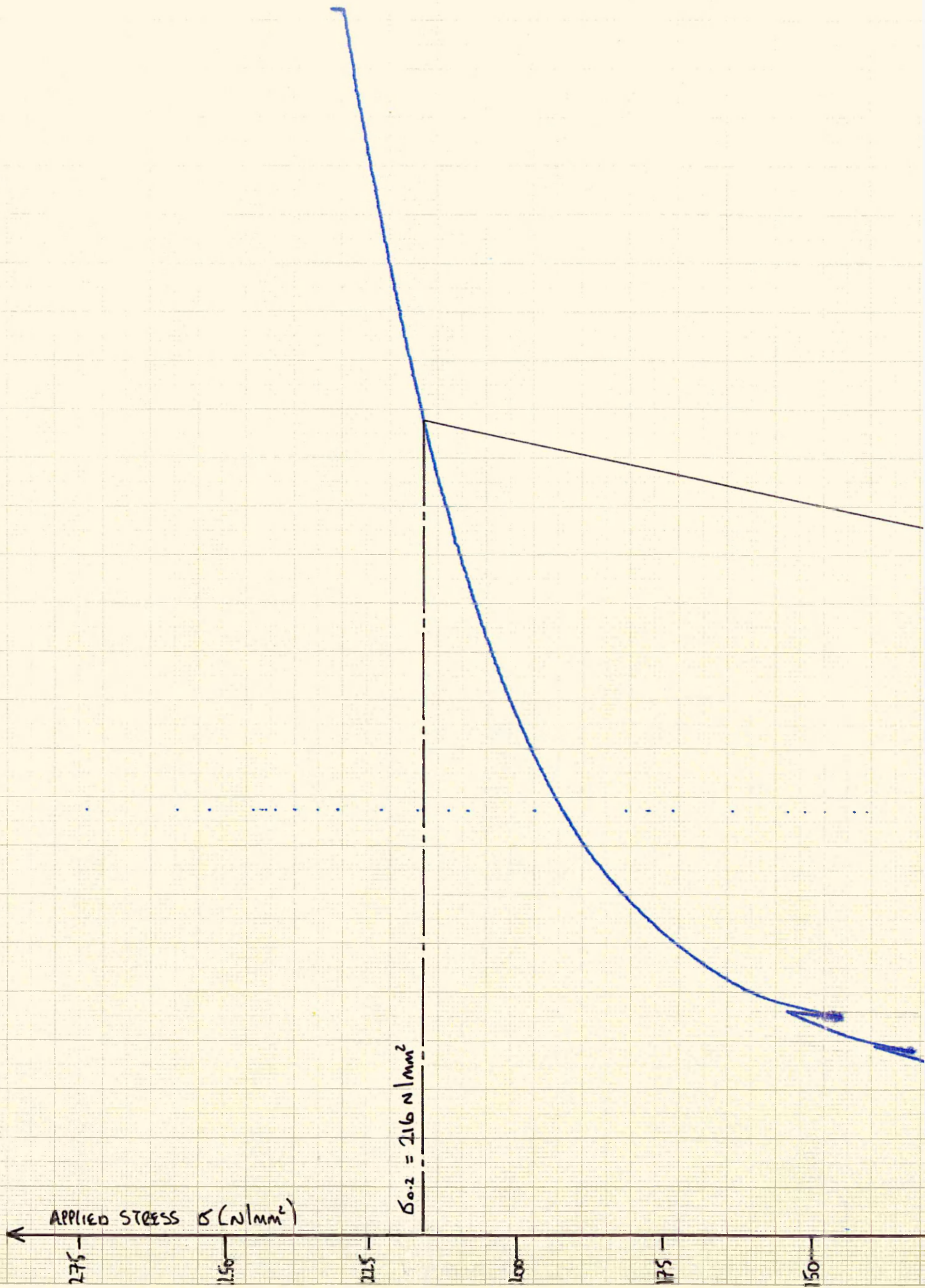
175

150

125

(N/mm²)





LATERAL STRAIN / $\mu\epsilon$

1000

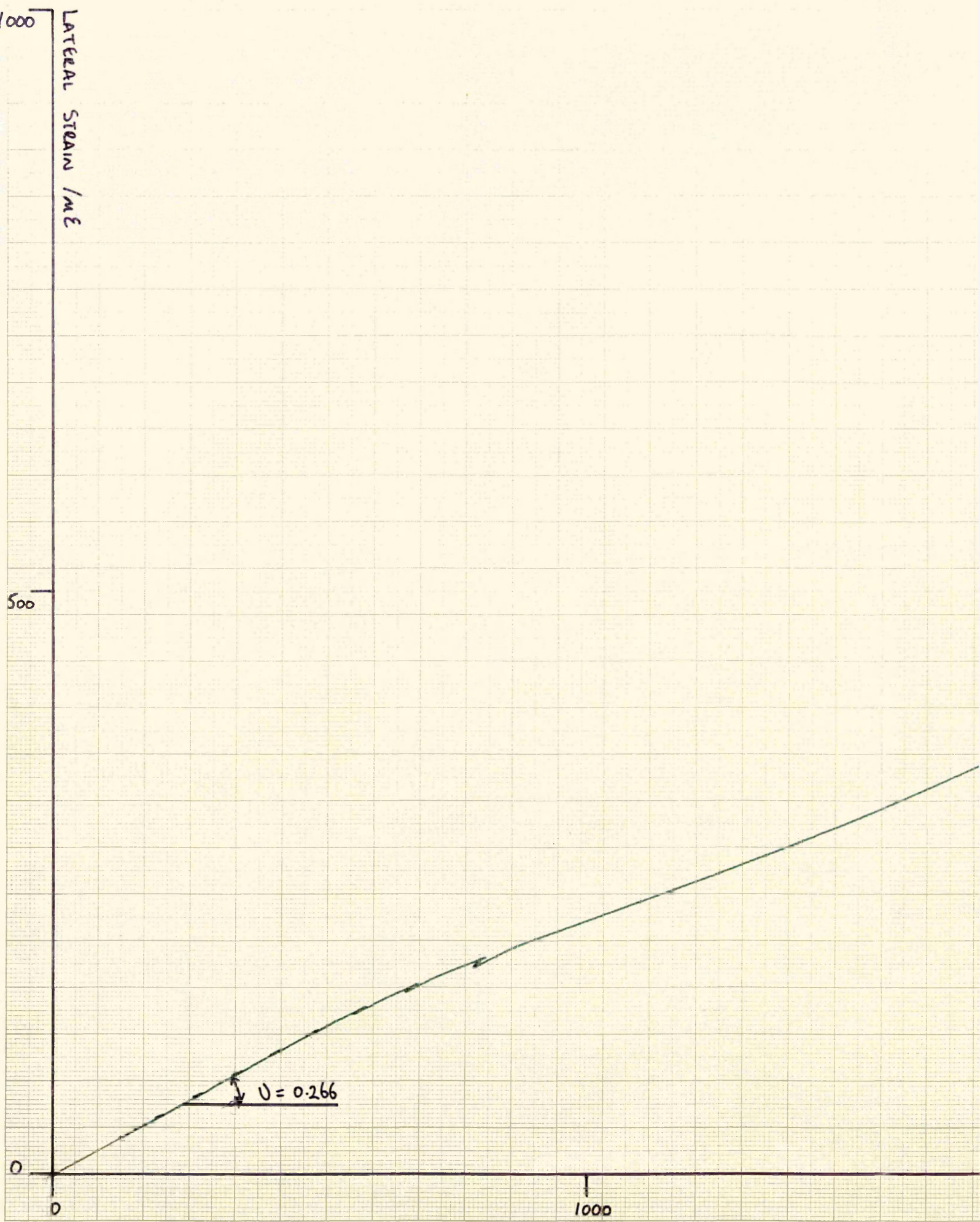
500

0

0

1000

$\nu = 0.266$



A summary of the mechanical properties found is shown in Table 5.8. below:-

Specimen Reference	Proportional stress (N/mm ²)	0.2 per cent proof stress (N/mm ²)	Failure stress (N/mm ²)	Poisson's ratio	Linear elastic modulus (kN/mm ²)	Average elastic modulus (kN/mm ²)
S1	116	233	570	0.271	181.6	195.5
S2	115	216	567	0.266	209.4	

Table 5.8.: Summary of mechanical properties found by tensile tests.

The values shown above when averaged correlate with standard table values for the material given below, after Mann [30] :-

Tensile strength : 510 N/mm² 0.2% Proof stress : 215 N/mm²

E at 20 °C : 201 kN/mm²

5.7. MAIN CONCLUSIONS.

The following conclusions maybe drawn from the experimental set-up and specimen preparation:-

- 1) With the use of the experimental apparatus described here, the objectives of the experimental programme were satisfied.

- 2) The chipboard packing rings when repeatedly loaded exhibit a stiffening response to applied load. This behaviour is confirmed by boot et al [22] and Milligan et al [23]. The elastic modulus should be taken as the tangent modulus at the stress state of the loaded cycle of the material under consideration.

- 3) Stainless steel coupling specimens were manufactured with rubber seals of constant cross section. The mechanical properties of the material are summarised in Table 5.8. and can be used to transpose surface strains to stresses in subsequent elastic stress analysis of the coupling specimens.

CHAPTER 6

INSTRUMENTATION AND EXPERIMENTAL PROGRAMME.

6.1. INTRODUCTION.

The experimental measurement of joint alignment, packing-pipe interaction, jacking forces, lateral forces and surface strains induced in the coupling are described in this chapter. The measures taken to control accuracy of the experimental data are also reviewed.

The experimental programme for verifying the structural interaction models presented in chapters 3 and 4 is described with reference to results and discussion given in chapter 7.

6.2. JOINT ALIGNMENT CHARACTERISTICS.

The pipe spigots were milled by rotating the pipe about its longitudinal axis, ensuring the pipe ends are perpendicular to the pipe axis. The angular deviation of the pipe axes was determined by deducing the angular inclination of the intersecting planes of the pipe section parallel to the pipe end. Analysis presented by Ripley et al [9] for the deduction of the misaligned angle (β) from three joint gaps spaced equidistantly around the pipe-end was utilised with the following amendment:-

- The joint gap was measured between 12 mm diameter by 10 mm long offset studs fixed to the external surface of the pipe barrel suitably clear of the coupling.

The three offset distances were measured by vernier calliper placed between adjacent studs. Table 6.1. shows the fixed offset distances of the studs used for the three pipe sizes investigated and Figure 6.1. illustrates the experimental measurement of β .

Pipe class (DN)	Radius to offset stud (mm)	Fixed offset distance to near side of stud, from pipe end (mm)
DN 250	180.0	80.0
DN 400	280.0	70.0
DN 600	385.0	80.0

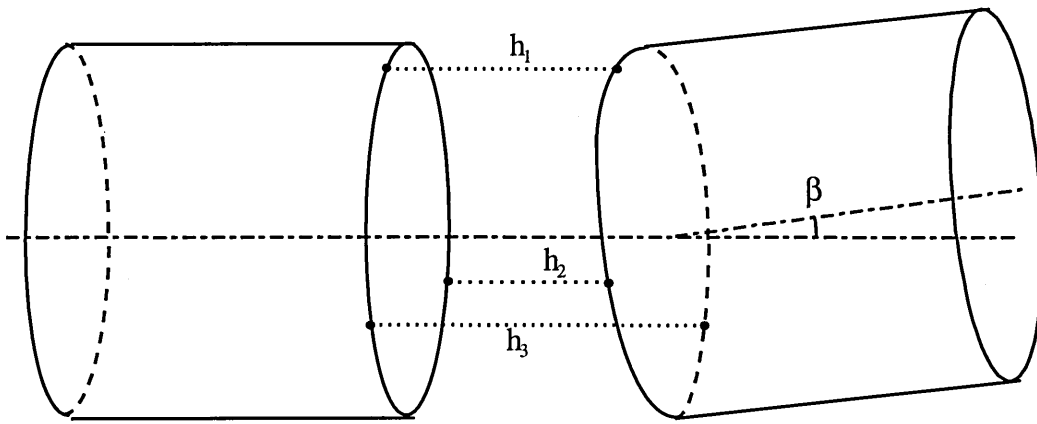
Table 6.1.: Summary of offset stud alignment for experimental measurement of β .

The deviation of the pipe axes can be deduced from:-

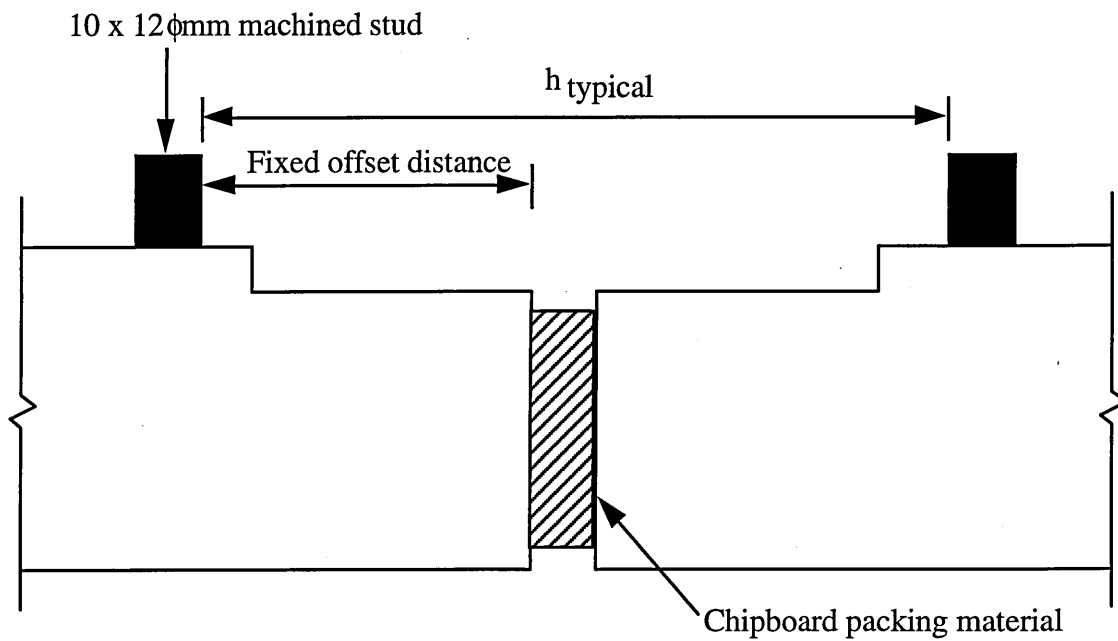
$$\beta = \cos^{-1} \left[\frac{1}{\sqrt{\frac{(h_3 - h_2)^2}{3R_s^2} + \frac{(h_2 + h_3 - 2h_1)^2}{9R_s^2} + 1}} \right] \quad [9] \quad (6.1)$$

Where:-

h_1, h_2, h_3 = distance between adjacent studs,



(a) : General arrangement of deflected joint studs.



(b) : Typical joint measurement - stud detail.

Figure 6.1: Experimental measurement of joint deflection for central misaligned joint.

and R_s = radius to stud.

The position of maximum compression in the packing material is important as this defines the line of symmetry for the coupling stress analysis. The theoretical position was deduced from the three joint gap measurements as the packing material deformed to the profile dictated by the joint deflection. The relative position (κ) is deduced from:-

$$\kappa = \tan^{-1} \left[\frac{\sqrt{3}(h_3 - h_2)}{(h_2 + h_3 - 2h_1)} \right] \quad [9] \quad (6.2)$$

Where κ is measured clockwise (looking at pipe A, Figure 5.1.), from offset stud h_1 within the following ranges:-

Ranges for κ	$h_3 > h_2$	$h_3 < h_2$
$h_2 + h_3 > 2h_1$	$0^\circ - 90^\circ$	$270^\circ - 360^\circ$
$h_2 + h_3 < 2h_1$	$90^\circ - 180^\circ$	$180^\circ - 270^\circ$

Table 6.2.: Identification of correct range for κ [9].

6.3. MEASUREMENT OF PIPE-PACKING-PIPE CONTACT ZONE.

The pipe-packing-pipe contact zone for open joints was determined by placing a 0.04 mm 'feeler gauge' between the packing material and the pipe-end and marking the position that the gauge was no longer able to penetrate, on both sides of the joint. The

radial distance from position h_1 (located at the open side of the joint) to the zero stress level in the pipe-packing (Figure 3.4b) was measured by tape measure. Plate 6.1. Illustrates the open joint and pipe-packing-pipe contact zone.

6.4. MEASUREMENT OF APPLIED JACKING FORCE.

The jacking force was applied by a large capacity hydraulic cylinder and operated by a constant pressure pump at working pressures up to 600 Bar gauge pressure. Two cylinders were used during the experimental programme depending upon the jacking force required. The cylinder details are summarised below:-

Cylinder Reference	Action	Capacity of cylinder (kN)
HC1	Single	1500
HC2	Dual	2000

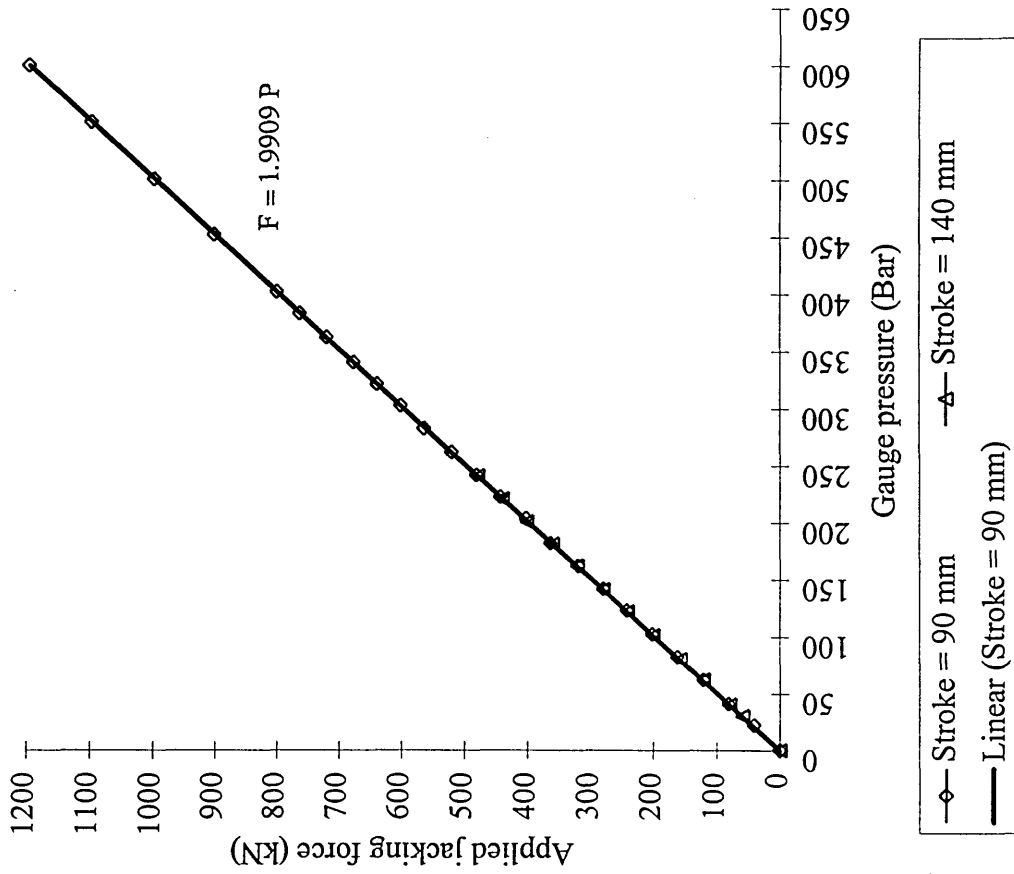
Table 6.3.: Summary of hydraulic cylinder details.

The cylinders were calibrated using a servo-controlled testing machine with calibrated readout (in kN) against a 250 mm diameter 0 to 600 Bar pressure gauge with resolution of 1 Bar gauge pressure. The calibration of gauge pressure with applied force for cylinders HC1 and HC2 is illustrated in Figures 6.2. (a) and (b) respectively.



Plate 6.1. Illustration of open joint showing packing ring and offset studs on DN 250mm pipes.

(a): Calibration function for cylinder HC1



(b): Calibration function for cylinder HC 2.

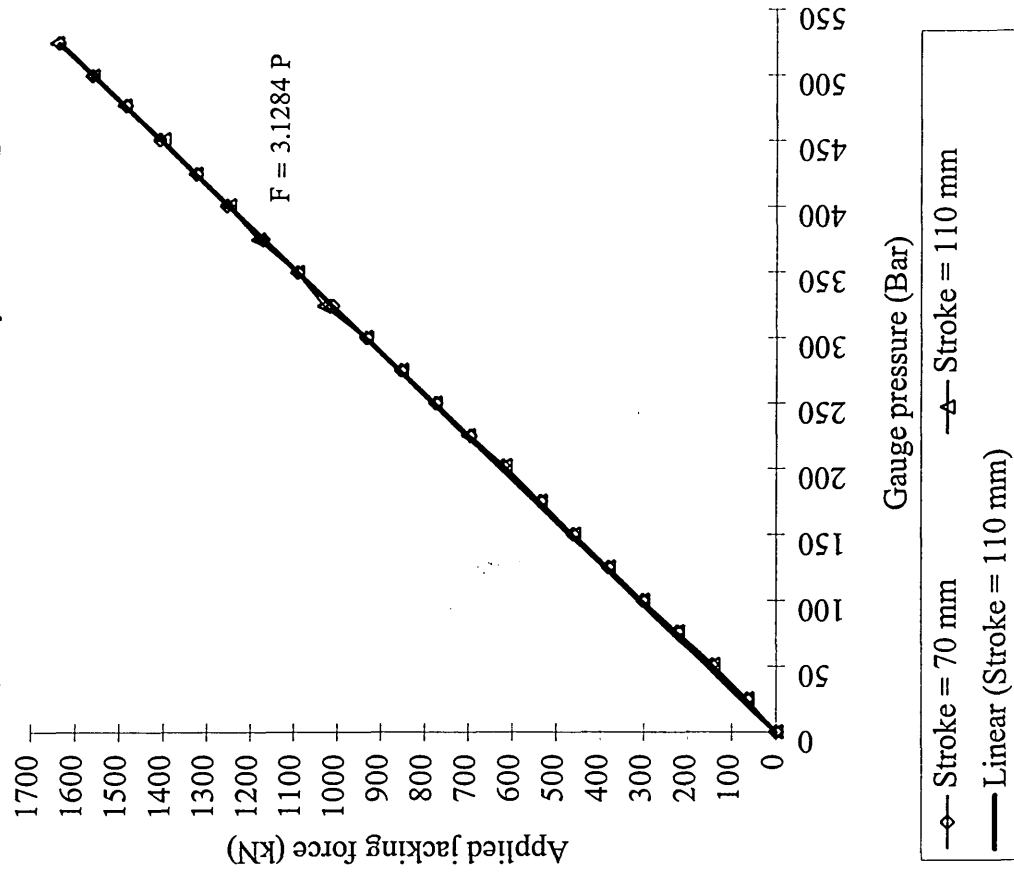


Figure 6.2.: Relationship between hydraulic gauge pressure and applied force for cylinders HC 1 and HC 2.

Increments of gauge pressure were transposed to applied jacking force using the following calibration functions:-

$$\text{For HC 1 : } F = 1.9909P \quad (6.3)$$

$$\text{For HC 2 : } F = 3.1284P \quad (6.4)$$

Where P = Gauge pressure recorded on dial gauge.

Plate 6.2. illustrates the calibration of cylinder HC 1.

6.5. MEASUREMENT OF LATERAL FORCE AT MISALIGNED JOINT.

The lateral force induced across the central misaligned joint was measured by placing a 250 kN load cell beneath the deflected spigot (Figure 6.3). Measurement of lateral force at each increment of jacking force was recorded. The accuracy of measurement for the load cell was 0.5 percent at full scale reading (250 kN) with a resolution of 1 kN.

6.6. MEASUREMENT OF COUPLING SURFACE STRAINS BY ELECTRICAL RESISTANCE STRAIN GAUGES.

To verify the coupling stress model presented in chapter 4, electrical resistance strain gauge rosettes were fixed to the surface of the coupling specimens and tested in

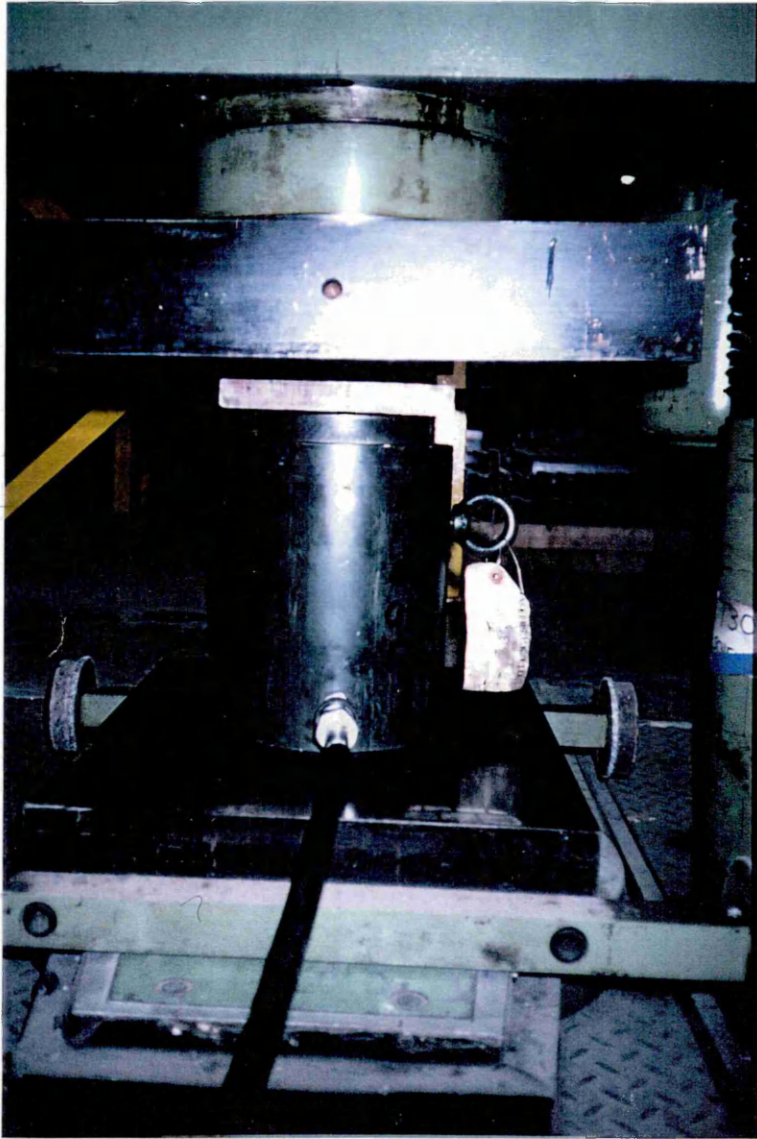
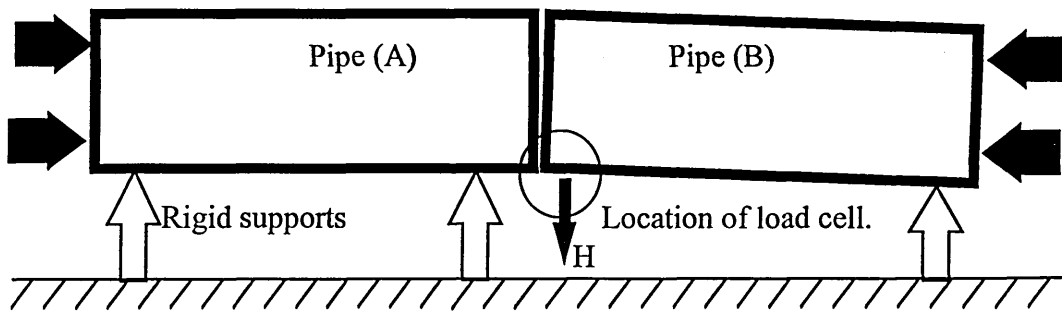
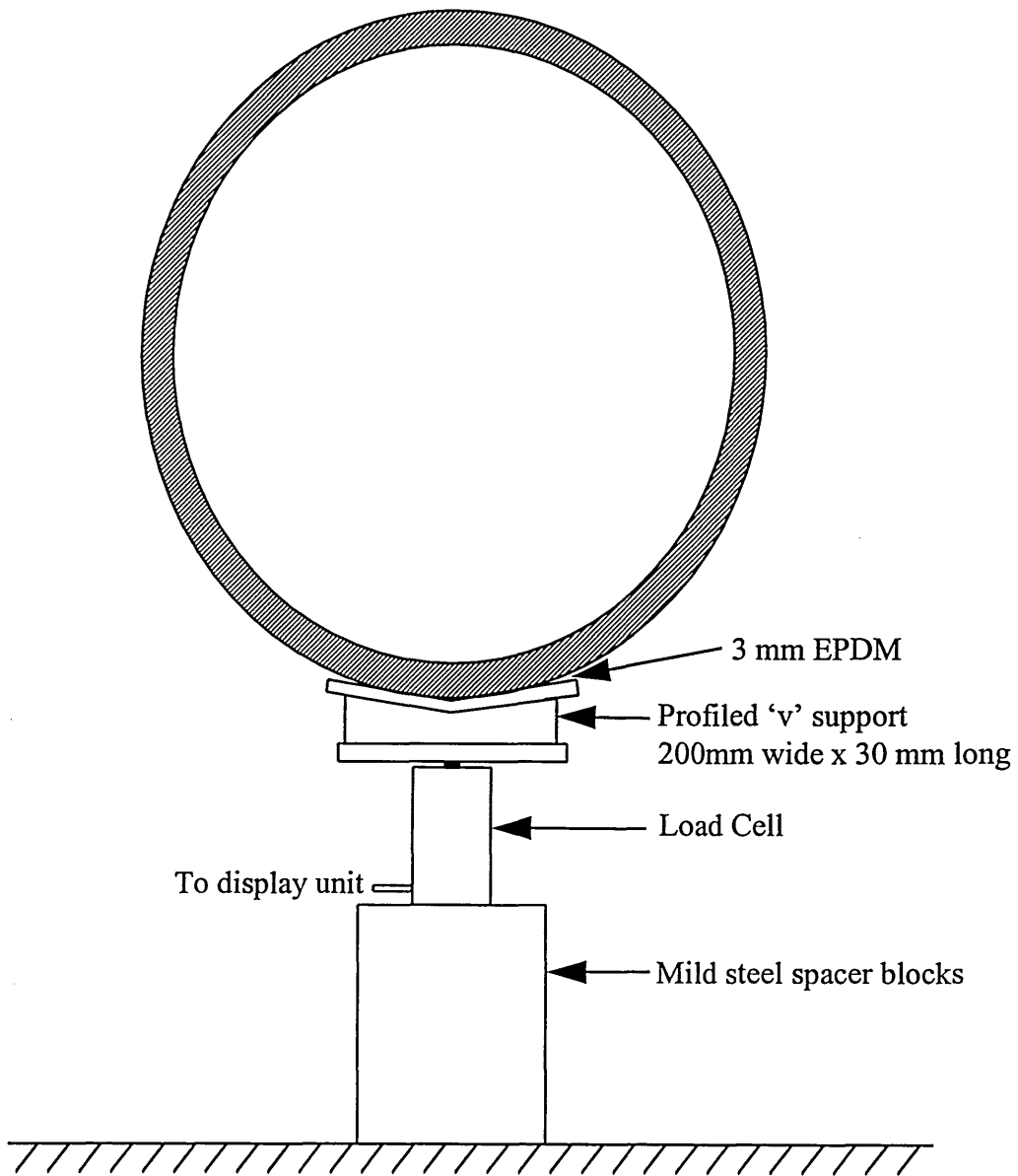


Plate 6.2. Calibration of cylinder HC1 using servo-controlled testing machine.



(a) Location of load cell.



(b) Detail of load cell arrangement.

Figure 6.3.: Load cell arrangement for lateral force measurement.

accordance with 6.9. The rosettes were linked to a multiplexer and scanned in turn by a PC driven strain monitoring work station.

Principal strain and maximum shear strain were measured using 45° rectangular strain gauge rosettes fixed at discrete intervals on the coupling surface. Principal stresses and maximum shear stresses were deduced using the material properties of stainless steel outlined in 5.6.1. and equations 6.5. and 6.6. (below).

Micro Measurements strain gauge rosettes [31] cast with polyimide backing and encapsulated, with a gauge length of 4 mm were used throughout the experimental investigation, and were fixed in accordance with the manufacturers recommendations [32,33,34].

Surface preparation of the gauge location was carried out in accordance with Measurements Group recommendations [34]. Typical gauge fixings are illustrated in Plate 6.3. for coupling test C2.

The principal stress and maximum shear stress can be found using the formula for the 45° rectangular rosette [35,36]:-

$$\begin{matrix} \sigma_{\max} \\ \sigma_{\min} \end{matrix} = \frac{E}{2} \left[\frac{\epsilon_1 + \epsilon_3}{1 - \nu} \pm \frac{\sqrt{2}}{1 + \nu} \sqrt{(\epsilon_1 - \epsilon_2)^2 + (\epsilon_2 - \epsilon_3)^2} \right] \quad (6.5)$$

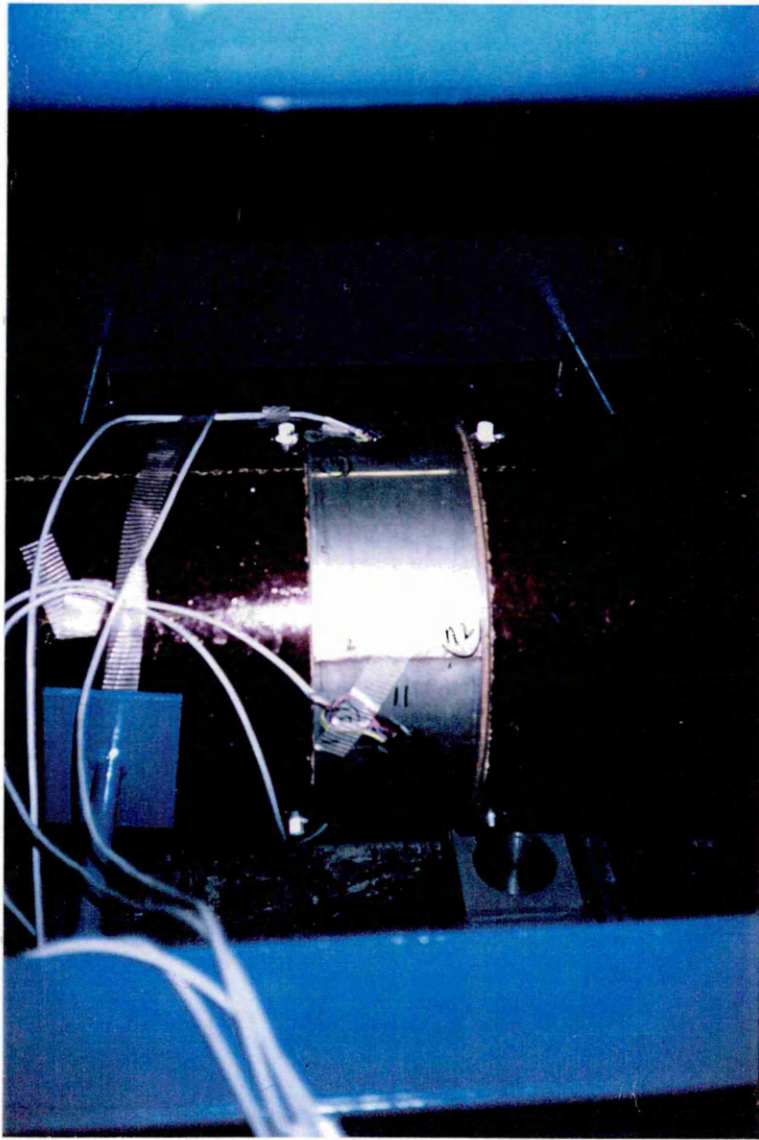


Plate 6.3. Strain gauge rosettes fixed to coupling specimen C2 under test conditions.

$$\tau_{\max} = \frac{(\sigma_{\max} - \sigma_{\min})}{2} \quad (6.6)$$

Where:

ε_1 and ε_3 are mutually perpendicular gauge readings of the rosette,

ε_2 is the gauge reading orientated at 45° to ε_1 and ε_3 ,

E is the modulus of elasticity of the stainless steel material, and

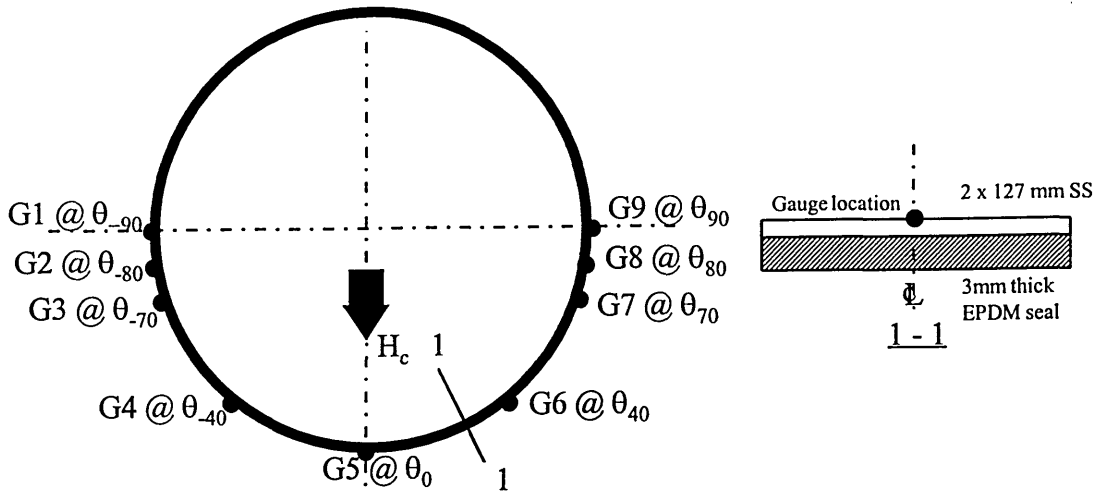
ν is its Poisson's ratio.

6.6.1. ELECTRICAL RESISTANCE STRAIN GAUGE ROSETTE FIXING DETAILS.

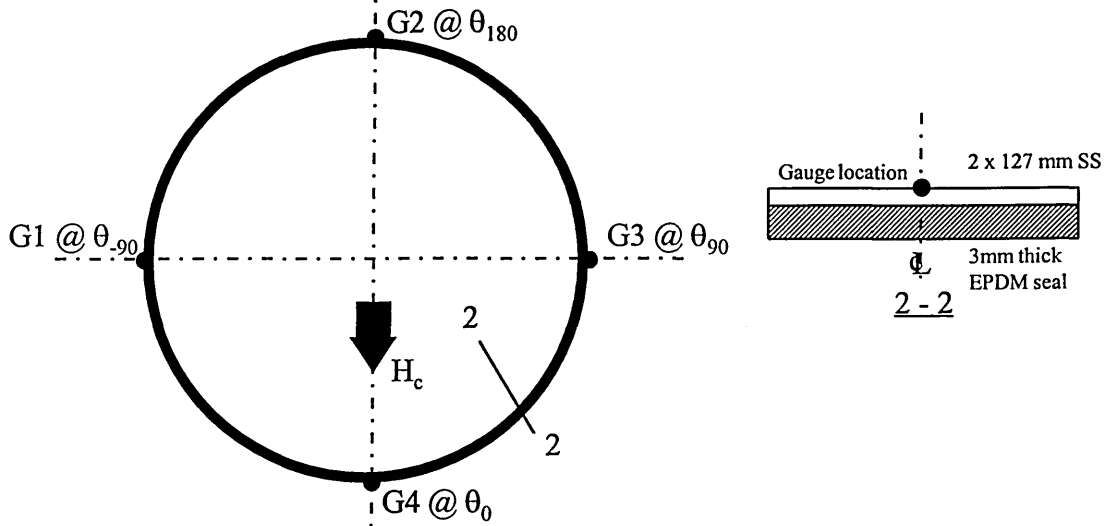
Figures 6.4.(a) to (c) illustrate the gauge locations used for coupling experiments C1 through C3 respectively.

6.7. SOURCES OF UNCERTAINTY AND ACCURACY IN EXPERIMENTAL MEASUREMENTS.

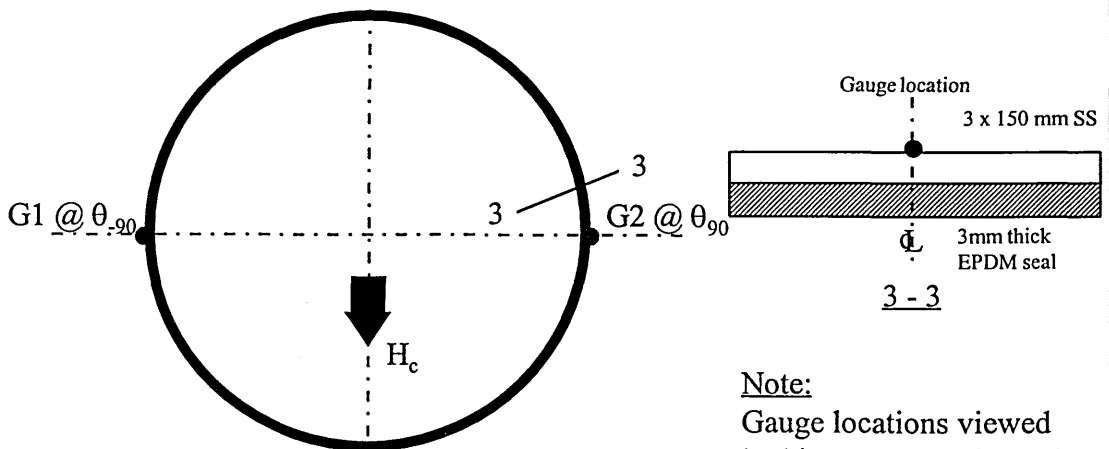
Possible sources of uncertainty in experimental measurements were identified in order to assess the accuracy of the experimental data. The possible sources of uncertainty and measures taken to control accuracy in experimental measurement during lateral force



(a): Strain gauge rosette location details for test C1.



(b): Strain gauge rosette location details for test C2.



(c): Strain gauge rosette location details for test C3.

Note:
Gauge locations viewed
looking towards pipe (A).

Figure 6.4. Electrical strain gauge rosette location details for coupling stress analysis.

determination and coupling stress analysis experiments (6.8., 6.9.), are shown in Table 6.4.

6.8. EXPERIMENTAL PROGRAMME FOR LATERAL FORCE MODEL VERIFICATION.

The experimental set-up used for the lateral force experiments is illustrated schematically in Figure 6.5. (a). The pipes were aligned such that the pipe-ends at the loading plate and reaction plate were in full contact with the jacking frame, resulting in concentric application of jacking force at the ends of the pipe.

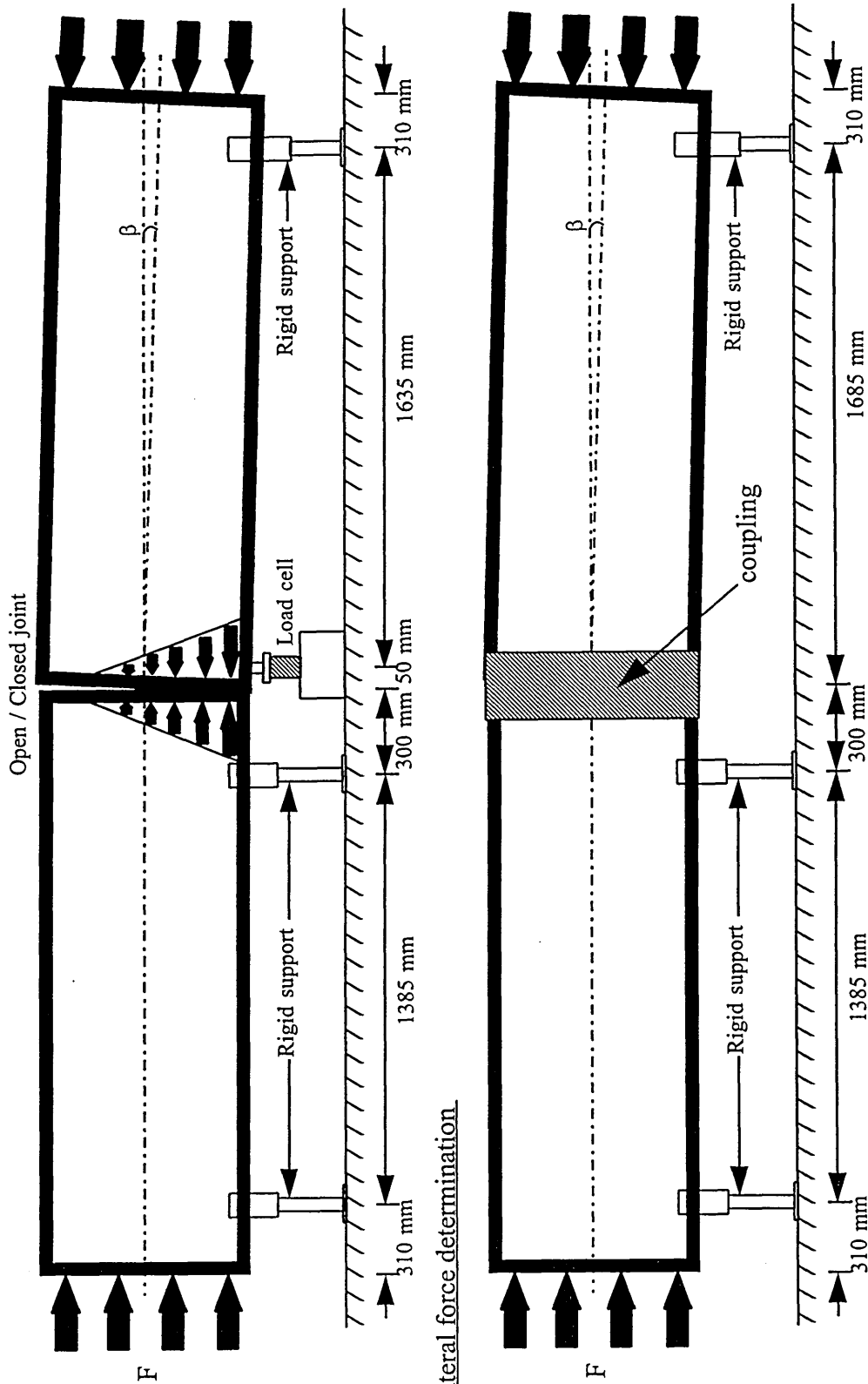
The deflected central joint was aligned such that the eccentricity of the jacking force was located in the lower half of the joint, resulting in the lateral force being directed towards ground through the load cell arrangement. Single thickness chipboard packing rings were inserted between all pipe-end interfaces (as specified in 5.5).

6.8.1. OPEN JOINT TEST PROCEDURE.

The joint misalignment was pre-set at an initial angle such that the joint was open. The jacking force was applied in increments of 25 Bar (78.183 kN for HC 2) with the following measurements taken at each increment:-

Measurement	Type of uncertainty	Source of uncertainty	Measures taken to reduce errors	Accuracy of measurements
Hydraulic Gauge Pressure	Systematic / Random	Instrumentation calibration / Flow control.	Flow calibrated against known load for each cylinder. Other experimental measurements made when steady flow achieved.	± 0.2 % Full scale reading. ± 2.0 % at 50 Bar gauge pressure.
Lateral Force	Systematic	Instrumentation calibration.	Certified calibration.	Load cell + Read out combined accuracy ± 0.5 % at Full scale reading
Joint Offset Distances	Random	Human Judgement.	Two measurements averaged.	$\beta \pm 1$ % for DN 250 reducing with increased pipe diameter. $\kappa \pm 40$ % at 1° (DN 250) $\kappa \pm 8$ % at 17° (DN 250)
Surface Strain	Systematic / Random	Instrumentation calibration / Gauge fixing precision.	Shunt calibration / Manufacturers installation procedures adhered to.	Calibrated against 1000 $\mu\epsilon \pm 0.1$ %. Resolution of $\pm 1.0 \mu\epsilon$

Table 6.4. Summary of uncertainty analysis and accuracy of measurements recorded during experimental programme.



(a): Lateral force determination.

(b): Coupling stress analysis.

Figure 6.5.: Experimental arrangement for lateral force determination and coupling stress analysis.

- Applied jacking force
- Lateral force less self weight of deflected pipe.
- Offset distances h_1 , h_2 and h_3 - for the determination of β and κ .
- Packing-pipe contact zone at open joint.

6.8.2. OPEN/CLOSED JOINT TEST PROCEDURE.

The joint misalignment was pre-set at an initial angle such that the joint was just open. The hydraulic pressure in the jack was applied in 25 Bar increments (78.183 kN thrust for HC 2) with the following measurement taken:-

- Applied jacking force
- Lateral force less self weight of deflected pipe.
- Offset distances h_1 , h_2 and h_3 - for the determination of β and κ .
- Packing-pipe contact zone while joint open.

The joint was initially open to investigate the effect of a joint closing under the action of a lateral force. The relative difference between the longitudinal jacking stress levels in the pipe barrel at either side of the joint ($\sigma_{p_{min}}$ and $\sigma_{p_{max}}$, Figure 3.2.) was not quantifiable, therefore the prediction of lateral force during the closed joint case was not possible. When the joint had closed the increase in lateral force induced at the misaligned joint was monitored with respect to the applied jacking force and the joint alignment.

6.8.3. LATERAL FORCE SHARING BETWEEN PIPE-PACKING FRICTION AND STRUCTURAL ELEMENT OF COUPLING.

To simulate the effect of the rubber seal element on the force acting on the coupling, a nominal 3.0 mm thick E.P.D.M. strip with a hardness value of 70, was placed between the pipe and the load cell. The open / closed joint lateral force tests were then repeated in accordance with 6.8.2. The value of ρ for equation 4.1. could then be assessed for the subsequent coupling experiments (see 6.9) for joint designs incorporating chipboard packing material.

A summary of the experimental programme for the determination of lateral force is shown in Table 6.5.

6.9. EXPERIMENTAL PROGRAMME FOR COUPLING STRESS ANALYSIS.

The experimental set-up used for the coupling stress analysis is illustrated in schematically in Figure 6.5. (b). The pipes were aligned such that the pipe-ends at the loading plate and reaction plate were in full contact with the jacking frame. The displaced joint was set-up such that the position of maximum compression in the packing material was located at the invert of the joint. The hydraulic gauge pressure in the jacking cylinder was applied in increments of 25 Bar (78.183 kN thrust for HC 2) with the following measurements taken:-

Test Reference	Pipe Class (DN)	Open / Closed Joint	3 mm Rubber sleeve	Packing material thickness, a_0 (mm)	Maximum Jacking force (kN)
ST 1A	250	Open	No	8	780
ST 1B	250	Open	No	8	780
ST 2A	250	Closed	No	8	780
ST 2B	250	Closed	No	8	780
ST 2C	250	Closed	No	8	780
ST 2D	250	Closed	Yes	8	780
ST 3A	400	Open	No	10	1485
ST 3B	400	Open	No	10	1485
ST 3C	400	Open	No	10	1485
ST 4A	400	Open/Closed	No	10	1485
ST 4B	400	Open/Closed	No	10	1485
ST 4C	400	Open/Closed	No	10	1485
ST 4D	400	Open/Closed	Yes	10	1485
ST 4E	400	Open/Closed	Yes	10	1485
ST 5A	600	Open/Closed	No	16	1560
ST 5B	600	Open/Closed	No	16	1560
ST 5C	600	Open/Closed	No	16	1560
ST 5D	600	Open/Closed	Yes	16	1560
ST 5E	600	Open/Closed	Yes	16	1560

Table 6.5: Summary of lateral force determination.

- Applied jacking force.
- Offset distances h_1 , h_2 and h_3 - for determination of β and κ .
- Strain induced in coupling for all gauge locations.

The electrical resistance strain gauge rosettes were fixed on the surface of the coupling in different configurations with the aim of verifying the coupling stress model. Table 6.6. illustrates the experimental programme for the coupling stress model verification.

Test reference	DN Class	Joint	Packing material thickness, a_0 (mm)	Maximum jacking force (kN)
C1	400	Open/Closed	10	1172
C2	250	Open/Closed	8	780
C3	250	Open	8	780

Table 6.6. Summary of coupling stress analysis programme.

6.10. MAIN CONCLUSIONS.

The following conclusions maybe drawn from the instrumentation and measurement of experimental parameters:-

- 1) The deflected joint characteristics can be deduced with sufficient accuracy using the procedure outlined in 6.2. and equations 6.1 and 6.2. Although the possible error in calculating the theoretical position of maximum compression in the packing material (κ) seems high (up to 40 % at low values of κ), errors in terms of κ in all cases result in approximately 1 degree, which is satisfactory.
- 2) The transformation from surface strains to principal stresses using 45° rectangular strain gauge rosettes can be made using equation 6.5. and the elastic properties for stainless steel coupling (5.6.1).
- 3) The experimental test set-up for the coupling stress analysis was identical to the lateral force experiments so that correlation between lateral force and coupling stresses could be assessed. An assessment of the value of ρ for equation 4.1. was made based on the load sharing characteristics of the joint configuration.

CHAPTER 7

EXPERIMENTAL RESULTS AND DISCUSSION.

7.1. INTRODUCTION.

The structural interaction of the pipe-packing-coupling system was investigated experimentally as described in chapter 6 with the aim of verifying the mathematical models presented in chapters 3 and 4. In this chapter the experimental results are presented and discussed in light of the model predictions in the following sequence:-

- 1) Pipe-packing interaction and correlation with modified Australian Concrete Pipe Association Linear Stress Approach (ACPALSA) for the prediction of pipe-packing contact zone at open joints.
- 2) Lateral force acting at open and closed joints and correlation with open joint lateral force model.
- 3) Coupling stress analysis and correlation with mathematical model.

In all experiments the deflected central joint was constantly monitored for changes in alignment in order that the models could be compared directly with experimental results.

7.2. PIPE-PACKING INTERACTION.

The prediction of pipe-packing contact zone available for transmission of longitudinal jacking force at open joints is necessary in order to predict the eccentricity of jacking force about the pipe axis. In turn the eccentricity of the jacking force determines the lateral force acting at a misaligned joint (see chapter 3). The contact zone was studied for chipboard packing material and clay pipes as described in 6.8.1.

Figures 7.1. to 7.3. show the change in pipe alignment and pipe-packing interaction at the misaligned joint with respect to longitudinal jacking force for tests ST1A, ST1B; ST3A, ST3B, ST3C; ST5A, ST5B, ST5C, ST5D and ST5E respectively.

The joint deflection in all cases reduced as a function of applied jacking force. Conversely, the pipe-packing interaction increased as a function of applied jacking force and joint deflection.

The concept of pipe bending has been proposed by Haslem [10] and supported by field evidence from Norris [9] for the reduction in pipe misalignment due to longitudinal jacking force through deflected joints. The eccentricity of the jacking force at the deflected joint induces bending in the pipe which causes elastic deformation tending to close the gap in a deflected joint. This phenomenon could explain the reduction in joint misalignment experienced during the experimental phase of this study.

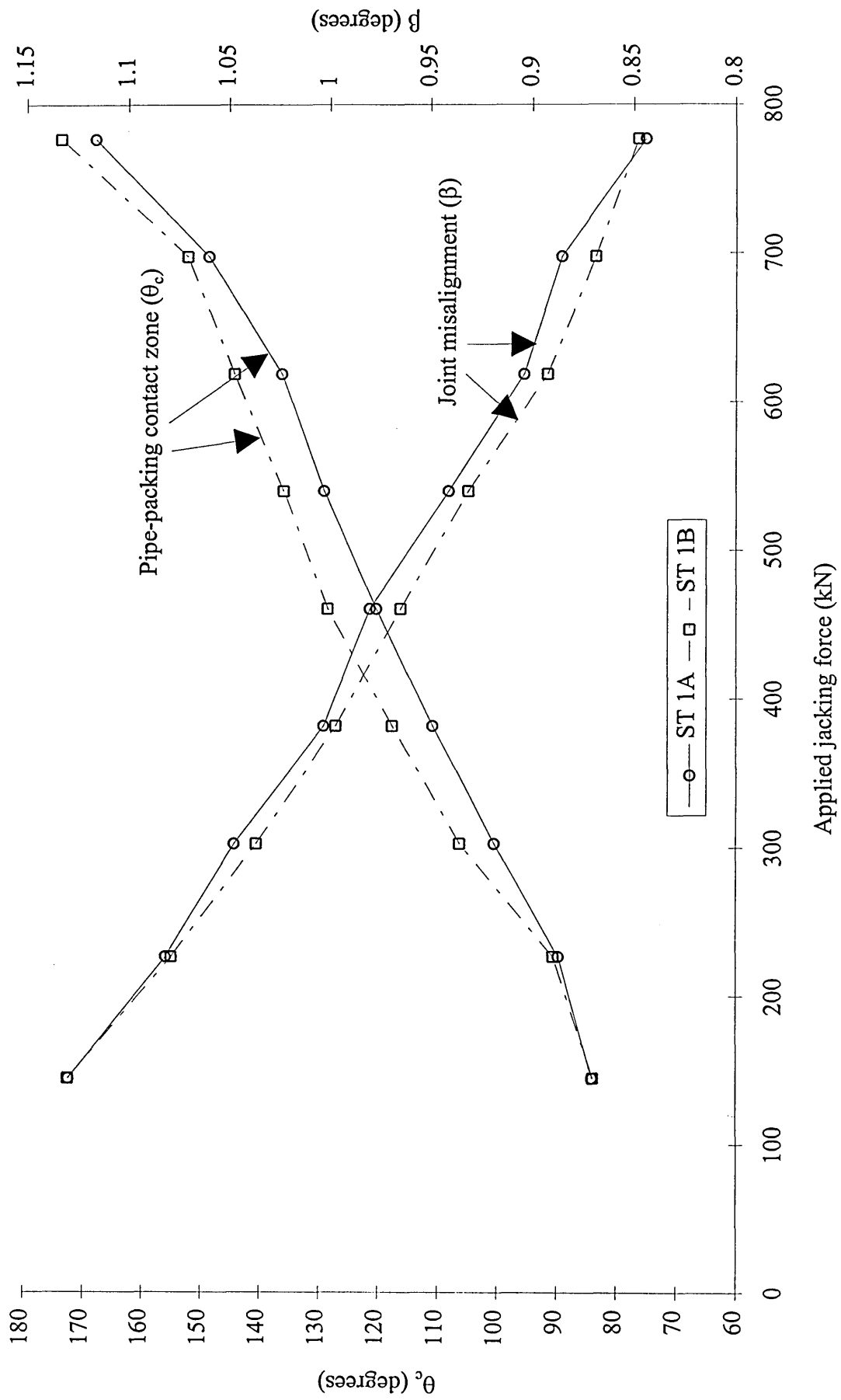


Figure 7.1. Misaligned open joint characteristics during lateral force tests ST1A-ST1B for DN 250 mm pipes.

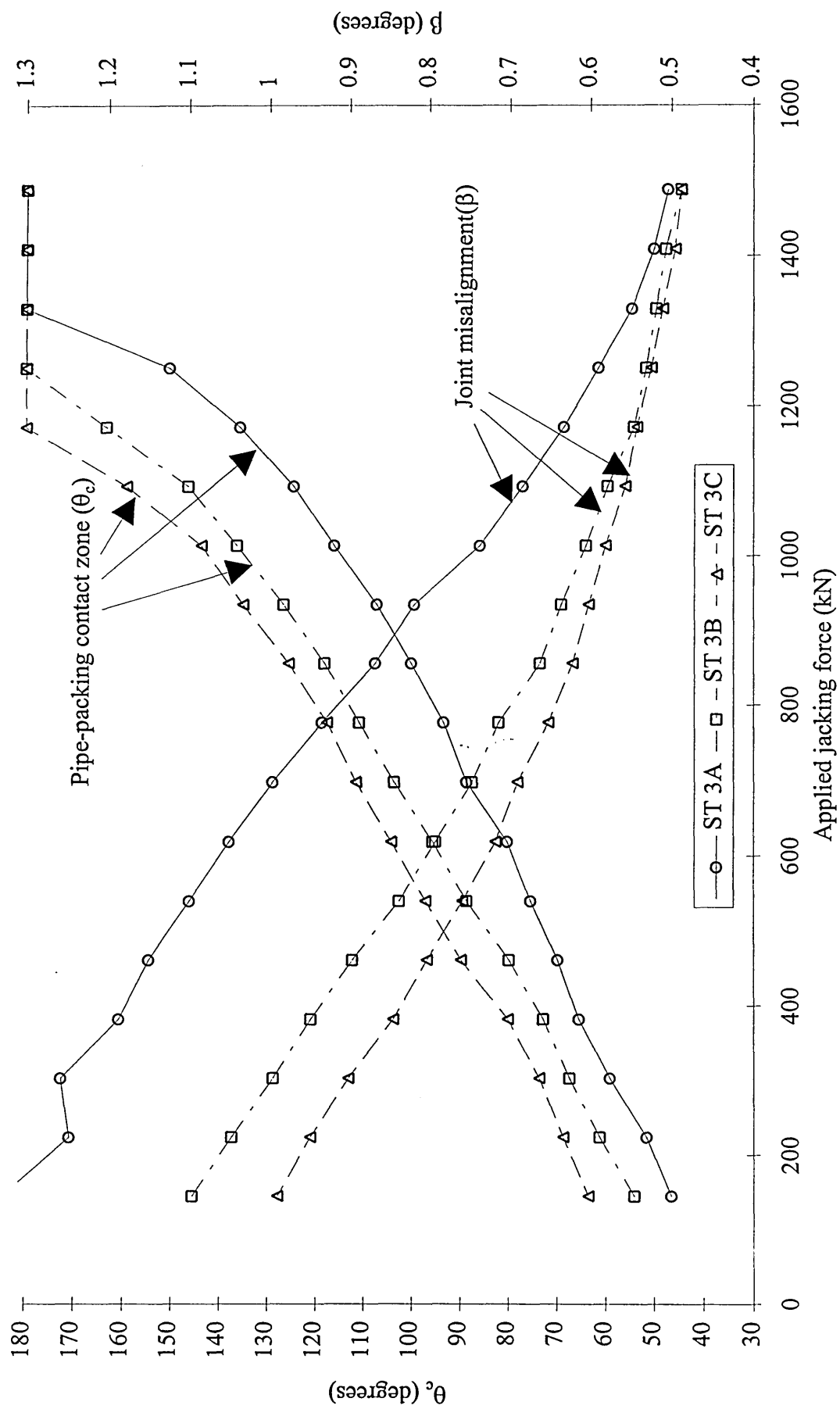


Figure 7.2. Misaligned open/closed joint characteristics during lateral force tests ST3A, ST3B and ST3C for DN 400 mm pipes.

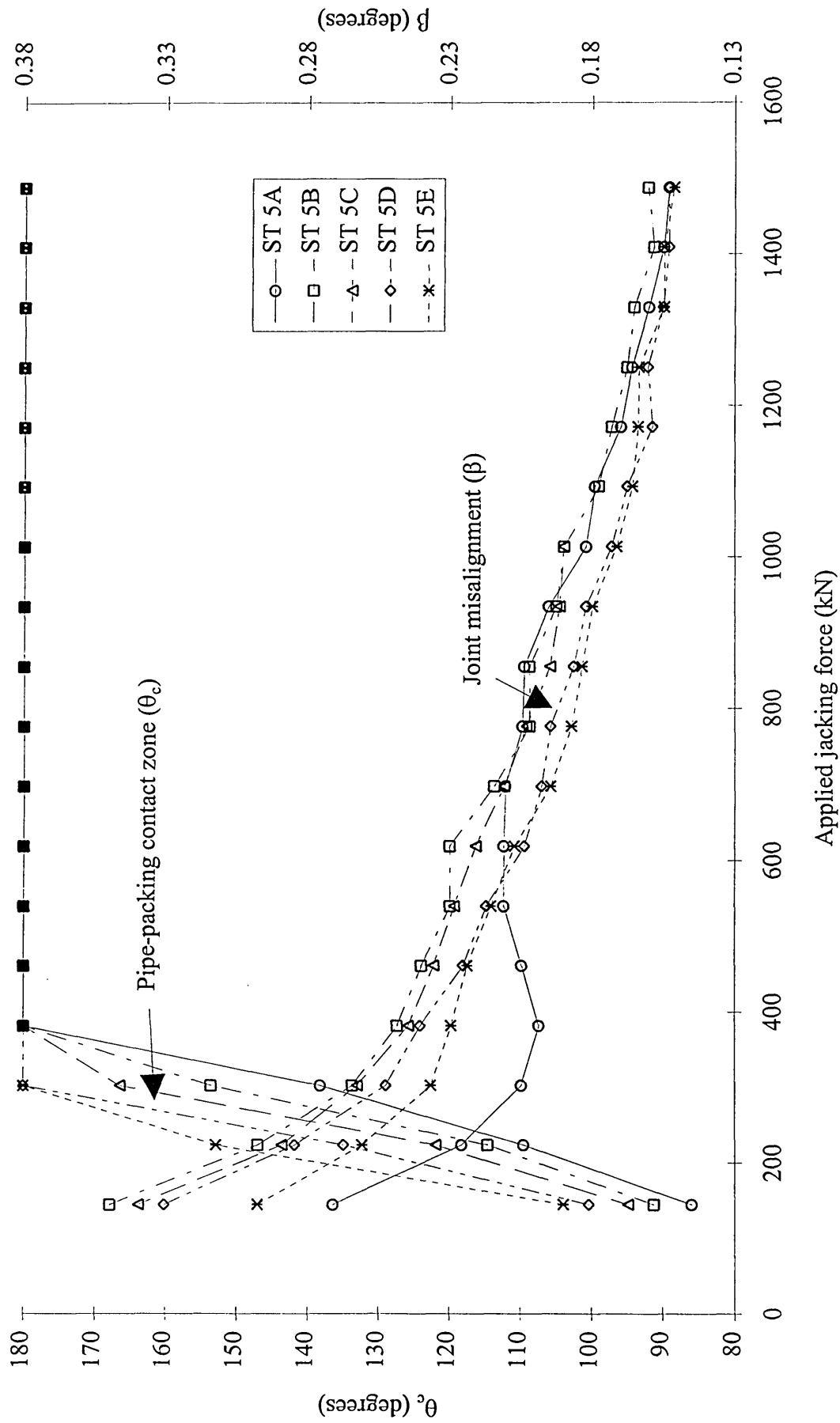


Figure 7.3. Misaligned open/closed joint characteristics for lateral force tests ST5A, ST5B, ST5C, ST5D and ST5E for DN 600 mm pipes.

It follows that the pipe-packing contact zone is a function of the following parameters:-

- 1) Misaligned joint deflection.
- 2) Applied jacking force.
- 3) Material properties of the pipe and packing material.

Any prediction of the contact zone interaction at open joints should therefore be related to the points above. It can be seen that the model for the prediction of pipe-packing interaction presented in chapter 3 (equations 3.30./2.7.) does incorporate all of the points discussed in (1) to (3) above indicating the validity of the model.

The joint elasticity (E_j) defined by equation 2.7. was determined from the following parameters:-

- 1) Stress-strain characteristics of the chipboard packing material.
- 2) The elastic properties of the clay pipes.
- 3) Geometric properties of the joint arrangements used in this study.

The stress-strain characteristics of the chipboard packing material used in this study are shown in Figures 5.3., 5.4. and 5.5. The tangent modulus of elasticity of the chipboard (E_p) was taken at a stress state corresponding to the applied jacking force, and equation 3.28. was used for the correlation between theory and experimental observations of the pipe-packing interaction. Due to the permanent deformation of the chipboard material

the tangent modulus was taken for the load cycle under consideration in tests ST1 to ST5.

The tangent modulus of elasticity of the chipboard was determined by differentiating the equation of the line of best fit of the stress-strain curve in the region of interest. Appendices A1 to A8 show the stress-strain relationships for chipboard packing material of nominal thickness of 8mm, 10mm and 16mm under the stress state encountered during pipe joint interaction experiments ST1A to ST5E.

Table 7.1. shows typical values of tangent modulus for chipboard packing material and the corresponding joint elasticity as defined by equation 2.7.

	DN Class (mm)	Jacking force, F (kN)	$\sigma_{p_{max}}$ (N/mm ²)	E_p (N/mm ²)	E_j (N/mm ²)
First cycle	250	302.7	21.9	113.6	74.8
	400	302.7	16.3	120.2	77.7
	600	302.7	6.32	62.3	57.8
Second cycle	250	302.7	20.9	308.1	128.1
	400	302.7	14.4	254.3	122.5
	600	302.7	5.95	126.9	95.0
Note: Modulus of elasticity for vitrified clay pipes = 50 kN/mm ² . [5]					

Table 7.1. Typical joint elasticity's derived for experimental programme.

During the first load cycle for the chipboard material the loose structure is consolidated by large compressive axial strain leaving a denser structure after removal of the load.

Applying the same stress level on subsequent load cycles produces less compressive strain therefore increases the modulus of elasticity. The tangent modulus for the first cycle is therefore significantly lower than on subsequent load cycles. This is shown in Table 7.1. The elasticity of the material is also stress dependant in the working stress region of the packing rings (less than 50 N/mm²). This can be seen in Figures 5.3. to 5.5. and ignoring the behaviour during cycle one.

The experimental parameters given in equation 3.30. were evaluated with regard to the previous discussion and plotted with respect to the contact zone (θ_c). Figure 7.4. shows the correlation with theoretical values. Two distinct trends were evident, the prediction of pipe-packing interaction for the first cycle and that of subsequent cycles.

The joint elasticity for virgin packing material is significantly lower than subsequent load cycles (Table 7.1) and leads to higher values of 'm' (for equation 3.31.) as indicated by the trend depicted in Figure 7.4. for the first cycle loading (ST1A, ST2A and ST3A). The correlation with equation 3.31. has been achieved in Figure 7.4. using values of η of 0.6 and 0.28 corresponding to the prediction of pipe-packing contact zone for the first and subsequent load cycles respectively.

It can be seen from Figure 7.4. that the modified relationship between 'm' and θ_c for the first and subsequent load cycles can be used for chipboard material for the prediction of packing-pipe contact zone. Packing rings of other materials should be tested to confirm the empirical scaling factors appropriate for the material.

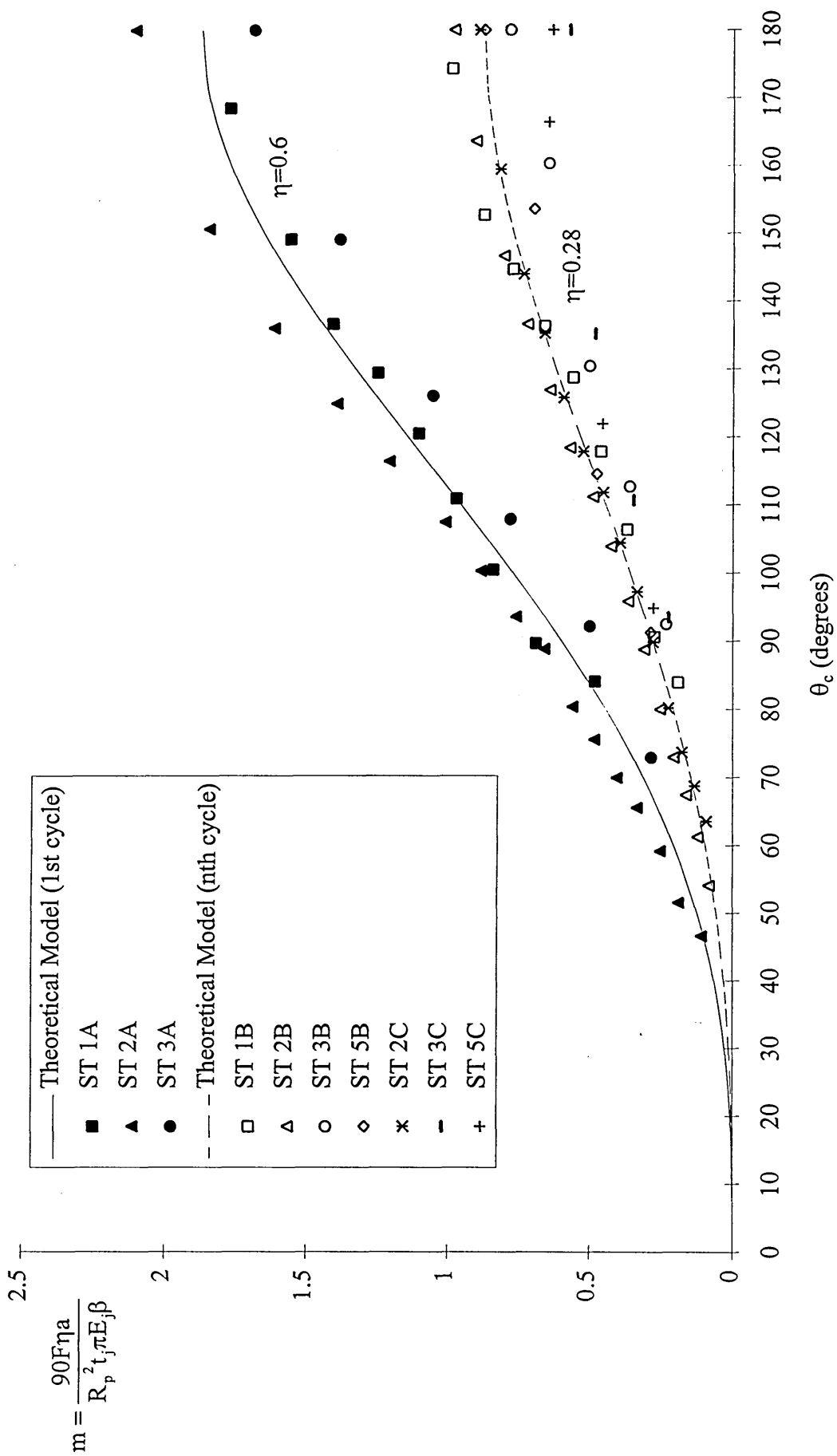


Figure 7.4. Correlation between experimental results and theoretical relationship for θ_c and m , for pipe diameters in the range 250mm to 600mm.

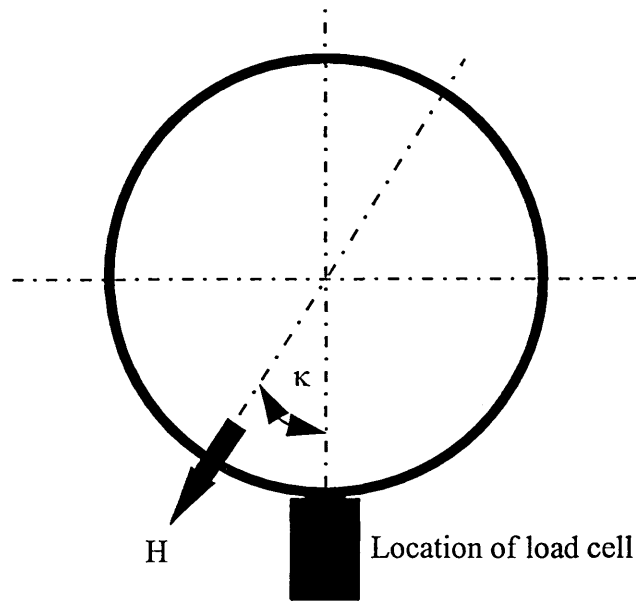
7.3. LATERAL FORCE ACTING AT A MISALIGNED JOINT.

The resultant lateral force acting at a misaligned joint was investigated in accordance with the experimental programme given in 6.8. A distinction was made between open and closed misaligned joints in chapter 3 and is adopted here in the analysis of the experimental results.

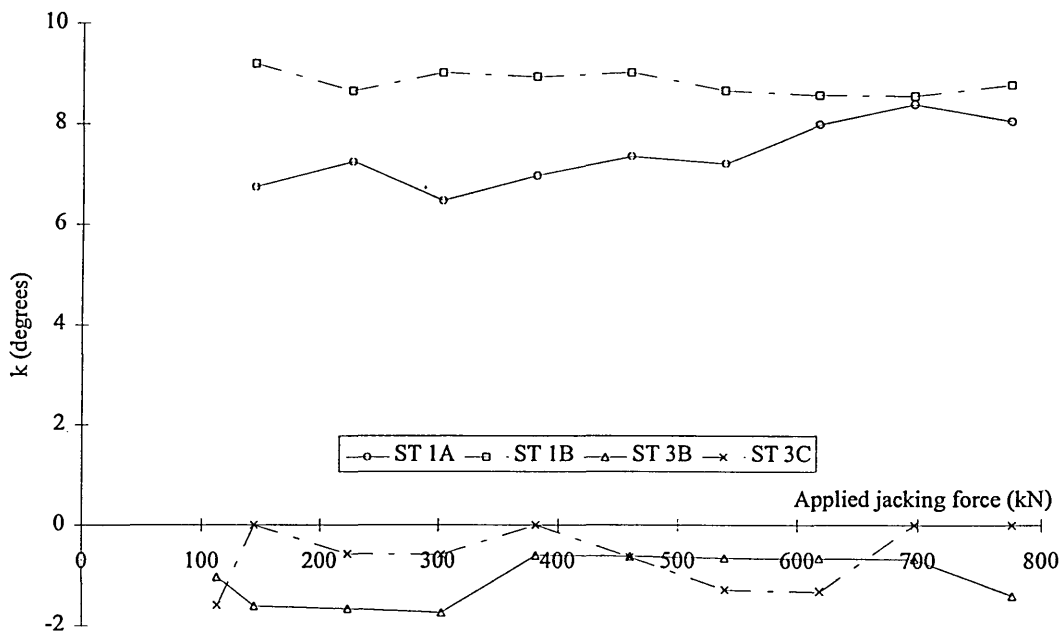
7.3.1. LATERAL FORCE ACTING AT AN OPEN MISALIGNED JOINT.

In order to correlate experimental measurement of lateral force with the theoretical model prediction as given by equation 3.1., the joint alignment parameters were monitored throughout the tests. The prediction of the lateral force acting across the deflected joint was determined using equation 3.27. and 3.2. and from the experimental measurement of the pipe-packing contact zone (θ_c).

Due to lateral movement of the pipe system under test conditions the position of maximum compression of the packing material moved from its original position at the pipe invert. This movement was monitored using equation 6.2. in order that the line of action of the lateral force could be defined relative to the position of the load cell. Figure 7.5. shows the relationship between position of maximum compression in packing material and applied jacking force for test ST1A/ST1B and ST3B/3C.



(a) General arrangement of experimental measurement of lateral force and its line of action.



(b) Relationship between applied jacking force and angular deviation of position of maximum compression in packing material for ST1A-ST1B and ST3B-ST3C.

Figure 7.5. Deviation of line of action of lateral force from vertical in open joint tests.

The prediction of lateral force throughout the test was made taking into account the conditions mentioned above. Figures 7.6. and 7.7. show the correlation between experimental measurement and the theoretical prediction for test ST1A/ST1B and ST3B/ST3C.

The Figures show good correlation between experimental and theoretical values with the theoretical model overestimating experimental observations in all cases. The difference between the theoretical prediction and experimental values decreased as the jacking force (i.e. lateral forces) increased. The percentage difference was observed to range from 30 percent down to 4 percent.

The good correlation outlined above confirms the validity of the theoretical model presented in chapter 3 for the analysis of open joints and in particular to the following parameters:-

- 1) Eccentricity of jacking force at open joint - equation 3.37.
- 2) Inclination of jacking force through deflected pipe train - equation 3.2.
- 3) Component of jacking force acting across deflected open joint (lateral force) - equation 3.1.

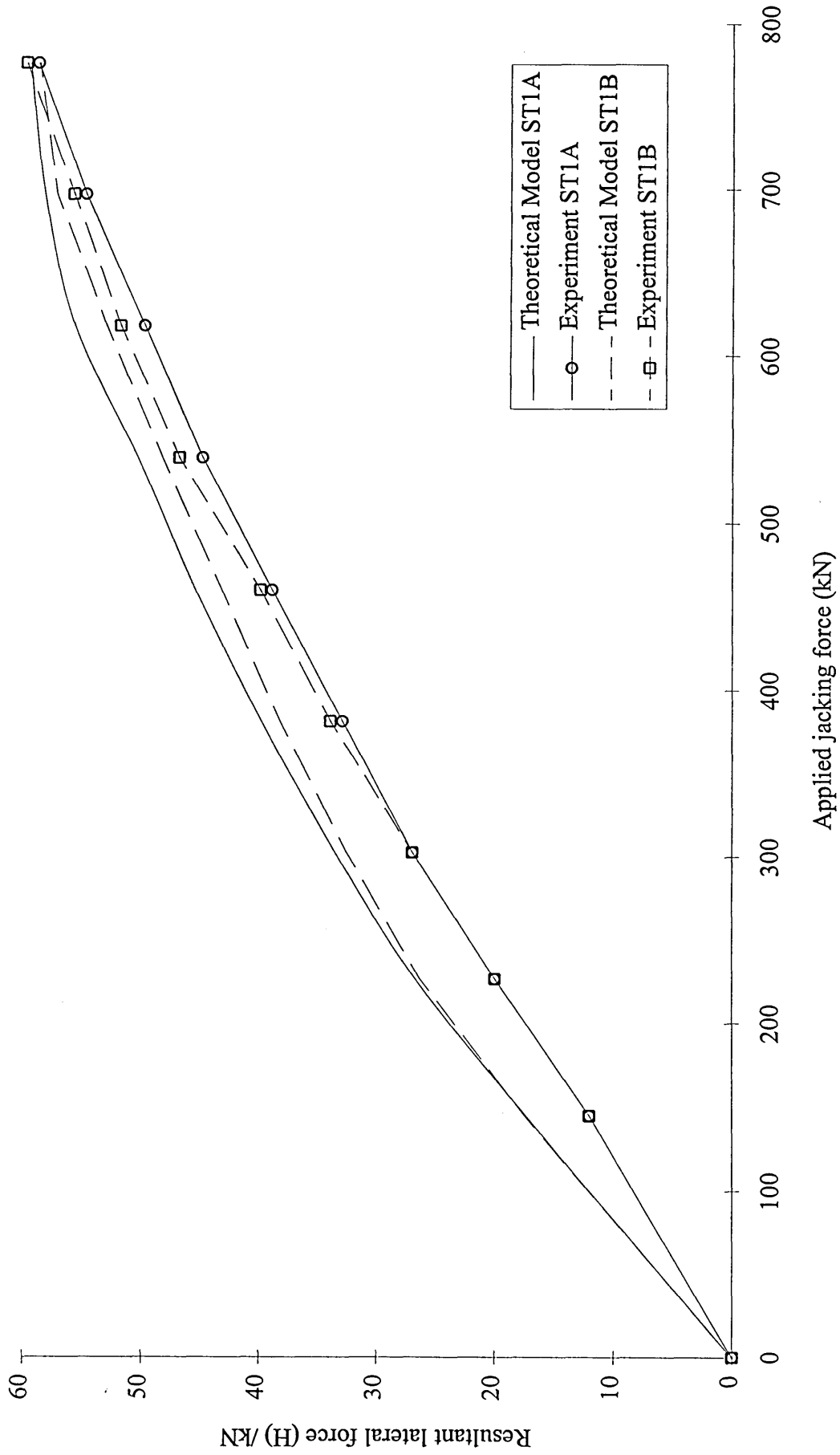


Figure 7.6. Correlation between experimental measurement and theoretical prediction for lateral force based on joint alignment data for tests ST1A and ST1B for DN 250mm pipes.

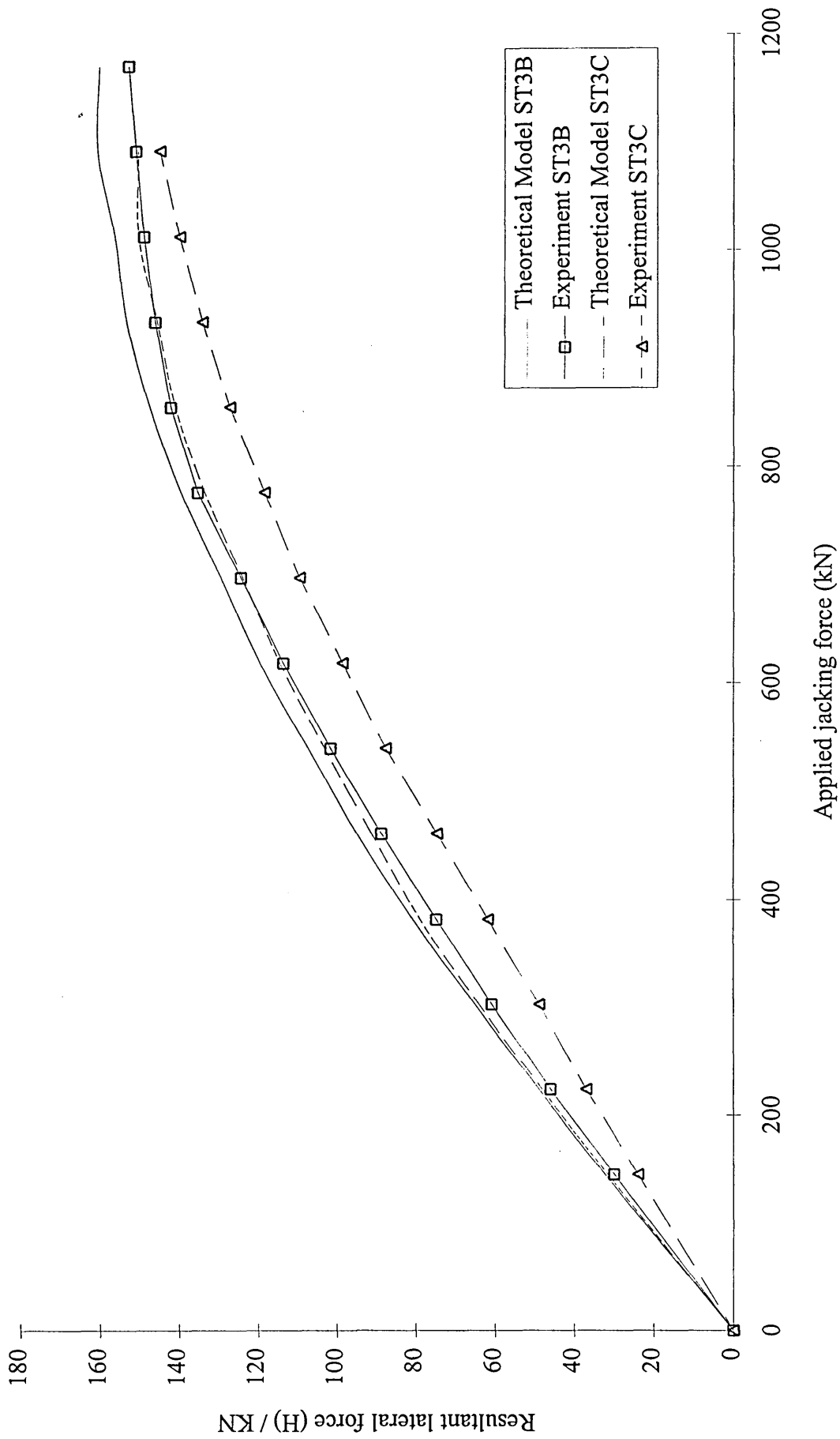


Figure 7.7. Correlation between experimental measurement and theoretical prediction of lateral force based on joint alignment data for tests ST3B and ST3C for DN 400 mm pipes.

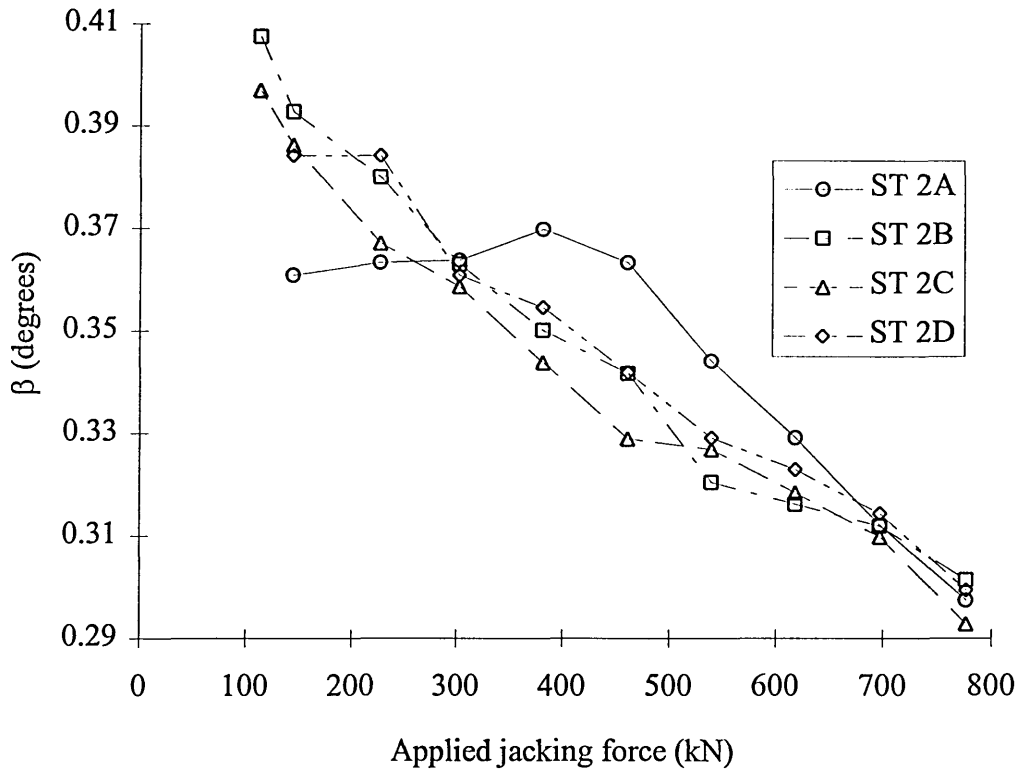
7.3.2. LATERAL FORCE ACTING AT OPEN/CLOSED MISALIGNED JOINT.

The relationship between lateral force and applied jacking force for open/closed joints was investigated in accordance with 6.8.2.

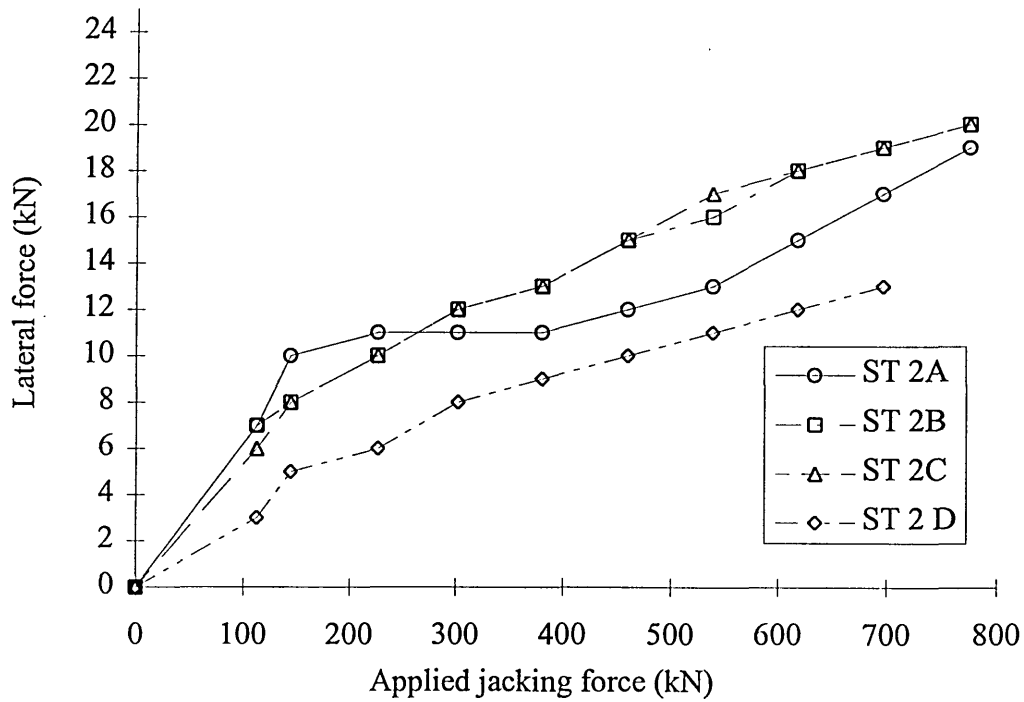
As the relative difference between the longitudinal jacking stress level at either side of the misaligned closed joint ($\sigma_{p_{min}}$ and $\sigma_{p_{max}}$) was not possible to measure experimentally, the prediction of lateral force at a closed misaligned joint was not made. The open joint phase of the test was correlated with the lateral force model up to the point where the joint closed. The lateral force was recorded for the closed phase until the limit of the safe working load of the pipes was reached.

Figures 7.8 to 7.10. show the misaligned joint characteristics, and the relationship between lateral force acting across the central misaligned joint and the applied jacking force for DN 250, 400 and 600 mm pipes respectively. Tests ST2A, ST2B, ST2C and ST2D were closed joint tests throughout.

The relationship between lateral force and applied jacking force during the first load cycle for the packing material showed a different trend to subsequent load cycles. This can be seen in Figures 7.8(b), 7.9(b) and 7.10(b). The joint misalignment angle increased and the lateral force decreased as the joint closed up (Figures 7.9(a) and 7.10(a)).

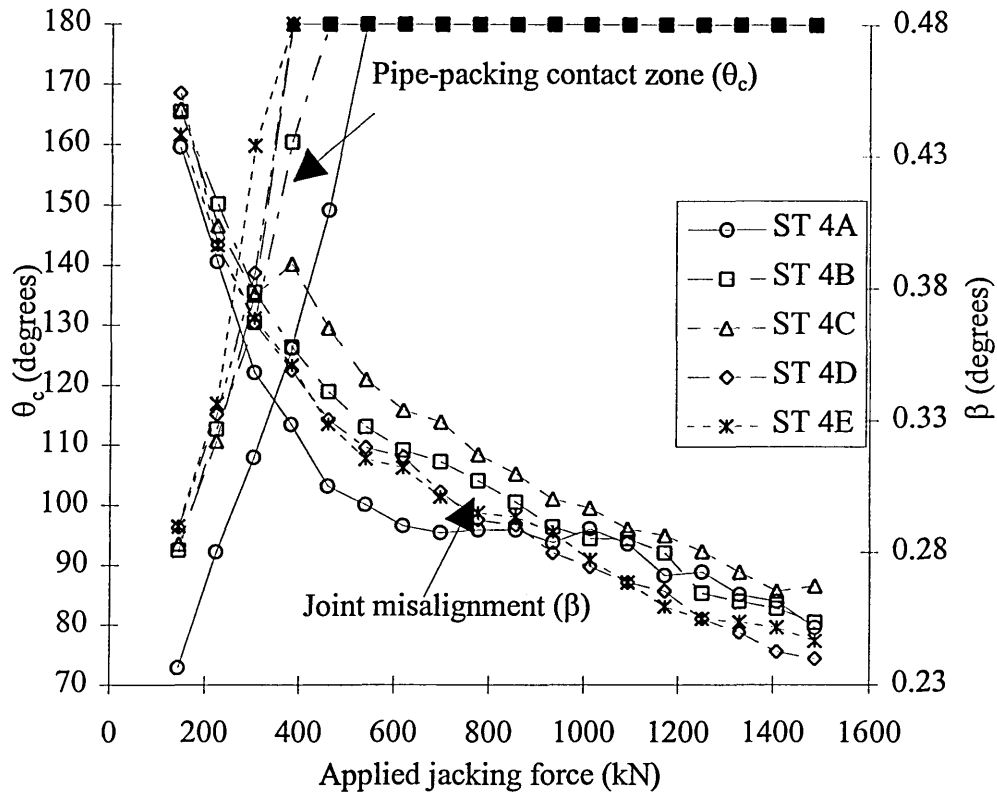


(a) Misaligned joint characteristics.

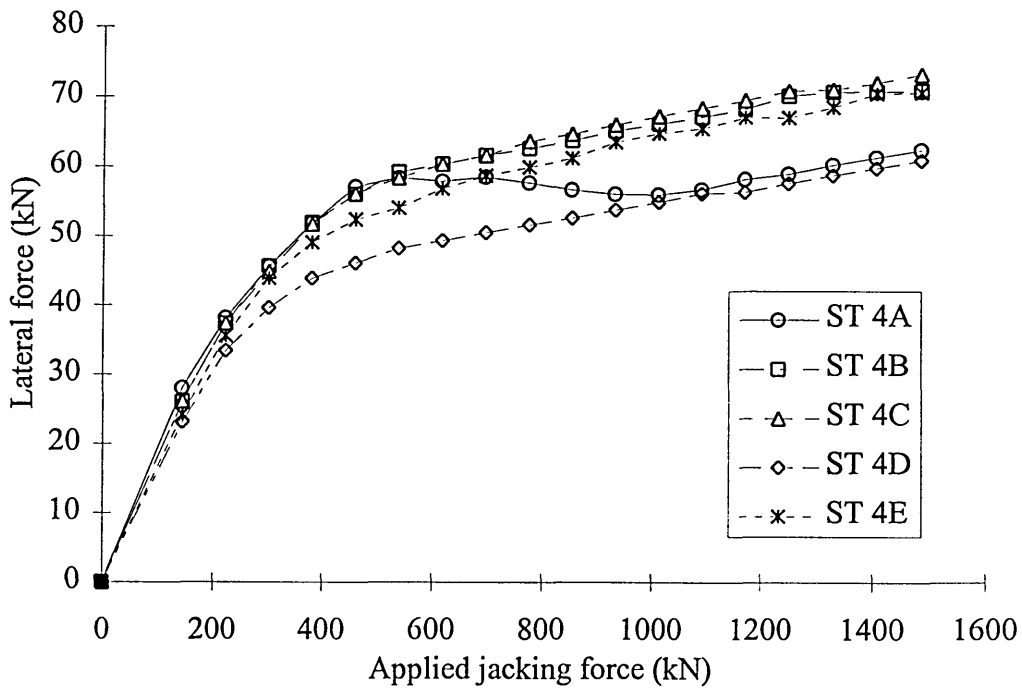


(b) Relationship between lateral force and applied jacking force.

Figure 7.8. Misaligned joint characteristics and relationship between lateral force and applied jacking force for tests ST2A, ST2B, ST2C and ST2D for DN 250mm pipes.

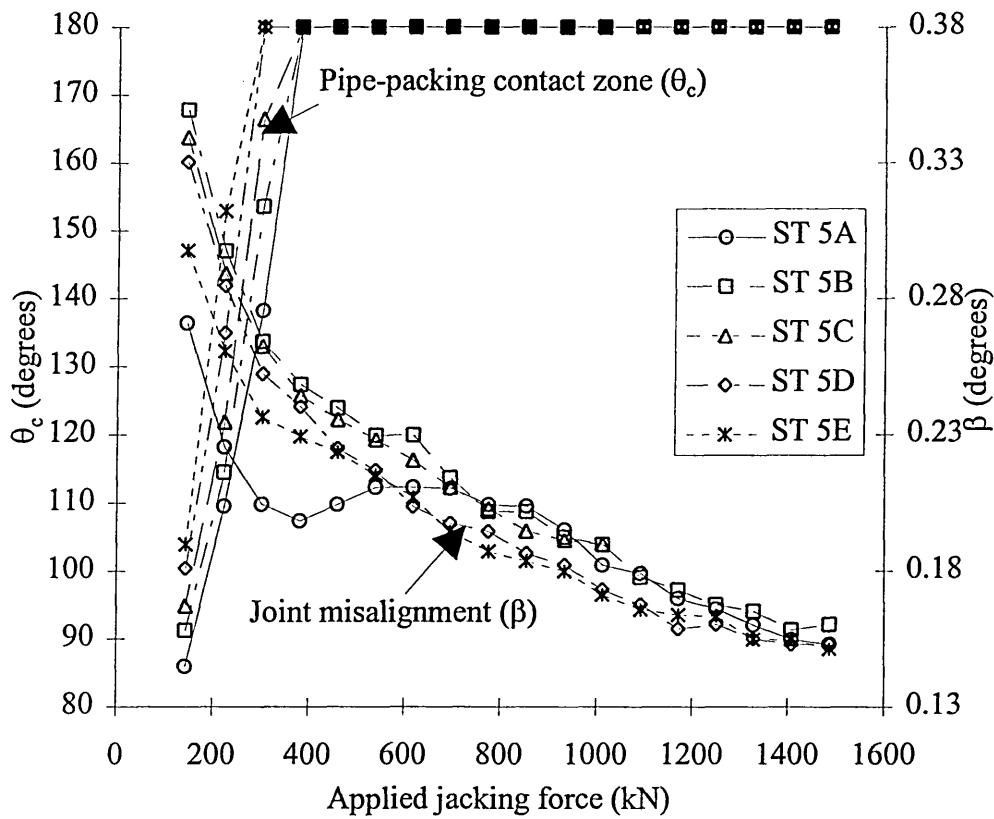


(a) Misaligned joint characteristics.

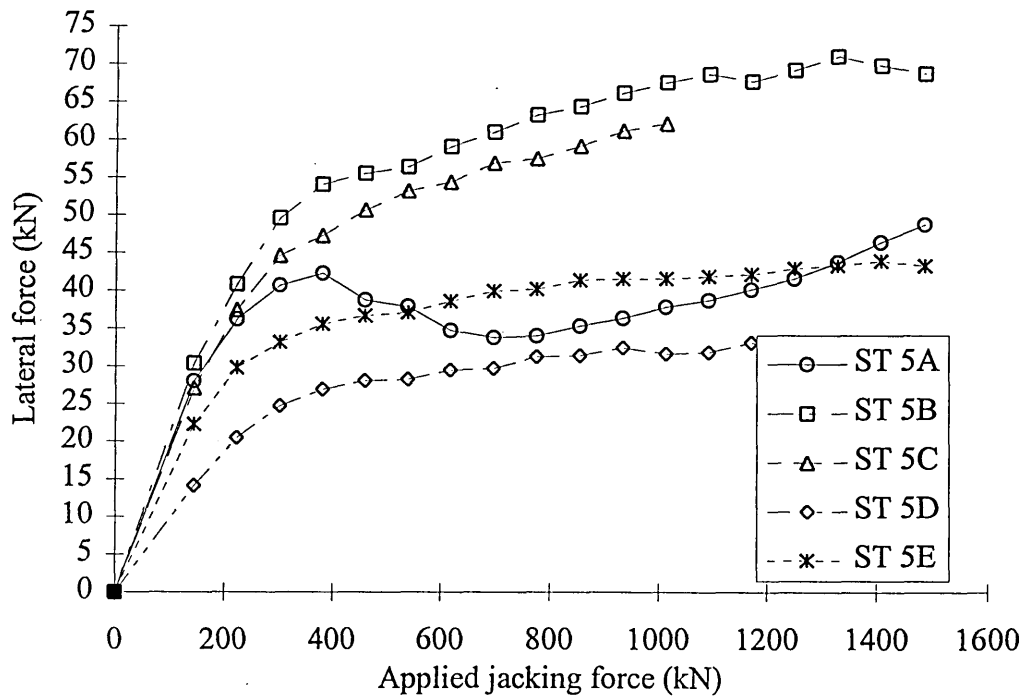


(b) Relationship between lateral force and applied jacking force.

Figure 7.9. Misaligned joint characteristics and relationship between lateral force and applied jacking force for tests ST4A, ST4B, ST4C, ST4D and ST4E for Dn 400mm pipes.



(a) Misaligned joint characteristics.



(b) Relationship between lateral force and applied jacking force.

Figure 7.10. Misaligned joint characteristics and relationship between lateral force and applied jacking force for tests ST5A, ST5B, ST5C, ST5D and ST5E for DN 600 mm pipes.

The difference in packing material characteristics between the first load cycle and subsequent cycles seems to be the most likely explanation for the phenomenon described above.

When the misaligned joint closes up, all the packing material is resisting longitudinal jacking force and the maximum stress level in the packing will be reduced. This can be seen from comparison of Figures 3.2. and 3.4. for the closed and open joint cases respectively. In addition, the eccentricity of the jacking thrust at the misaligned closed joint will reduce therefore the component of jacking force acting perpendicular to the pipe axis (lateral force) will reduce as compared with the open joint case. This is clearly shown in Figures 7.8(b), 7.9(b) and 7.10(b) for the three pipe sizes investigated.

When the central deflected joint was closed the eccentricity of the jacking force was located within the core of the cross section. Taking the rate of increase in lateral force for the closed joint into account, the ratio of r in Figure 3.3. is likely to be greater than 0.75 indicating approximately uniform axial compression.

7.3.3. LATERAL FORCE SHARING BETWEEN STRUCTURAL ELEMENT OF COUPLING AND FRICTIONAL RESISTANCE OF PIPE-PACKING INTERFACE.

The effect of lateral force sharing between the coupling and pipe-packing friction was investigated experimentally in accordance with 6.8.3.

Figures 7.8(b), 7.9(b) and 7.10(b) for DN 250, 400 and 600mm pipes respectively show the reduction in lateral force resisted by the load cell (hence coupling) for open/closed tests ST2D, ST4D/ST4E and ST5D/ST5E. The joint misalignment characteristics for the tests were consistent with previous tests in each series, therefore the difference in lateral force recorded is due to the 3mm E.P.D.M. rubber seal alone.

Table 7.2. shows the reduction in lateral force resisted by the load cell (hence coupling) due to the load sharing characteristics of the joint configuration:-

	Test	ρ	Test	ρ	ρ_{average}
	Reference		Reference		
DN 250	ST2D	0.66	-	-	0.66
DN 400	ST4D	0.84	ST4E	0.95	0.89
DN 600	ST5D	0.49	ST5E	0.62	0.56

Table 7.2. Summary of load sharing characteristics for closed joint tests.

The variation in the load sharing coefficient (ρ) for ST4D/ST4E is noteworthy. Little reduction in lateral force was recorded in comparison with ST2D and ST5D/ST5E where the value of ρ was reasonably consistent. Further investigation into the load sharing characteristics of joints considering different seal profiles and packing ring dimensions is necessary to make proper engineering judgement of the application of ρ as given in Table 7.2. However, the values of ρ given above were used to assess the lateral force acting on the coupling for subsequent coupling stress analysis.

7.4. EXPERIMENTAL STRESS ANALYSIS OF LOOSE SLEEVED PIPE-JACKING COUPLING.

In order to verify the mathematical model for the prediction of principal stresses induced in loose sleeved jacking pipe couplings due to the installation method, a full scale experimental investigation was carried out in accordance with 6.9. The following sections compare the experimental results with the theoretical model predictions. The analysis of the results consider both the lateral force model and the coupling stress model.

The internal radial pressure distribution exerted on the coupling at a misaligned joint (see 4.2.2.) was defined by the parameter φ in the theoretical analysis of the coupling. From the theoretical model, the bending stress distribution about the minor member axis was found to be very sensitive to the radial pressure distribution and in particular the value of φ .

Therefore, different pressure distributions were assumed with the resulting principal stresses compared with experimental values. The value of φ that gave the closest overall correlation with the three different coupling experiments (C1 to C3) was found to be 0.005. This value is used throughout the following sections. The resulting radial pressure distribution exerted on the coupling is therefore virtually constant. This would be expected due to the confined nature of the tightly fitted pipe-coupling system.

7.4.1. RESULTS OF COUPLING TEST C1 FOR 400 MM DIAMETER CLAY PIPES.

Electrical resistance strain gauge rosettes were fixed on the surface of the coupling specimen C1 as illustrated in Figure 6.4.(a) and tested in accordance with 6.9. In order to verify the coupling stress model, the lateral force resisted by the coupling was determined first.

The joint misalignment characteristics for test C1 are shown in Figure 7.11. The procedure adopted for the determination of the relationship between lateral force resisted by the coupling and the applied jacking force is outlined below:-

- 1) From misalignment angle, applied jacking force, packing material characteristics and joint geometry, - the contact zone between packing material and pipe (for open joint phase of test) was determined.
- 2) The eccentricity of jacking force at deflected joint, based on open joint analysis, was determined (from equation 3.27).
- 3) The inclination of jacking force through the pipes was determined, thereby total lateral force was calculated (equation 3.2. and 3.1).
- 4) The proportion of lateral force resisted by the coupling, ρ , was observed (Table 7.2.).

The above procedure leads to the prediction of lateral force resisted by coupling at each increment of jacking force. Steps (1-4) above were repeated until the value of θ_c reached 180°. For test C1, the deflected joint was found to close up when the applied jacking force was greater than 381 kN.

Table 7.3. shows the analysis of open joint phase of test C1:-

Jacking force, F, (kN)	β (degrees)	m	θ_c (degrees) (Figure 7.4)	e/R_p (Figure 3.5)	H (kN)	H_c (kN)
144.734	0.370	0.352	74	0.845	30.3	26.1
223.729	0.300	0.672	97	0.750	41.8	36.0
302.724	0.257	1.062	117	0.670	50.9	43.8
381.719	0.216	1.590	146	0.565	54.3	46.7
461.714	0.207	2.011	>180	-	-	-

Notes:
 $E_j = 88 \text{ N/mm}^2$ $t_j = 53\text{mm}$ $t_w = 61\text{mm}$ $E_c = 50000\text{N/mm}^2$ $E_p = 125 \text{ N/mm}^2$
 $a = 10\text{mm}$ $L_p = 1999\text{mm}$ $R_p = 261\text{mm}$
 $\rho = 0.86$

Table 7.3. Analysis of open joint phase of coupling test C1.

The joint elasticity (E_j) was assumed to be constant at low stress levels of the packing material. This assumption is reasonable as the elasticity of packing material at low

stress levels was approximately constant. This is shown by Figure 5.4. for cycle one. The value of ρ used in the open joint analysis was 0.86 as obtained from test ST4D.

Figure 7.11. shows that the misalignment angle (β) remains approximately constant at 0.19° after the jacking force has reached 381 kN, therefore, the lateral force acting across the misaligned joint was a function of applied jacking force alone.

The lateral force increases at a constant rate for the closed joint case (Figure 7.9.). The determination of lateral force throughout test C1 was determined by combining the theoretical approximation given by Table 7.3. with the constant increase given by Figure 7.9. The lateral force resisted by the coupling for test C1 can be seen in Figure 7.12.

In order to compare the coupling stress model with strain gauge rosette readings, the position of maximum compression in the packing material was determined thereby defining the line of symmetry for the theoretical stress system. Figure 7.11. shows the variation in position of maximum compression (κ) during test C1.

The theoretical principal tensile stress derived from equation 4.44. (for stress element 1) was compared with the maximum principal stress obtained directly from the strain gauge rosettes. Figures 7.13 to 7.15 show the correlation between the theoretical model and the experimental results.

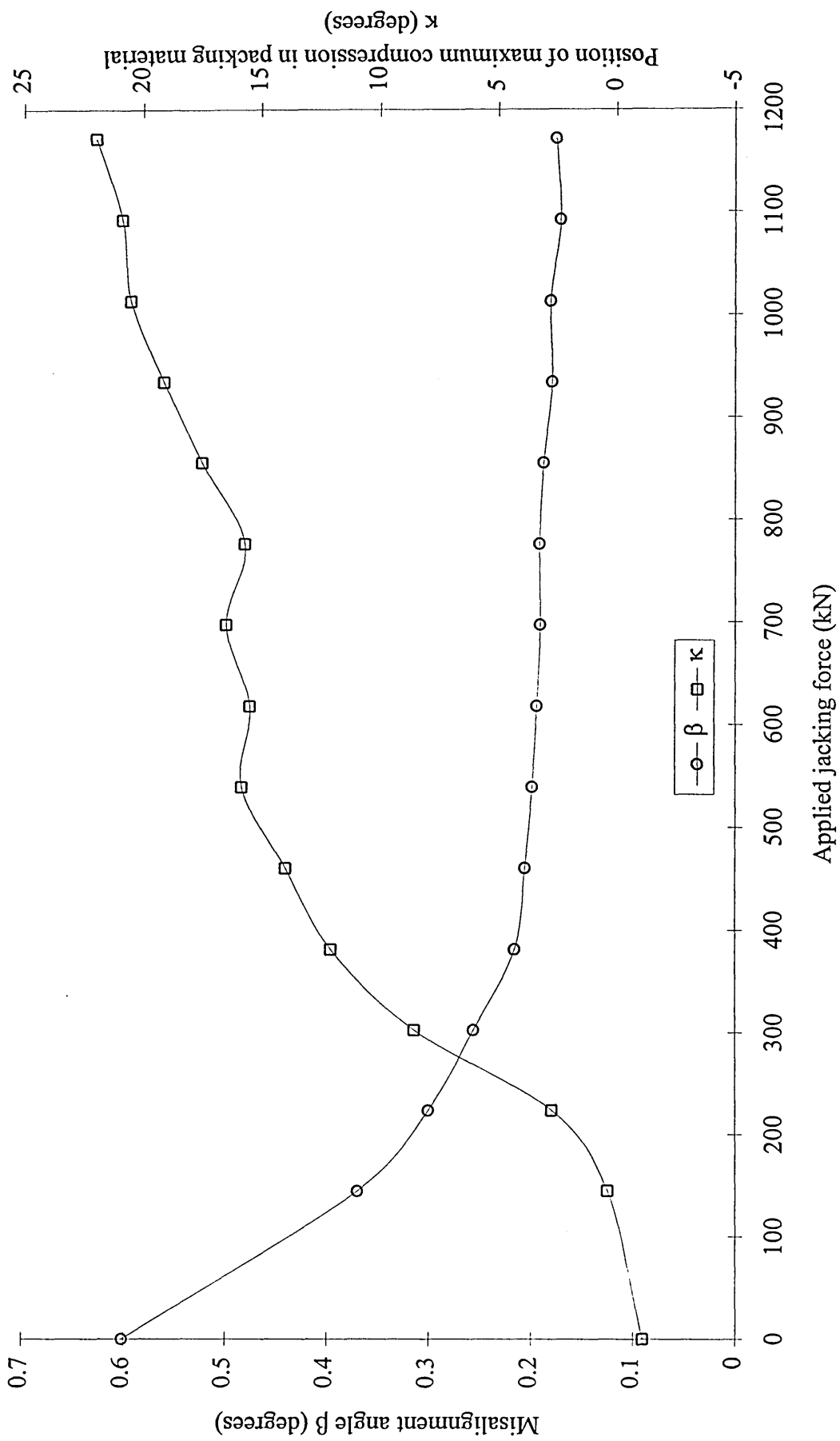


Figure 7.11. Misaligned joint characteristics during test C1 for DN 400mm pipes.

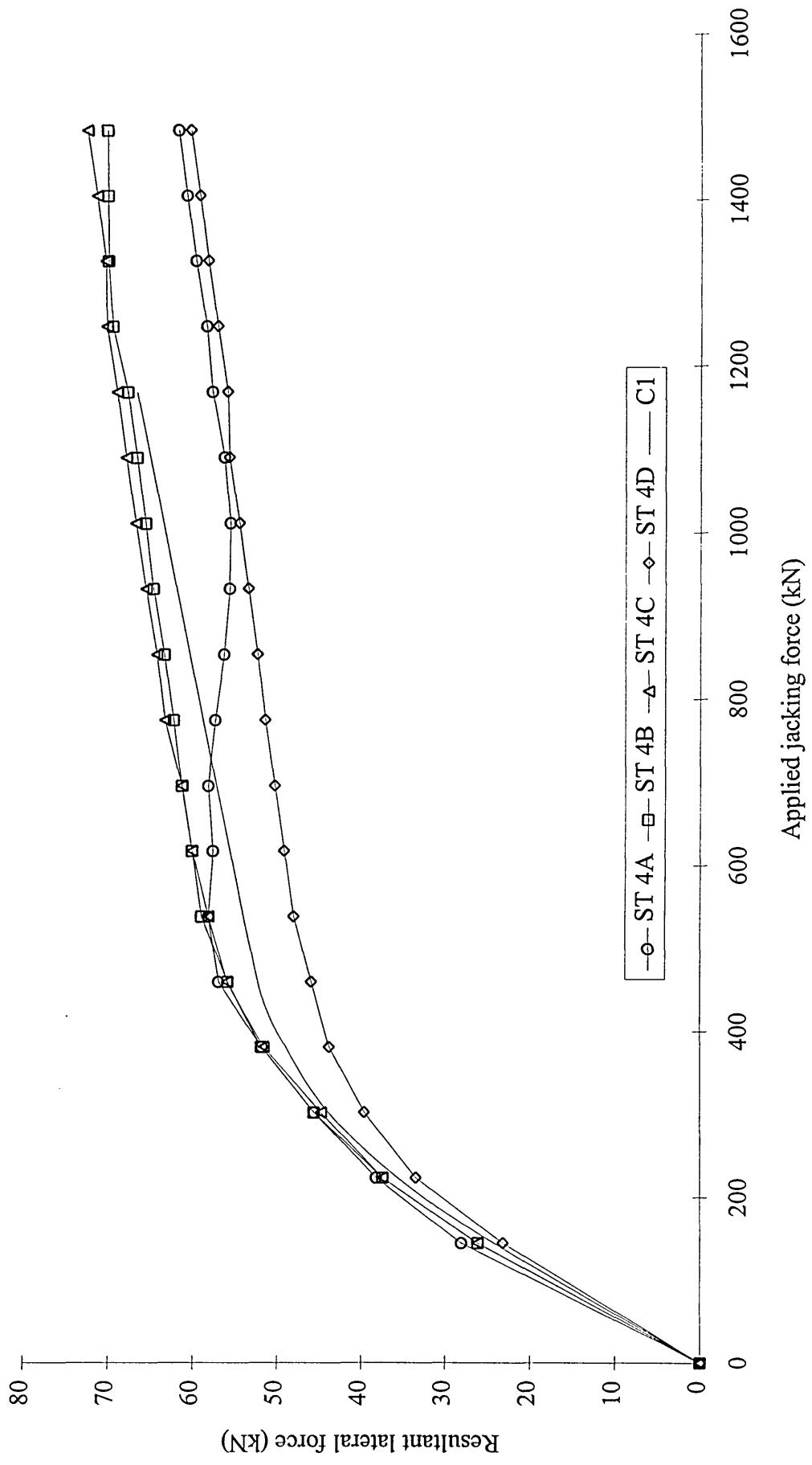
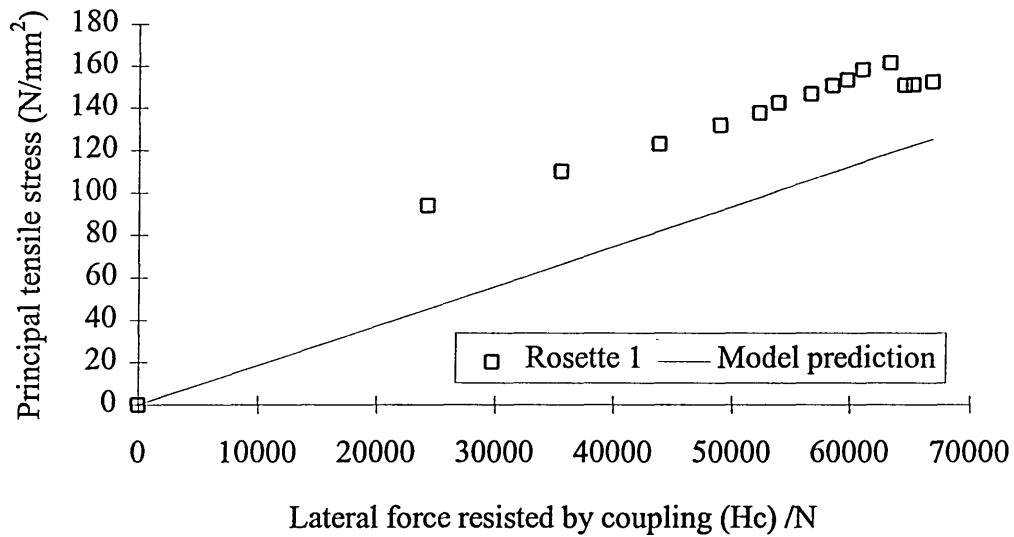
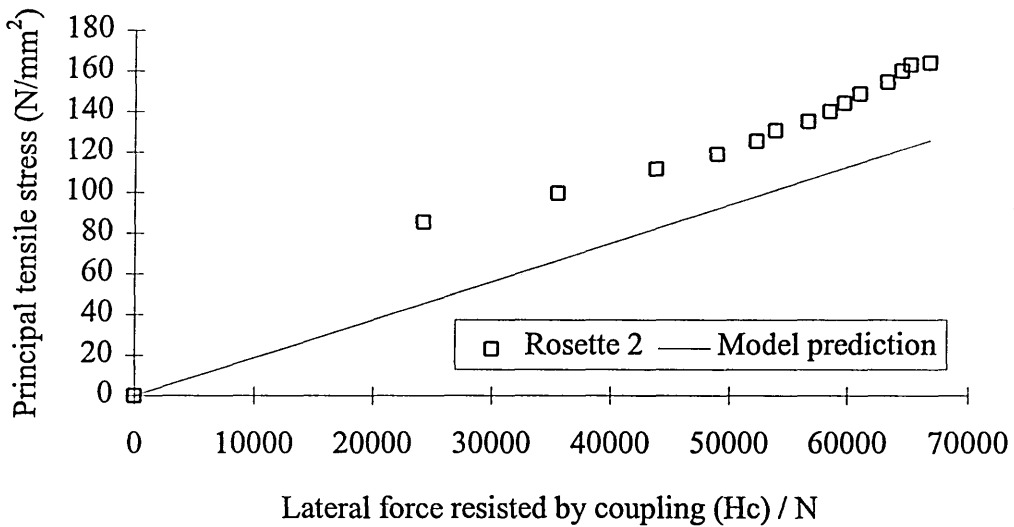


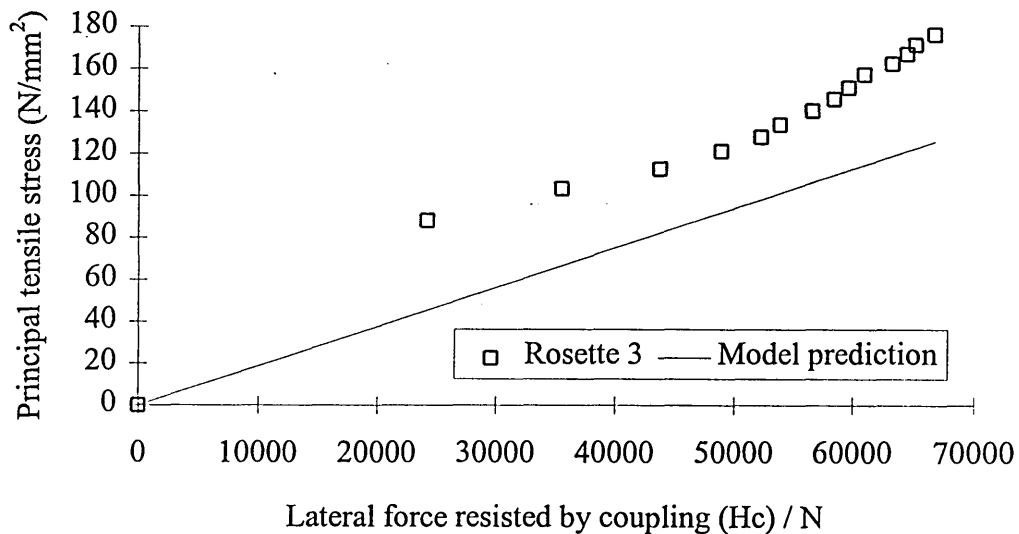
Figure 7.12. Relationship between lateral force resisted by coupling and applied jacking force for test C1.



(a) Correlation for rosette 1.

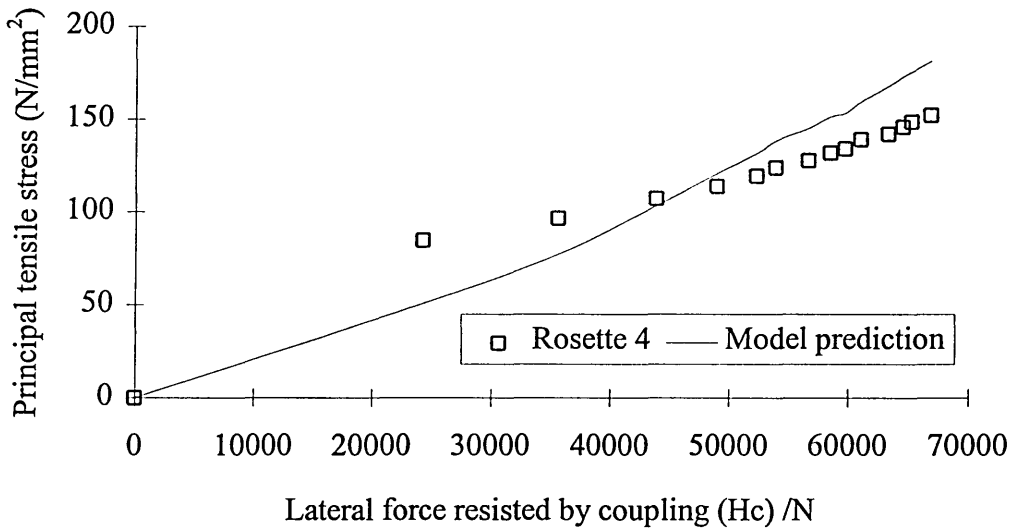


(b) Correlation for rosette 2.

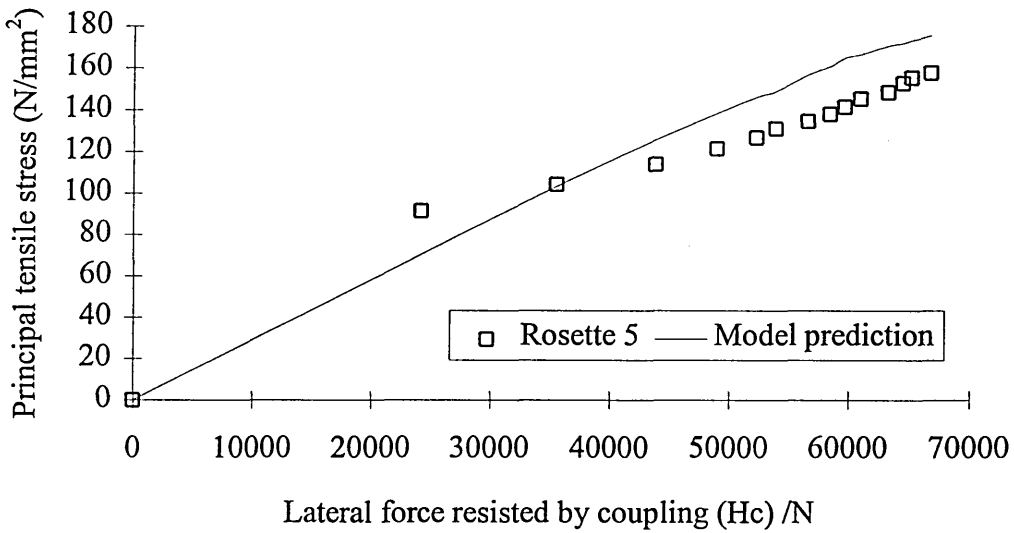


(c) Correlation for rosette 3.

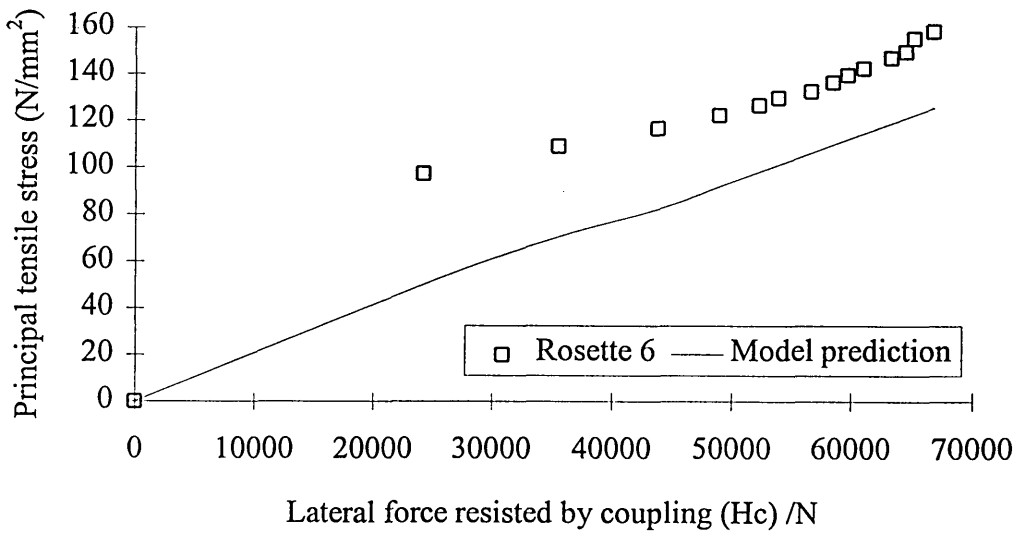
Figure 7.13. Correlation between theoretical model and experimental results for test C1.



(a) Correlation for rosette 4.

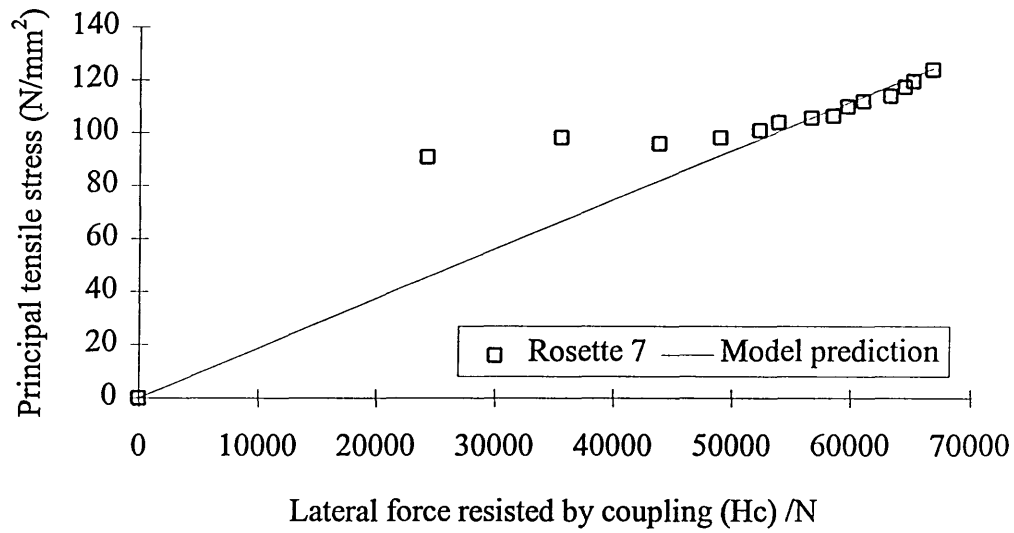


(b) Correlation for rosette 5.

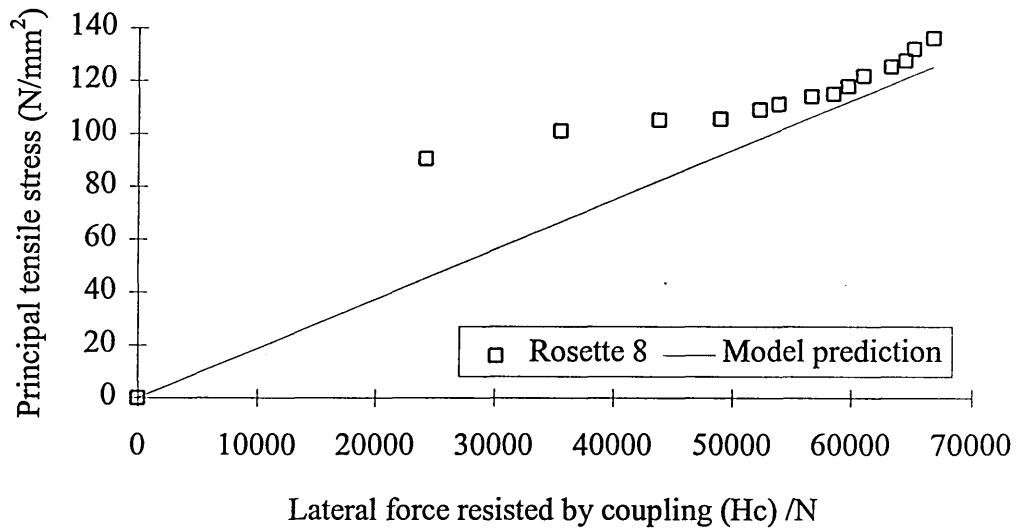


(c) Correlation for rosette 6.

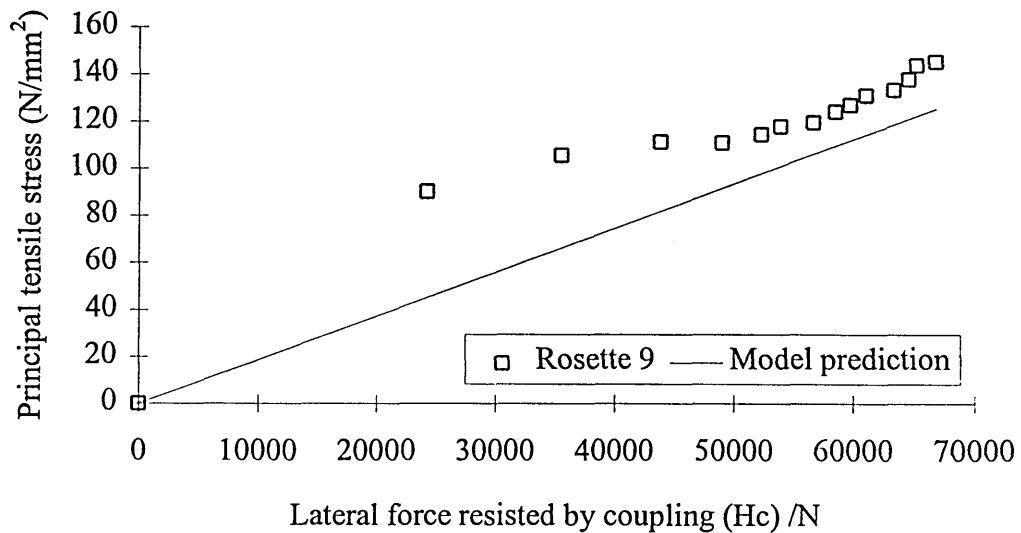
Figure 7.14. Correlation between theoretical model and experimental results for test C1.



(a) Correlation for rosette 7.



(b) Correlation for rosette 8.



(c) Correlation for rosette 9.

Figure 7.15. Correlation between theoretical model and experimental results for test C1.

The relationship between lateral force and principal tensile stress is linear for the elastic range of the stainless steel for any discrete location on the coupling surface. However, the changes in the position of maximum compression in the packing material (therefore line of symmetry for stress system) are amplified in the stress model to a greater extent over the range of $45^\circ < \theta < -45^\circ$ (i.e. rosettes 4,5 &6) than other locations. This is seen from Figure 4.12.

Generally, correlation between theory and experiment is good with theoretical values underestimating experimental values slightly for test C1 (Figures 7.13. through 7.15). However, the linear relationship between lateral force and principal tensile stress was observed which confirms the validity of the theoretical model.

7.4.2. RESULTS OF COUPLING TEST C2 FOR 250 MM DIAMETER CLAY PIPES.

The procedure illustrated in 7.4.1. for the determination of the relationship between lateral force resisted by the coupling and applied jacking force was adopted for the open/closed joint coupling test C2 for DN 250mm pipes. The strain gauge rosette fixing locations are shown in Figure 6.4.(b) and the test was carried out in accordance with 6.9.

The joint misalignment characteristics for test C2 are shown in Figure 7.16. The position of maximum compression in the packing material shows significant

fluctuations after the jacking force reached 500 kN. However, the joint misalignment angle (β) showed a constant decrease throughout the test.

Table 7.4. shows the open joint analysis for test C2:-

Jacking force, F, (kN)	β (degrees)	m	θ_c (degrees) (Figure 7.4)	e/R_p (Figure 3.5)	H (kN)	H_c (kN)
98.484	0.567	0.281	90	0.787	11.78	7.80
148.412	0.522	0.461	112	0.695	15.70	10.40
198.339	0.493	0.652	134	0.604	18.07	11.92
248.267	0.440	0.914	>180	-	-	-

Notes:
 $E_j = 94 \text{ N/mm}^2$ $t_j = 38\text{mm}$ $t_w = 41\text{mm}$ $E_c = 50000\text{N/mm}^2$ $E_p = 87 \text{ N/mm}^2$
 $a = 5.5\text{mm}$ $L_p = 1991\text{mm}$ $R_p = 165\text{mm}$
 $\rho = 0.66$

Table 7.4. Open joint lateral force analysis for coupling test C2.

Using the open joint analysis above, the joint was predicted to close up when the misalignment angle was approximately equal to 0.44° . This was also evident from Figure 7.8. with β in the range of 0.36° to 0.41° at a jacking force of 144kN. This is in agreement with the theoretical model for the prediction of contact zone and therefore

lateral force acting across central deflected joint. The value of ρ of 0.66 as obtained from test ST2D was used.

The relationship between lateral force and applied jacking force used for correlation of coupling stresses for test C2 is shown in Figure 7.17.

The Correlation between the theoretical prediction of principal tensile stress (taking account of joint alignment characteristics) and experimental measurements of maximum principal stress was excellent for rosettes 1,3 and 4. This is shown by Figure 7.18. Rosette 2 is not presented here due to poor gauge output.

The non-linear relationship predicted by the stress model is due to the variable nature of the position of maximum compression of the packing material (κ). However, taking this into account gives excellent correlation for test C2.

7.4.3. RESULTS OF COUPLING TEST C3 FOR 250 MM DIAMETER CLAY PIPES.

Test C3 was classified as ‘open joint’ throughout the duration of the test. As a consequence the open joint analysis (see 7.4.1.) was adopted in the derivation of the lateral force resisted by the coupling for the stress analysis of the coupling. In order to generalise the theoretical model the coupling section was changed to 3 x 150 mm. The strain gauge rosette locations are illustrated in Figure 6.4.(c).

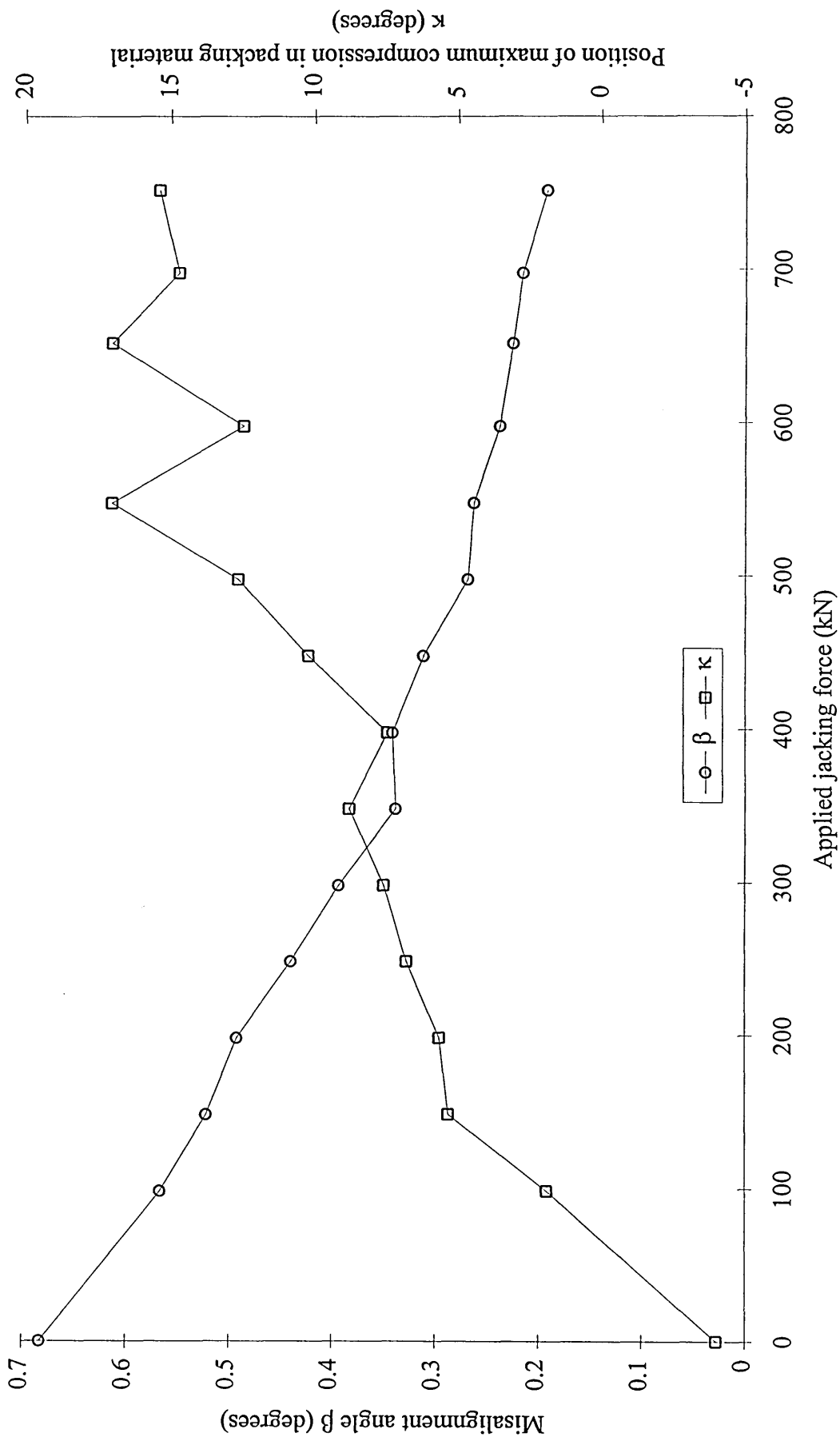


Figure 7.16. Misalignment joint characteristics for test C2 for DN 250mm pipes.

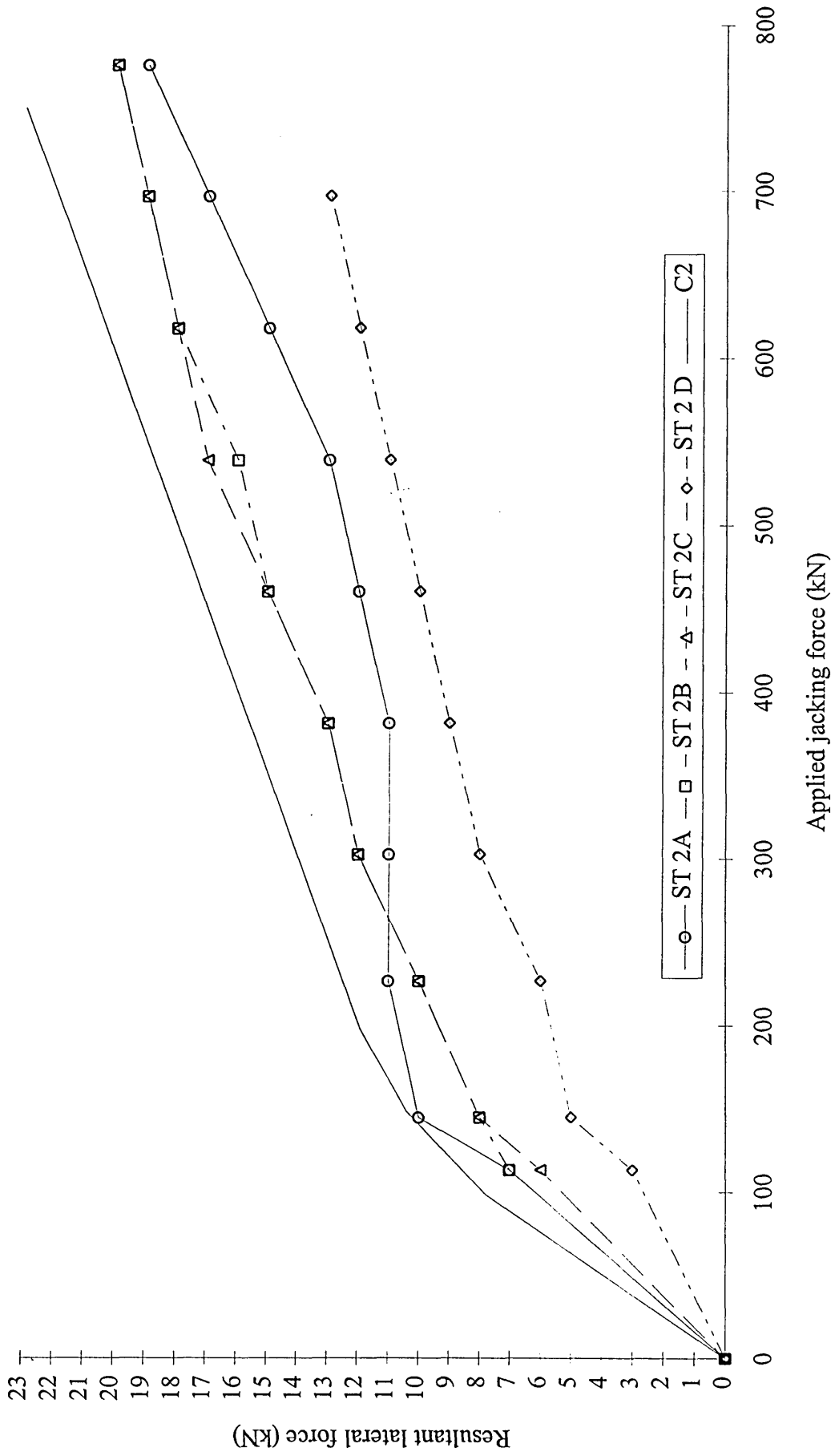
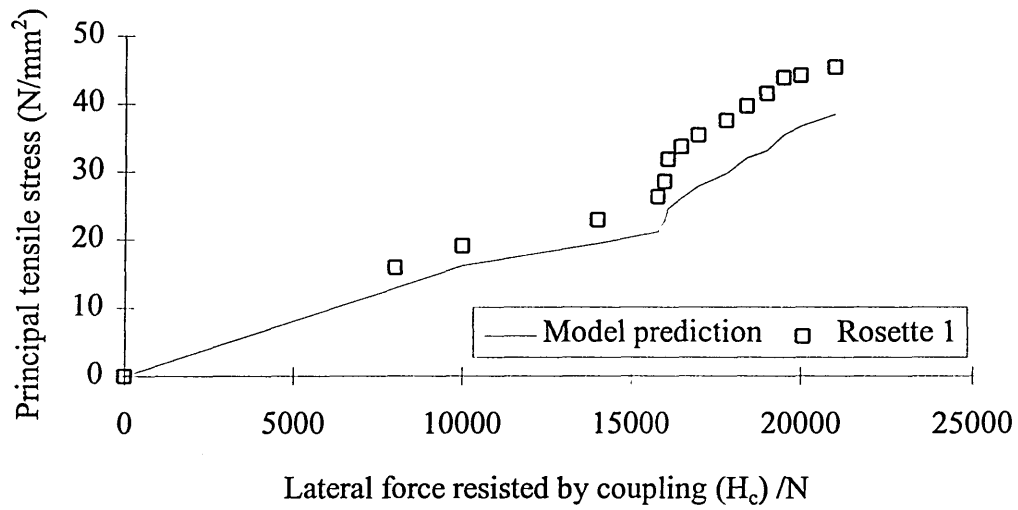
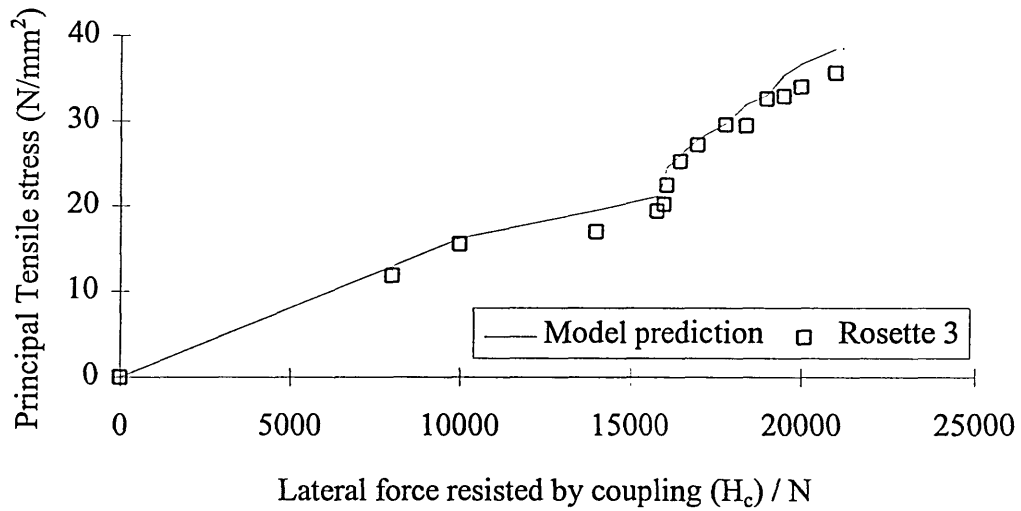


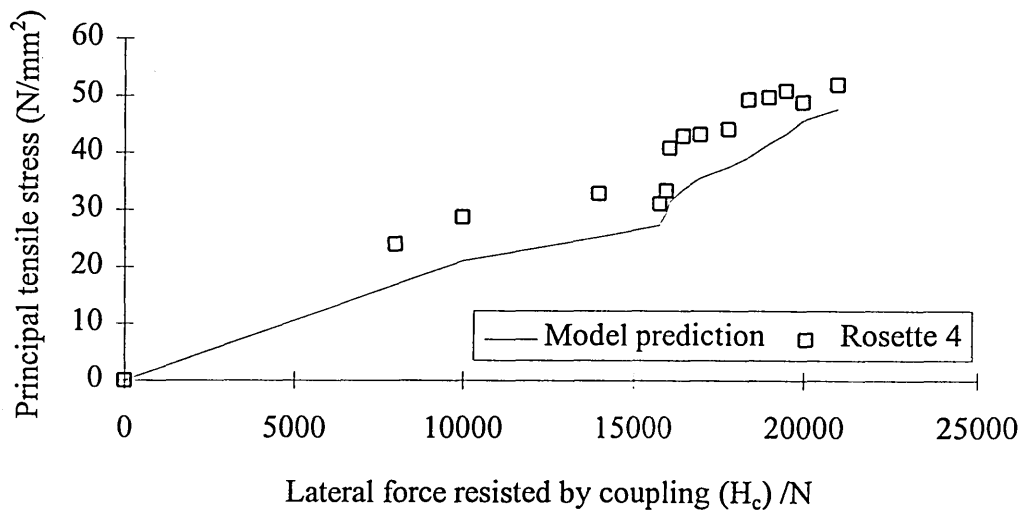
Figure 7.17. Relationship between lateral force resisted by coupling and applied jacking force for test C2.



(a) Correlation for rosette 1.



(b) Correlation for rosette 3.



(c) Correlation for rosette 4.

Figure 7.18. Correlation between theoretical model and experimental results for rosettes 1, 3 and 4 for test C2.

The joint misalignment characteristics for test C3 are shown in Figure 7.19. The joint misalignment showed a constant decrease throughout the test while the position of maximum compression of the packing material was well controlled with maximum value of κ of approximately 5.3° .

The relationship between lateral force resisted by the coupling and applied jacking force is shown in Figure 7.20. using the value of ρ as 0.66 (Table 7.2.). Correlation between theory and experiment was excellent for points located on the centre of the coupling width (stress element 1 in Figure 4.11.) as shown in Figure 7.21.

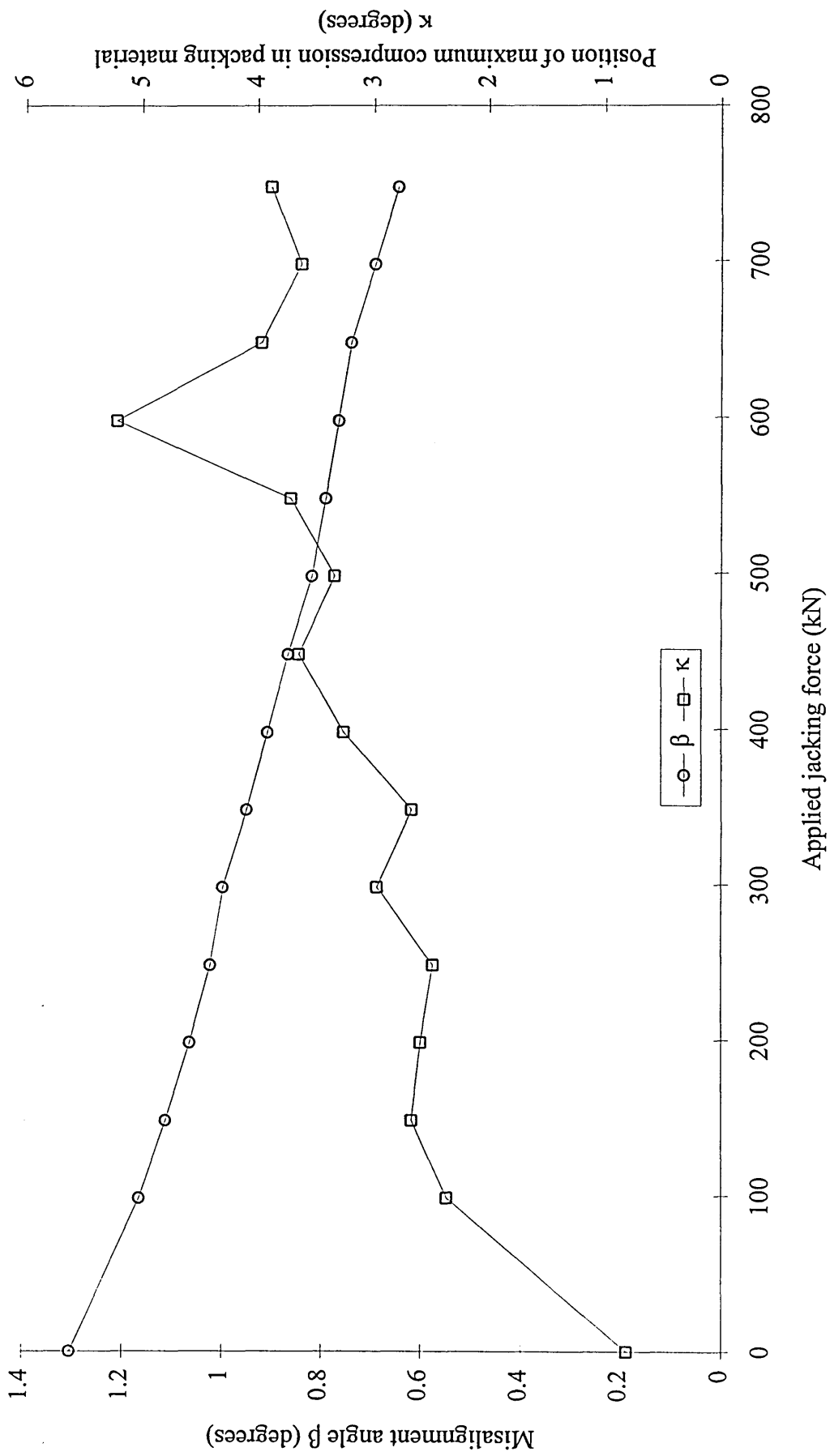


Figure 7.19. Misalignment joint characteristics for test C3 for DN 250mm pipes.

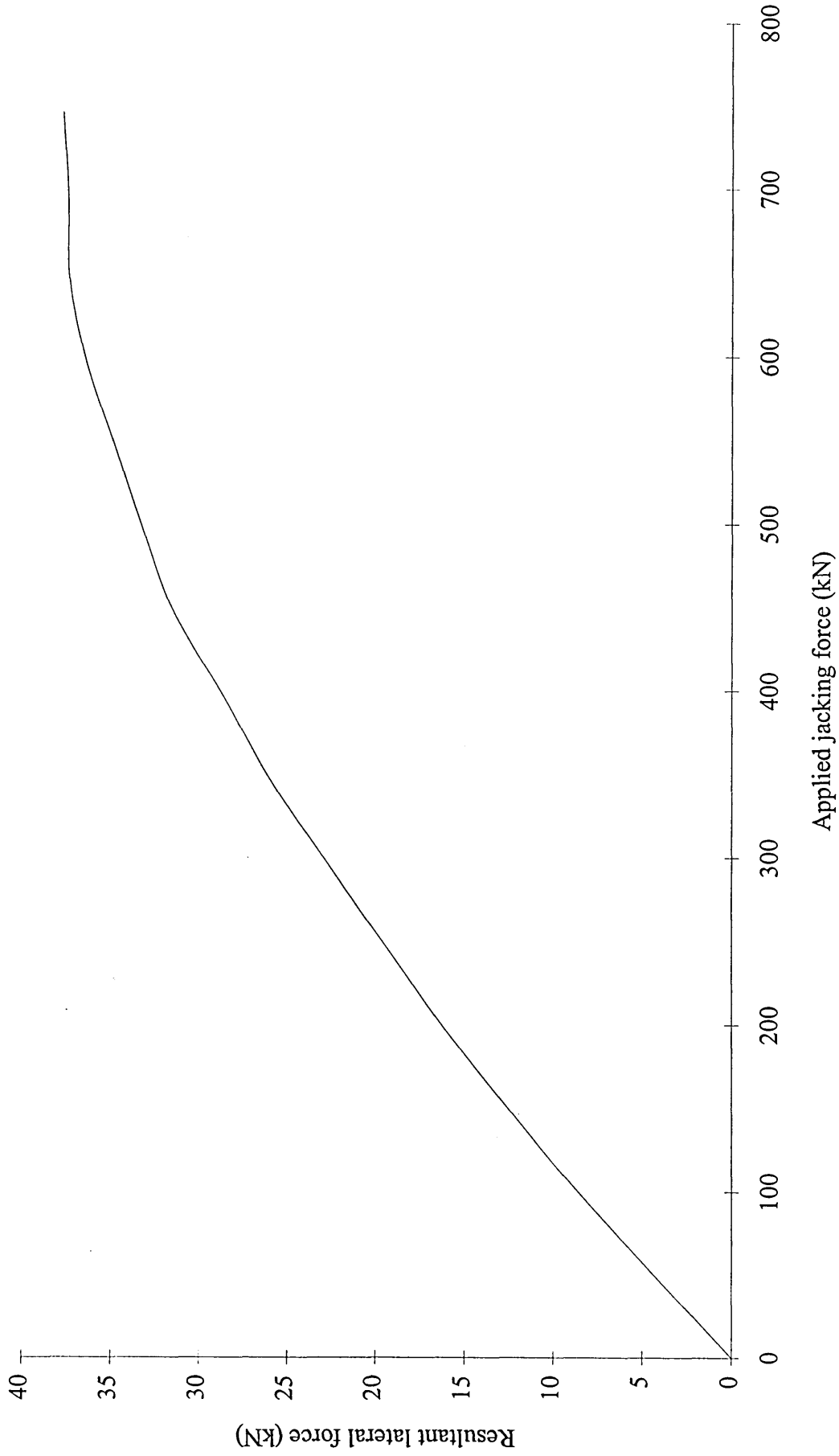
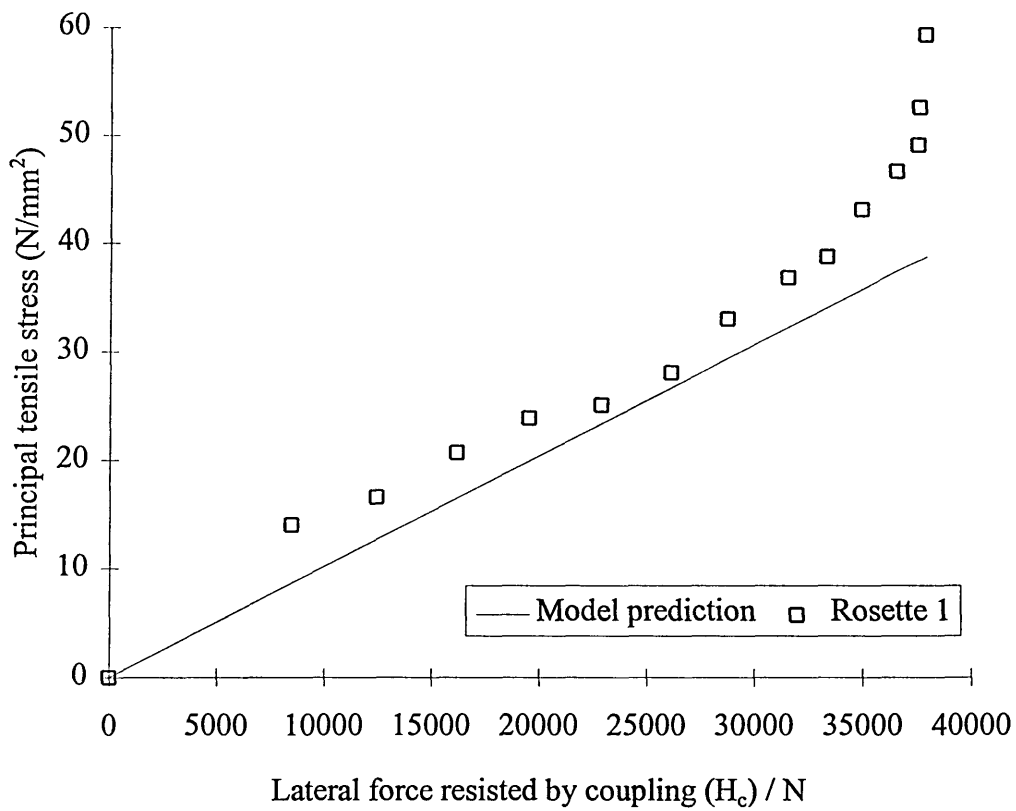
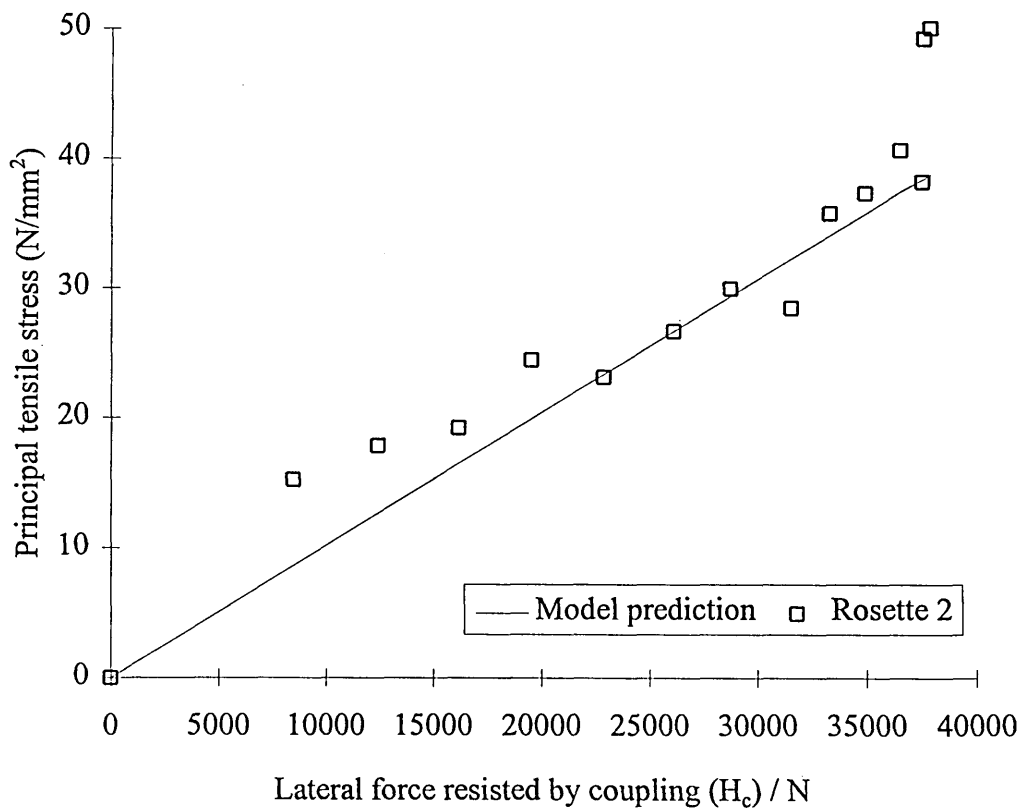


Figure 7.20. Relationship between lateral force resisted by coupling and applied jacking force for test C3.



(a) Correlation for rosette 1.



(b) Correlation for rosette 2.

Figure 7.21. Correlation between theoretical model and experimental results for rosettes 1 and 2 for test C3.

7.5. MAIN CONCLUSIONS.

The following conclusions may be drawn from the experimental investigation of the pipe-packing-coupling interaction:-

1) A misaligned joint will tend to close up when subjected to longitudinal jacking force due to eccentricity of jacking force and deformation of the packing material.

2) Prediction of the pipe-packing contact zone was found to be dependant on the following parameters:-

- Misalignment angle (β).
- Applied jacking force.
- Material properties of pipe and packing material.
- Geometric properties of joint configuration.

3) Chipboard packing material exhibits different stress-strain behaviour during the first load cycle compared with subsequent load cycles. The structure of the material becomes permanently deformed upon removal of load. As a consequence the tangent modulus of elasticity of the material increases after the first load cycle for the same stress state.

4) The theoretical model for prediction of pipe-packing contact zone at an open misaligned joint (given by equation 3.31) gives good correlation with experimental

observations for chipboard. The following values of η should be used for chipboard packing material:-

- Prediction of pipe-packing contact zone for first load cycle of packing material - 0.6
- Prediction of pipe-packing contact zone for n^{th} load cycle of packing material - 0.28

5) Correlation between theoretical prediction of lateral force at a misaligned open joint and experimental observations was excellent using the analysis presented in chapter 3. The difference between theory and experiment was found to be less than 4 percent for large lateral forces.

6) The lateral force acting on a closed misaligned joint was found empirically to be insignificant as the longitudinal jacking force was located within the core cross section of the pipe. The lateral force in all cases was found to be a linear function of applied jacking force.

7) The load sharing characteristics of the pipe-packing-coupling system used in this study were found empirically. From the experimental evidence the reduction coefficient (ρ) was not found to be dependant on the lateral force acting across the joint alone. Further investigation into this area would provide useful data for different joint configurations.

- 8) The lateral force acting on couplings C1, C2 and C3 was derived using the open joint lateral force model (see 3.1. and 3.3.) and empirical data for the closed joint phase of the tests where applicable.

- 9) The distribution of internal radial pressure exerted on the coupling was determined by correlating theoretical principal tensile stresses with experimental stresses to give the most appropriate value of ϕ for equation 4.2. This was found to be 0.005.

- 10) Correlation between the coupling stress model and experimental observations was generally excellent for points located on the centreline of the coupling band.

- 11) The design of loose sleeved jacking pipe couplings can be made using the mathematical models presented in chapters 3 and 4. Using the coupling stress model for the design of fixed sleeved collars will give slightly conservative results as the coupling ring will retain its profile due to the rigid confinement of the concrete pipe.

CHAPTER 8

CONCLUSIONS FROM PRESENT STUDY AND RECOMMENDATIONS FOR FUTURE WORK

8.1. CONCLUSIONS FROM PRESENT STUDY.

The following conclusions maybe drawn from the theoretical and experimental investigation of the pipe-packing-coupling system reported in this thesis:-

- 1) The structural interaction of the pipe-packing-coupling system developed in this study is based on field evidence of the global interaction of the pipe train with the tunnel bore.

- 2) Misalignment of the pipe train leads to deflected joints and eccentric loading of the pipes. The inclination of the resultant jacking force through the pipe leads to a component perpendicular to the pipe axis and is resisted by friction between the packing material and the pipe-end, and the structural element of the coupling.

- 3) Small angular joint deflections can be accommodated by compression of the packing material, leading to a closed joint where the eccentricity of the resultant jacking force is located within the core of the cross section of the pipe and no tensile stresses are

induced in the pipe wall. The lateral force acting at a closed joint is a function of the applied jacking force and is negligible compared with the open joint case.

4) Large joint deflections lead to opening of joints where the resultant jacking force is located outside the core of the cross section of the pipe. This situation is more critical than (3) above leading to the development of tensile stresses in the pipe wall and greater lateral force transferred to the packing-coupling system.

5) The structural interaction of the pipe-packing-pipe interface is dependant on the following parameters:-

- Applied jacking force.
- Misalignment angle between successive pipes.
- Mechanical and geometrical properties of pipe-joint configuration.

6) The prediction for the pipe-packing-pipe contact zone for open joints can be made using the modified Australian Concrete Pipe Association Linear Stress Approach (ACPALSA) as given by equation 3.31. and the values of η for chipboard packing rings:-

$\eta = 0.6$ for prediction of pipe-packing interaction during the first load cycle.

$\eta = 0.28$ for prediction of pipe-packing interaction during subsequent load cycles.

- 7) The lateral force acting across a misaligned joint is a function of the applied jacking force and its differential eccentricity at each pipe-end adjoining the deflected joint. The lateral force can be predicted using equation 3.1. for an open joint.
- 8) The presence of a compressible rubber seal element located between the pipe and the coupling ring facilitates lateral force sharing between the frictional resistance of the pipe-packing interaction and the structural element of the coupling. The extent of the load sharing is dependant on the joint configuration.
- 9) Due to the confinement of a loose sleeved coupling ring and the presence of a compressible rubber seal element, the distribution of internal radial pressure exerted on the coupling is defined by equation 4.2. with a suitable value for ϕ of 0.005.
- 10) The critical location of principal tensile stress induced in the coupling was measured and compared with the theoretical results. The correlation was found to be very good and this confirms the validity of the theoretical model proposed in this study.

8.2. RECOMMENDATIONS FOR FUTURE RESEARCH.

The following recommendations for future research are based on the findings of this thesis:-

- The use of alternative coupling ring materials such as reinforced plastic for use with a generic range of couplings.
- Further investigation of the load sharing characteristics of different joint configurations, including packing material and seal design. The formulation of a predictive model would be beneficial for a general coupling system.
- The development of an optimum seal design to give required performance against ingress or egress of fluids and to optimise the load sharing characteristics of a misaligned joint.

REFERENCES

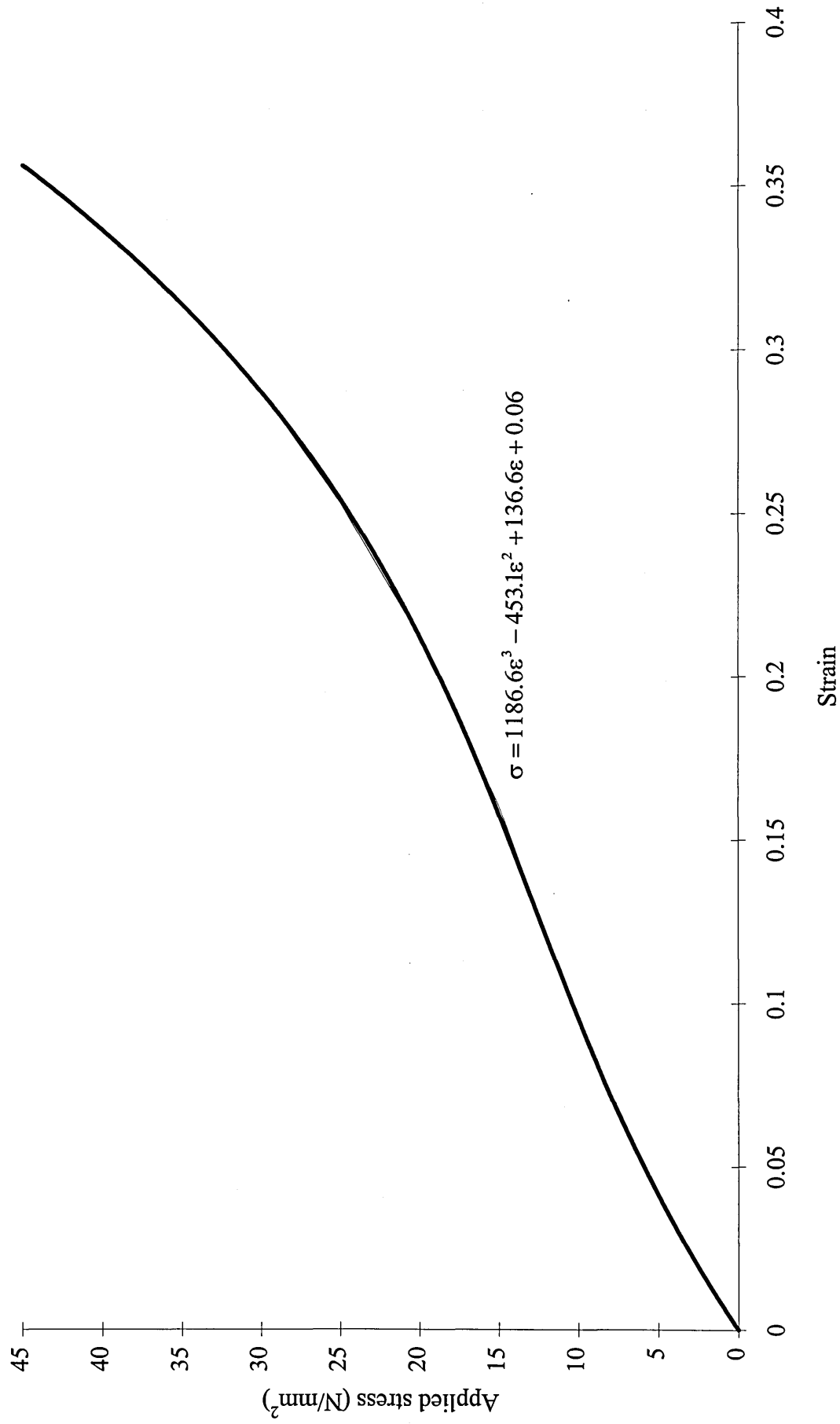
- [1] American Concrete Pipe Association.
'Jacking reinforced concrete pipelines'. 1960.
- [2] Pipe Jacking Association of Great Britain publication.
'A guide to pipe jacking and microtunnelling design'
- [3] Thompson, J.
'Pipejacking and microtunnelling' 1993. Published by Chapman & Hall.
- [4] CSR Hummes Technical Literature. 1994.
- [5] Steinzeug GmbH Handbook. 1996.
'Natural components for modern sewerage systems'.
- [6] Hobas Durotec GmbH Product Information. 1993.
- [7] Stein, D., Bielecki, R., & Maass, U.,
'Small-diameter jacked pipes : development and experiences from Hamburg'.
1983. Europipe'83 Conference, Switzerland. Paper 17.
- [8] Boot. J.C., Woods, G. & Streatfield, R.,
'On-line replacement of sewers using vitrified clayware pipes'. 1987.
International No-dig Conference. Paper 2.3.
- [9] Milligan, G.W.E. & Norris, P.,
'Pipe jacking - research results and recommendations'. 1994. Pipe Jacking
Association / Oxford University.
- [10] Haslem, R.F.,
'Structural interaction at joints in pipejacked tunnels'. 1996. Journal of the
Institution of Structural Engineers. Volume 74. Number 10.
- [11] Moss, A.,
'The guide to best practice for pipe jacking and microtunnelling'. July/Aug.
1995. Underground Utility Construction.
- [12] BS 5911:part 120 : 1989
'Specification for reinforced jacking pipes with flexible joints'.
- [13] EN 295: part7 : 1995
'Requirements for vitrified clay pipes and joints for pipe jacking'.

- [14] Craig, R.N.,
‘Pipe jacking: a state-of-the-art review’. 1983. CIRIA technical note 112.
- [15] O’Reilly, M.P., Rodges, C.D.F.,
‘Pipe jacking forces’. 1987. Proceedings of International Conference on Foundations and Tunnels 87, Edinburgh, Volume 2, Engineering technical press.
- [16] Haslem, R.F.,
‘Pipe jacking from practice to theory’. 1986. Proceedings of ICE North West Association Centenary Conference on Infrastructure Renovation & Waste Control, Manchester, UK.
- [17] Auld, F.A.,
‘Determination of pipe jacking loads’. 1982. Proceedings of Seminar on Renewing Sewerage Infrastructure, Manchester, London. Pipe Jacking Association.
- [18] Terzaghi, K.,
‘Theoretical soil mechanics’. 1943. Wiley, New York.
- [19] Norris, P., & Milligan, G.W.E.,
‘Pipe end load transfer mechanisms during pipe jacking’. 1992. International No-Dig Conference. Washington, USA.
- [20] Concrete Pipe Association of Australia.,
‘Pipe jacking’. 1990. Bulletin.
- [21] Kanari, H., Nobuyuki, N., Kawaguchi, N., & Shiomi, M.,
‘Effect of stress absorbers on pipe splitting during jacking in curves’. 1996. Proceedings of International No-Dig Conference, New Orleans, USA. Paper 3A-3
- [22] Boot, J.C., & Husein, N.M.,
‘Vitrified clay pipes subject to jacking forces’. 1991. Proceedings of Pipe Jacking and Microtunnelling Conference. Pipe Jacking Association.
- [23] Milligan, G.W.E., & Ripley, K.J.,
‘Packing material in jacked pipe joints’. 1989. Proceedings of International No-Dig Conference. Paper 2.1.

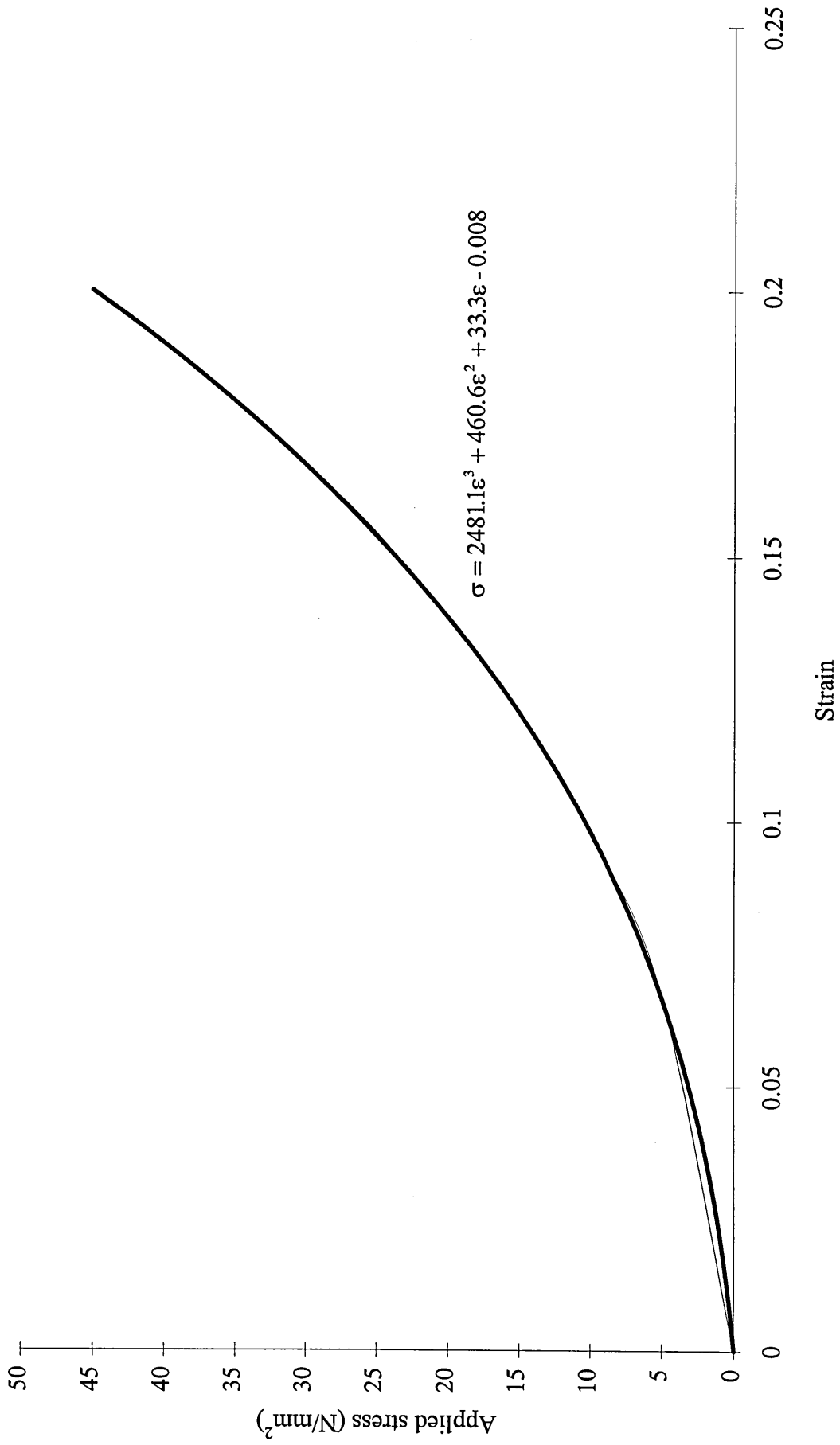
- [24] Gere, J.M., & Timoshenko, S.P.,
‘Mechanics of materials’. 2nd SI Edition, 1987. PWS Publishers USA.
- [25] Timoshenko, S.P., & Goodier, J.N.,
‘Theory of elasticity’. 1970. International Student Edition. McGraw-Hill.
- [26] prEN 312: part 1,
‘Particle boards : General requirements for all board types’
- [27] BS 1449 part 2 : 1983,
‘Specification for stainless and heat-resisting steel plate, sheet and strip’.
- [28] EN 2430,
‘Aerospace series. Ethylene-Propylene rubber (EPM/EPDM). Hardness 70 IRHD’
- [29] BS EN 10 002-1 :1990 :part 1,
‘Tensile testing of metallic materials. Method of test at ambient temperature’.
- [30] Mann, A.P.,
‘The structural use of stainless steel’. 1993. Journal of the Institution of Structural Engineers. Volume 71. Number 4.
- [31] Micro-Measurements.
Catalogue 500 ‘Precision strain gauges’. 1993.
- [32] Micro-Measurements. Technical Tip TT-606,
‘Soldering techniques for lead attachment to strain gauges with solder dots’. 1983.
- [33] Micro-Measurements. Technical Tip B-137-16
‘Strain gauge applications with M-Bond AE-10, AE-15 and GA-2 adhesive systems’. 1979.
- [34] Micro-Measurements. Bulletin 309,
‘Student manual for strain gauge technology’. 1983.
- [35] Micro-Measurements. Technical Note TN-515,
‘Strain gauge rosettes - selection, application and data reduction’. 1990.
- [36] Dally, J.W., & Riley, W.F.,
‘Experimental stress analysis’. 1991. 3rd Edition. McGraw-Hill International Edition.

BIBLIOGRAPHY

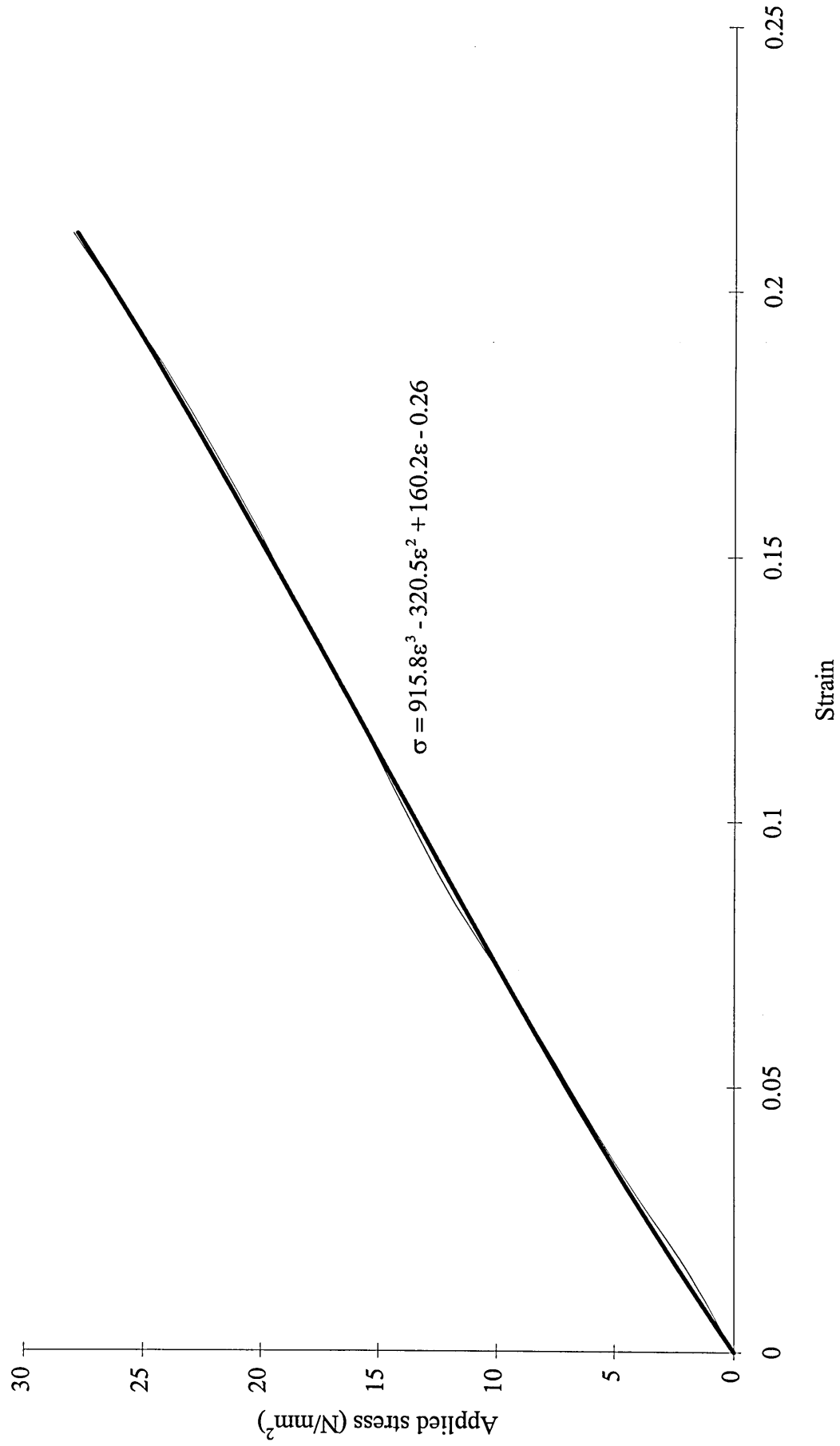
- Stein, D., Mollers, K., & Bielecki, R.,
‘Microtunnelling : Installation and renewal of nonman-size supply and sewerage lines by the trenchless construction method’. 1989. Ernst & Sohn. Berlin.
- Woods, G., Boot, J.C., & Beaumont, T.,
‘Trenchless installation of vitrified clay pipes using microtunnelling techniques’.
- Watson, T.J.,
‘Trenchless construction for underground construction’. 1987. CIRIA Technical Note 127.
- Husein, N.M.,
‘Vitrified clay pipes installed by trenchless techniques’. 1989. PhD. Thesis. Bradford University. UK.
- Rees, D.W.A.,
‘Mechanics of solids and structures’. 1990. McGraw-Hill. UK.
- Holman, J.P.,
‘Experimental methods for engineers’. 1984. International Student Edition. McGraw-Hill.
- Hayward, A.T.J.,
‘Repeatability and accuracy’. 1977. Mechanical Engineering Publications Limited. UK.
- Rangan, C.S., Sarma, G.R., & Mani, V.S.V.,
‘Instrumentation, devices and systems’. 1983. McGraw-Hill.



APPENDIX A1: Stress-strain relationship for chipboard packing material of nominal thickness 8mm on first application of load.

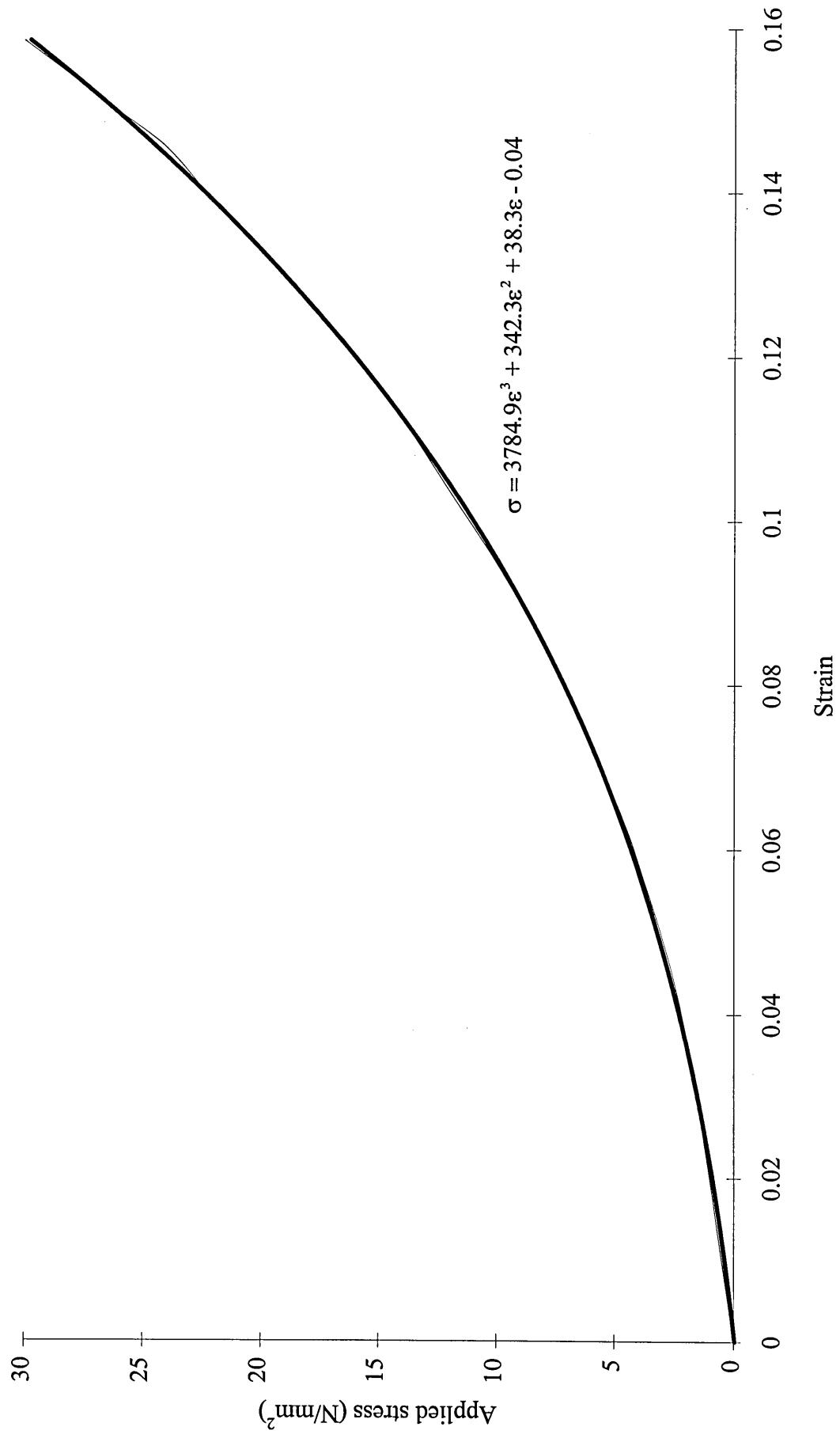


APPENDIX A2: Stress-strain relationship for chipboard packing material of nominal thickness 8mm on second application of load.

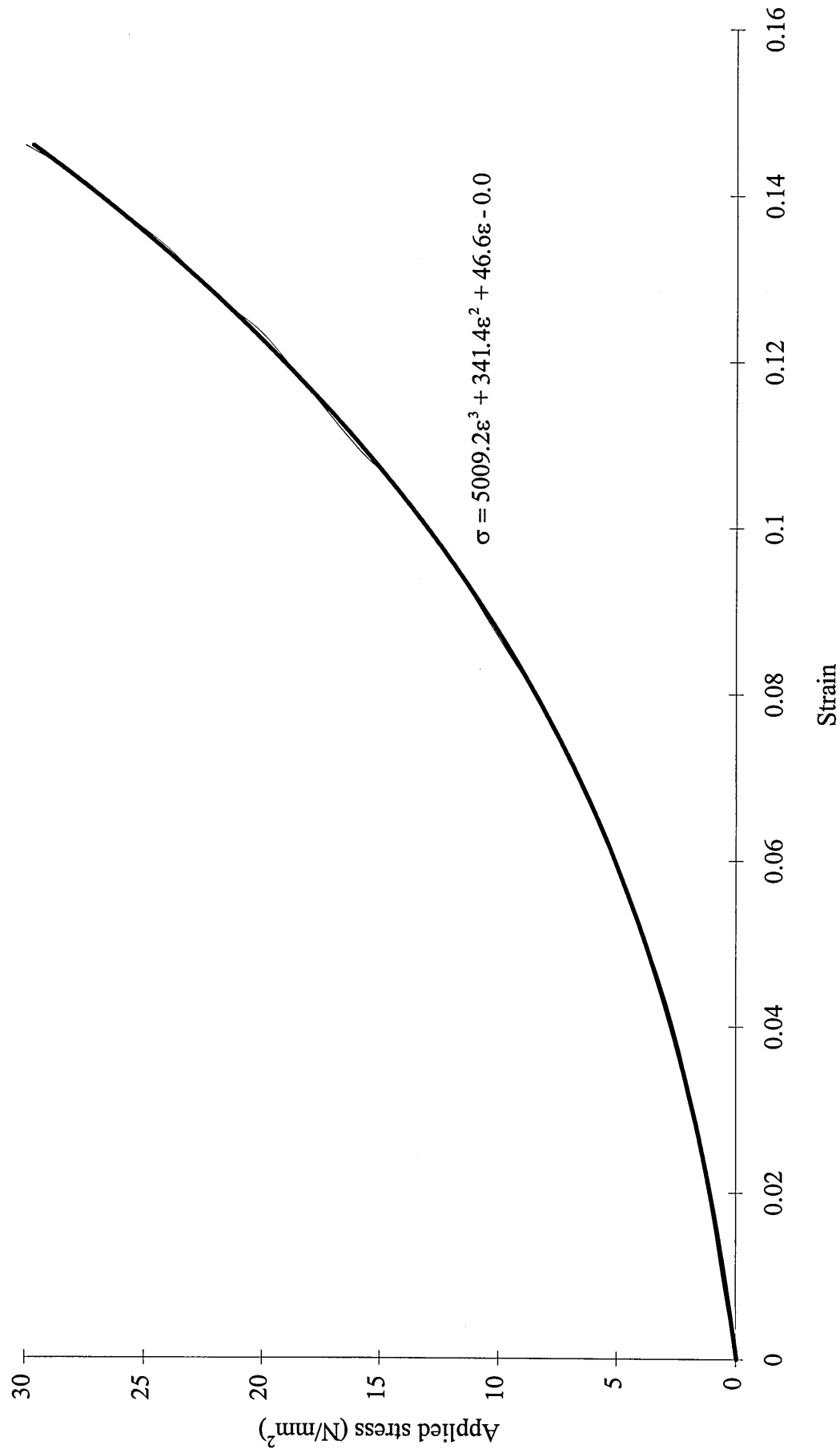


A3

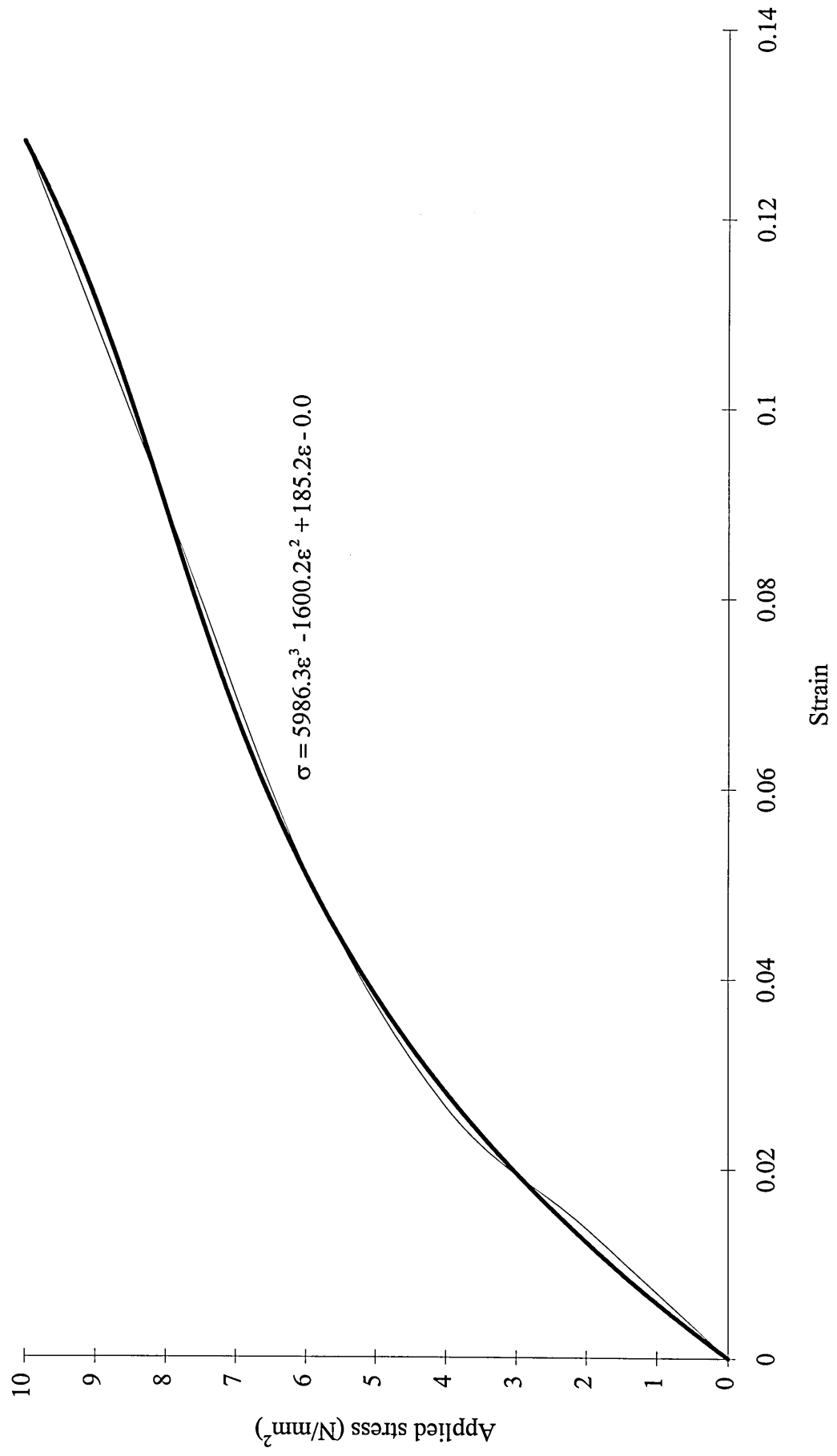
APPENDIX A3: Stress-strain relationship for chipboard packing material of nominal thickness 10mm on first application of load.



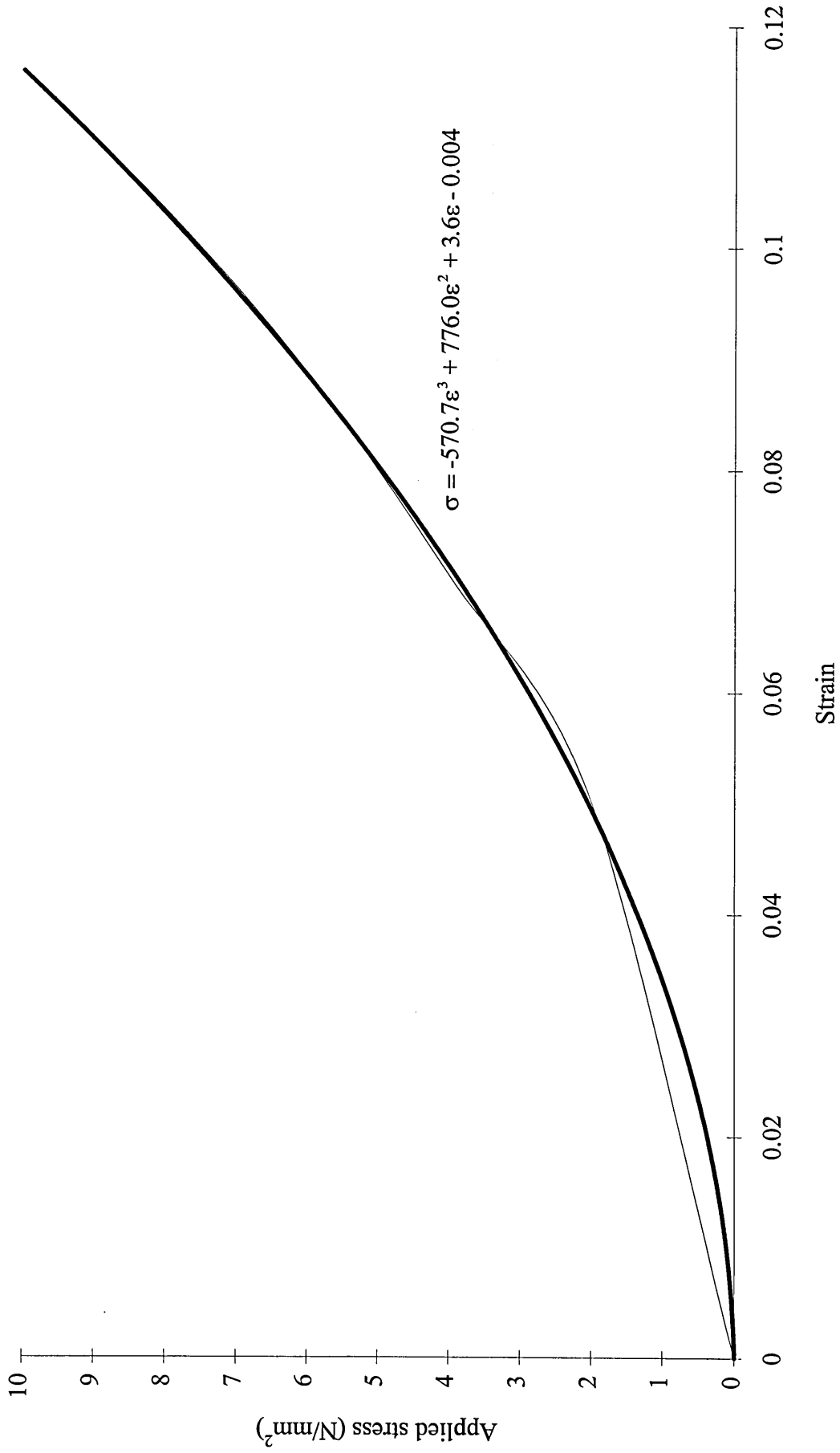
APPENDIX A4: Stress-strain relationship for chipboard packing material of nominal thickness 10mm on second application of load.



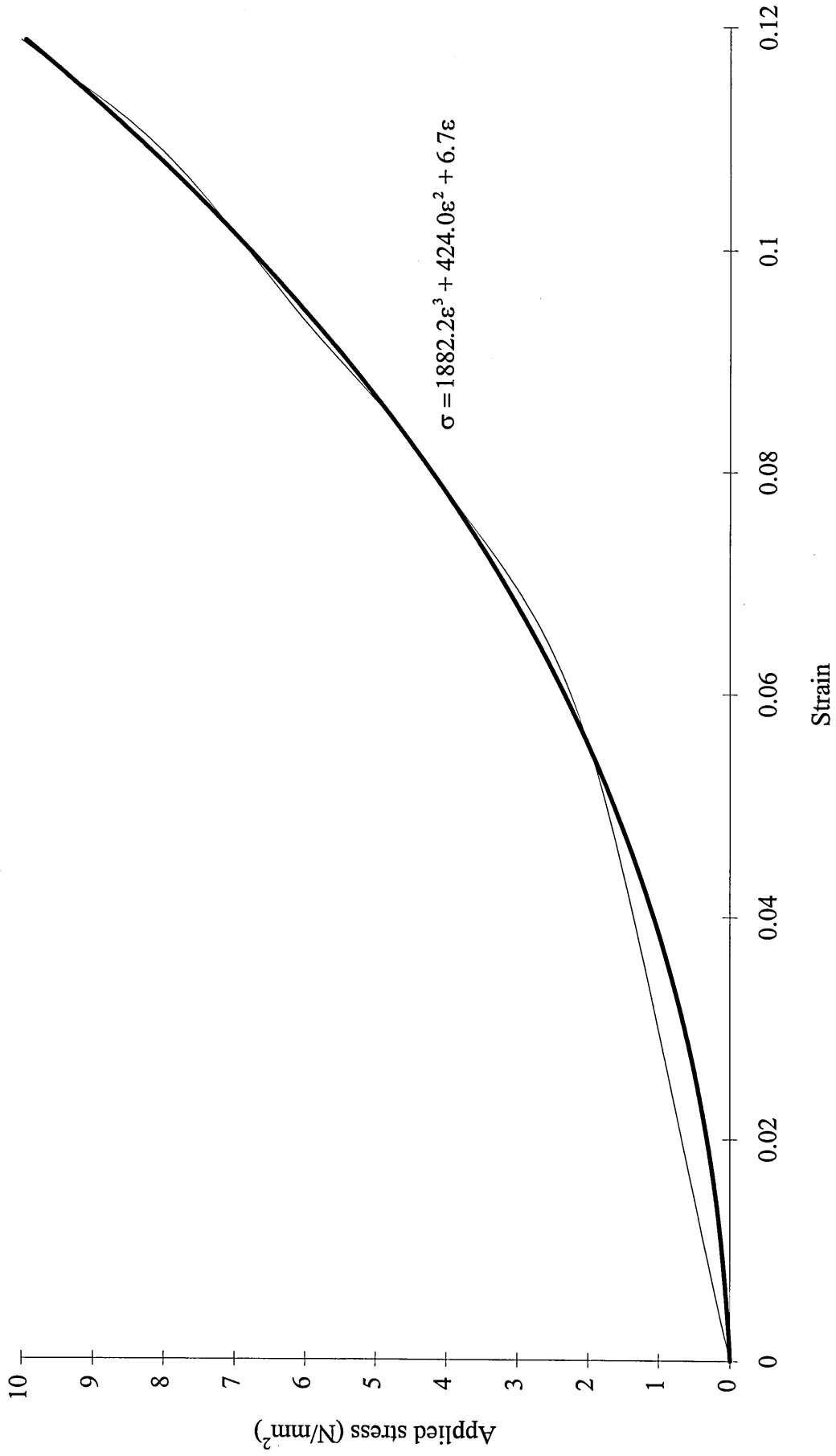
APPENDIX A5: Stress-strain relationship for chipboard packing material of nominal thickness 10mm on third application of load.



APPENDIX A6: Stress-strain relationship for chipboard packing material of nominal thickness 16mm on first application of load.



APPENDIX A7: Stress-strain relationship for chipboard packing material of nominal thickness 16mm on second application of load.



APPENDIX A8: Stress-strain relationship for chipboard packing material of nominal thickness 16mm on third application of load.